Binary Stars in Globular Clusters

Thesis by

Lin Yan

In Partial Fulfillment of the Requirements
for the Degree of
Doctor of Philosophy

California Institute of Technology
Pasadena, California

1996
(Submitted November 2, 1995)

Acknowledgements

Looking back over the past six years at Caltech, I realize that many people have influenced my career in one way or another. Firstly, I would like to thank my advisor Judith Cohen. From her I learned how to do optical observations. Her acute understanding of optical instruments has always been a source of knowledge and inspiration. She helped me through many difficult observing runs and read and corrected the drafts of my thesis again and again with patience.

I did a part of my thesis with Mario Mateo, who was a Hubble Fellow at the Observatories of the Carnegie Institution of Washington and is now an assistant professor at the University of Michigan. Without him, this thesis would have been impossible. I have learned how to do science from him. The collaboration with him has been an enriching experience. I also wish to thank Professor Carlton Pryor at Rutgers University for providing unreserved help and consultation whenever I had questions about the spectroscopic binary survey.

Among the faculty in astronomy at Caltech, I wish to thank our Executive Officer Roger Blandford for dealing with thorny situations with competence and experience. I thank Tony Readhead for providing me with financial support to participate in an astronomy conference in which I was very interested. I also appreciate a great deal the guidance and support from a former Caltech professor Jeremy Mould. Since the day I came to Caltech from China, Peter Goldreich has been my source of advice and encouragement, especially during many difficult times. Finally, I wish to thank Neill Reid for working with me, for many stimulating conversations about astronomy and for reading and correcting early versions of my thesis.

During these six years, my fellow graduate students and postdocs have been a major source of knowledge on virtually every subject, including departmental gossip. I thank Todd Small for his knowledge about the Norris Spectrograph and for his help during many observing runs at Palomar. During conversations with Todd Small, Ian Smail, Donna Womble, David Hogg and my former officemate David Thompson, I have learned a great deal, from little observation tricks and clever data reduction methods to inspiring ideas and unbridled enthusiasm about astronomy. I thank Martin Shepherd, the computer guru in Robinson lab, for helping me on countless occasions. I also wish to thank Gautam Vasisht, Angela Putney, my officemate Julia Kennefick, John Gizis, Chris Fassnacht, Jagmit Sandhu and Rudi Danner for being my friends and for making my life at Caltech more enjoyable.

Finally, for always believing in me and bringing me up to face life with courage and optimism, I thank my mother, Ruilan Yu. And most of all, I thank Sterl Phinney for being always there, for his encouragement and support.

Abstract

This thesis consists of several surveys to search for binary stars and to estimate the frequencies of binary populations in globular clusters. The motivations for these searches are that 1) binary populations (even with a fraction as small as 3%) dominate the dynamical evolution of a globular cluster by producing a tremendous amount of energy through stellar encounters; 2) binary stars provide important information for understanding several apparently different phenomena such as blue stragglers, millisecond pulsars and X-ray sources.

Two different techniques were employed in our surveys. The first survey is based on radial velocities obtained using the Norris Multi-fiber Spectrograph on the Palomar 200 inch telescope. We discovered 5 spectroscopic binary candidates among a total of 65 stars in the globular cluster NGC 5053. A total of 223 velocities were obtained for these 65 stars over a timespan of 3 years with a typical velocity error per measurement of 3 kms^{-1}. With detailed computer simulations we calculated the fraction of binaries which might have been missed in our detection sample due to unfavourable binary orbital configurations. Thus, we derived a binary frequency of 19−26% depending on the adopted period distribution function and orbital eccentricities.

The second part of this thesis utilized a different technique — the analysis of time series photometry. This method is efficient in searching for eclipsing binaries with periods of a few days, as demonstrated in our surveys in the two globular clusters M 71 and M 5. We discovered a total of 11 eclipsing binaries in the clusters, with periods of 0.3−0.7 days. All variables are main-sequence stars except one in M 5, which is a possible blue straggler. Their light curves indicate that one variable

in M 71 and one in M 5 are detached or semi-detached eclipsing binaries; the rest of the 11 systems are W UMa type contact binaries. Based on a simple model of the evolution of contact binaries from initially detached short-period binaries, we estimated a lower limit of 1.3% on the frequency of primordial binaries in M 71 with initial orbital periods of 2.5−5 days. This implies that the primordial binary frequency is 22% assuming a flat logarithmic period distribution. This frequency is for binaries with initial periods shorter than 800 years since any longer-period binaries would have been disrupted over the lifetime of the cluster. A similar calculation was done in M 5. Adopting a flat logarithmic period distribution and a contact binary lifetime of 3 Gyr, we estimated an overall primordial binary frequency of 28^{+11}_{-6}% for systems with periods of 2.5 days to 550 yrs. The discovery of 11 short-period main-sequence eclipsing binaries for the first time provides strong physical evidence which supports the scenario that some blue stragglers are formed by mass transfer and mergers in short-period main-sequence binary systems.

Contents

List of Figures

List of Tables

Chapter 1

INTRODUCTION

1.1. Overview

1.1.1. Binary Stars and the Energetics of Globular Cluster Evolution

A globular cluster is a roughly spherical self-gravitating system, composed of $\sim 10^5$ to 10^6 14 billion years old metal poor stars. For any bound, finite self-gravitating system, its heat capacity is *negative*[†]. The negative heat capacity implies that by losing energy the system gets hotter. For example, when a binary star loses its binding energy, its orbit gets tighter, hence the orbital velocity gets higher, *i.e.*, the orbital kinetic energy becomes higher. Since the system has a negative heat capacity, this means it gets hotter.

In a globular cluster, many dynamical processes have contributed to the evolution to its state in which we observe the cluster today. Internally, gravitational two-body encounters are the major driver of the evolution. Each star slowly strays away from its initial orbit after every two-body encounter. After a two-body relaxation timescale $t_{relax} \approx 0.1\mathrm{N}/\ln(\mathrm{N}) \times \mathrm{t_{cross}}$, where N is the total number of stars in a globular cluster and $\mathrm{t_{cross}}$ is the time for a star to move across a whole cluster, cluster stars have completely lost the memory of their initial trajectories, and the cluster

[†] By analogy with the ideal gas, we can define the system temperature T as $\frac{3}{2}k_B\mathrm{T} = \frac{1}{2}\mathrm{m}\bar{\mathrm{v}}^2$, where m is the stellar mass and k_B is Boltzmann's constant. The total kinetic energy of this system with N stars is then $K = \frac{3}{2}Nk_B\bar{\mathrm{T}}$, here $\bar{\mathrm{T}}$ is the averaged system temperature. According to the virial theorem, the total energy of the system is $\mathrm{E} = -\mathrm{K}$, and hence $\mathrm{E} = -\frac{3}{2}Nk_B\bar{\mathrm{T}}$. Now from the above equation, we can define the system heat capacity $C \equiv \frac{d\mathrm{E}}{d\mathrm{T}} = -\frac{3}{2}Nk_B$.

has evolved. A series of weak, distant encounters can gradually give a star slightly positive energy and cause it to escape from the cluster (*evaporation*). Encounters between stars also tend to establish equipartition of kinetic energy. The more massive stars lose kinetic energy and sink toward the center, while the lighter ones gain kinetic energy and their orbits expand (*mass segregation*). Therefore, on the two-body relaxation timescale of 10^8 to 10^9 years (Binney & Tremaine 1987) mass segregation essentially transfers kinetic energy, *i.e.*, "heat," from the cluster core to the outer parts of the cluster. Because a globular cluster has a negative heat capacity, the process of "heat transferring" from the cluster core by two-body encounters pushes the cluster towards higher and higher central density, which eventually leads to a *gravothermal catastrophe.*

Externally, on a cluster's passages through the Galactic disk and close to the Galactic bulge, the Galaxy's tidal gravitational field can perturb the orbits of stars, particularly those in the outer regions of the cluster, and remove them from the cluster (*tidal stripping*). Furthermore, the Galactic tidal force and the disk shocking can substantially increase the evaporation rate and the mass segregation, and thus accelerate the cluster evolutionary process. Core collapse happens roughly around ten times the half-mass relaxation timescale, *i.e.*, $10t_{rh}$.

The Sun loses heat on its thermal diffusion timescale of $\sim 10^7$ years, and its core would contract if energy were not supplied to the core by nuclear burning. Similarly, a globular cluster loses "heat" on its gravitational two-body relaxation timescale of $\sim 10^8 - 10^9$ years, and the cluster core would collapse and infinite central density would occur in a few half-mass relaxation timescales if energy were not supplied to the core. This energy source in globular clusters is binary stars, just as nuclei are the heat source for the Sun. The energy provided by the binaries can halt core collapse by cooling the central core and thereby reversing the outward flow of energy from core to halo that lies at the root of the gravothermal catastrophe.

Binary stars are very efficient energy sources for the dynamical evolution of a globular cluster. This is demonstrated in the following simple calculation. The total binding energy of a binary, with two $0.7M_\odot$ stars and $2R_\odot$ orbital separation, is $\sim 10^{47}$erg. For a typical globular cluster with a total number of 10^5 stars, the cluster total energy is roughly $-\frac{1}{2}M\sigma^2$, where M is $10^5 M_\odot$, the total mass of a globular cluster, and σ is $\sim$ 10km s^{-1}, the cluster stellar velocity dispersion. This gives the total energy of a typical globular cluster of $\sim 10^{50}$erg. If 1% of all stars are short period binaries, the total energy in these binaries would be equal to the total

energy in the whole cluster. This implies that binary stars can potentially supply a significant amount of energy to a cluster, especially the so called hard binaries. The latter are defined as a type of binary systems where their orbital periods are short enough that their orbital kinetic energy is higher than the cluster single star kinetic energy, *i.e.*, $|\mathrm{E}/\mathrm{m}\sigma^2| > 1$. In other words, these hard binaries are hotter than single stars in the cluster. Thus, during star-binary encounters, energy will flow from hotter binary stars to cooler single stars. This is how hard binaries provide heat to the cluster. Because of its negative heat capacity, the binary star gets hotter after each encounter, as Heggie's law says: *hard binaries get harder and soft binaries simply get disrupted during star-binary encounters.*

For a globular cluster composed initially of single stars, energy can be supplied to the core by binaries which are formed in dissipationless three-body encounters and in two-body tidal captures (Fabian, Pringle & Rees 1975; Heggie 1980). However, because the binary formation rates by these two processes are very sensitive to the cluster density ($\propto n^3$ and $\propto n^2$ respectively), they are inefficient in producing enough binary stars to stave off the core collapse in most clusters. To be significant energy generating mechanisms, they require extremely small, dense cores. The nearly contact binaries produced by the three-body and two-body captures within the small, dense core usually result in rapid and frequent mergers. The products of these mergers are more massive and more luminous than single stars. The problem is that this scenario produces an extremely small and luminous cluster core, which is in contradiction with observations (Goodman 1989).

Theorists understood the dynamical importance of a primordial binary population in globular clusters many years ago. However, only very recently because of mounting observational evidence, they started to take binaries into account seriously in the calculations. Numerous detailed theoretical studies, both analytical and numerical (Gao *et al.* 1991; Heggie & Aarseth 1992; McMillan & Hut 1994; Vesperini & Chernoff 1994), have shown that the primordial binary stars, even with a fraction as small as 3%, can dominate the cluster dynamical evolution. Models without primordial binaries result in too many clusters on the verge of core collapse, as well as extremely small and luminous cores which are not observed in the core collapsed clusters. When the cluster core starts to contract around $10t_{rh}$, the energy generated by primordial binaries stabilizes it and maintains the core size around an almost constant radius, $\sim$4 times larger than in the single-star case for much a longer period of time, almost four times the core collapse timescale for the single-star

cluster (McMillan, Hut & Makino 1990; Gao *et al.* 1991; Hut, McMillan & Romani 1992). Binary stars provide cluster cores a much wider time period window to be at moderate densities before cluster cores exhaust all primordial binaries and undergo core collapse. This gives a natural explanation why we don't observe as many core collapsed clusters as predicted in the single-star case.

1.1.2. Observational Evidence

In above section, we have shown the importance of binary stars for the energetics of the globular cluster evolution. However, is there any observational fact which suggests that a binary star population indeed exists in globular clusters?

Indisputable evidence for the binary existence in globular clusters came from discoveries of millisecond pulsars. These millisecond pulsars are rapidly rotating neutron stars, which were spun up previously by accreting material from close companion stars. Among a total of ~40 millisecond pulsars in globular clusters, ~12 were found in binary systems. And of these 12 binary millisecond pulsars, 2 were found with periods as long as 200-300 days (McKenna *et al.* 1988; Kulkarni *et al.* 1991) in the low density clusters M 4 and M 53. Binaries with such long periods cannot be formed through single star-star tidal capture. They have to be formed by star-binary and binary-binary encounters, or their progenitors are primordial binary stars. In fact, the millisecond pulsar PSR B1620-26 in M 4 is a triple star system (Backer 1993; Backer, Foster & Sallmen 1993; Thorsett, Arzoumanian & Taylor 1993; Bailyn *et al.* 1994), which can only be formed by binary-binary encounters. The inferred high birth-rate of pulsars in globular clusters suggests a primordial binary frequency of 5% −20% (Phinney 1995).

Bright X-ray sources in globular clusters, indistinguishable from those in the galactic disk, are understood as low mass X-ray binaries (thereafter LMXBs) containing neutron stars accreting material from low mass companions. A total of 12 low mass X-ray binaries (two of which have accurately measured periods) were discovered in all globular clusters, while only 120 LMXBs were found in our Galaxy. The mass ratio of all globular clusters and the Galaxy is $10^8/10^{11}$, *i.e.*, 10^{-3}. This implies that relative to the number of stars, the abundance of LMXBs in globular clusters is 1 to 2 orders of magnitude higher than it is in the Galactic disk. Therefore, there must be another much more efficient way of forming these LMXBs in globular

clusters. Due to the high density environment in globular clusters, single star-star, star-binary and binary-binary encounters together naturally provide much more efficient formation mechanisms than in our Galaxy. However, because the lifetime of LMXBs are poorly understood, it is not clear if star-binary and binary-binary encounters are required in order to explain all LMXBs in globular clusters, or perhaps single star tidal captures or dissipationless three-body encounters are sufficient. Recent studies have shown that two-body tidal captures may not be nearly as efficient at forming binaries as was commonly believed in the 1980's (Podsiadlowski 1991).

In 1992, Meylan et al. discovered two high-velocity stars within the core region of the high density globular cluster 47 Tuc. These two stars are located 4″ and 7″ from the cluster center respectively, and their radial velocities are almost three to four times of the radial velocity dispersion of the cluster core. After examining the cluster membership and the statistical possibility of both stars having high velocities by chance within the small central region, the authors concluded that the two high velocity stars are probably members. The possible explanation could be that the two stars are produced by ejections of star-binary and/or binary-binary close encounters in the dense cluster core environment.

1.1.3. Searches for Binary Stars and Determination of Binary Frequency in Globular Clusters

All the above observational evidence has, to some extent, suggested the existence of a significant population of binary stars in globular clusters. In the following section, we will discuss the binary stars discovered through direct observational techniques and the new results of recent surveys. Many ambitious surveys have been carried out to obtain a better understanding of binary star populations in globular clusters. One of the drivers behind these efforts is to understand many apparently different phenomena in globular clusters which may be intimately related to binary stars. For example, such phenomena include blue stragglers, colour/stellar gradient in the cores of post-core-collapsed clusters (Djorgovski & King 1986; Stetson 1994), X-ray sources and numerous "recycled" radio pulsars (Phinney 1992; Phinney 1995).

There are basically three kinds of techniques which directly measure binary stars in globular clusters. The first method is to detect binary systems by measuring the radial velocity changes with time. The first large radial velocity survey was carried

out by Gunn & Griffin (1978). They measured radial velocities of 33 giant stars, each with two measurements, in the globular cluster M 3. The stars in their sample are bright giant stars with V magnitudes of 12−14. They did not find any binary stars, and concluded that binaries with periods in the range of 0.1−10AU are deficient in globular clusters compared to the field binary population.

However, Harris & McClure (1987) criticized this conclusion by pointing out that low metallicity giant stars in globular clusters have much smaller masses compared to field K giants. Field K giants have typical masses of $2M_{\odot}$ as compared to $0.8M_{\odot}$ giants in globular clusters. According to the standard stellar evolutionary models, main sequence stars more massive than $1.5M_{\odot}$ don't increase their luminosity by large factors when they evolve to giants, unlike the evolution of low mass stars. A $2M_{\odot}$ giant is, in fact, fainter than a $0.8M_{\odot}$ bright giant in a globular cluster. Thus it also has a smaller radius than that of a bright globular cluster giant. Including these effects, they statistically compared the distribution of maximum velocity variation (one maximum velocity change per star) of the simulated data containing 54% binaries with that of the real data in M 3. They claimed that the Gunn & Griffin's failure to detect any spectroscopic binaries among 33 giants in globular clusters is *not inconsistent* with the high value of binary frequency as in the field.

Encouraged by the Harris & McClure result, Pryor et al. (1988) extended Gunn & Griffin's sample from 33 to 112 giant stars in the similar magnitude range and increased the number of velocity measurements per star. They discovered one spectroscopic binary candidate VZ 164, which was later confirmed with the period of 7.3 year. Around the same time, significant evidence from observations of pulsars and X-ray sources (as described above) suggested strongly the existence of primordial binary populations in globular clusters. This was the start of a new period when both observers and theoreticians realized that binary populations indeed exist in globular clusters, and many large ambitious surveys were carried out to estimate the binary frequency in globular clusters.

The radial velocity survey technique for finding binary stars in globular clusters suffers two fundamental limitations: technical limitations and the intrinsic difficulties of the problem itself. For binaries with periods in the range of 10 days to 10 years, the only way of determining the binary frequency is to systematically measure radial velocity variations in individual stars of a globular cluster. Technically, only recently with the advent of high resolution multi-object spectrographs on 4-meter class telescopes did it become possible for the first time to sample a large number of

stars and to obtain multi-epoch observations with a reasonable amount of telescope time. With telescopes smaller than the Keck 10-meter telescope, we are limited to bright red giants and subgiants even in the closest globular cluster. These bright low metallicity giant stars have smaller masses and larger radii compared to the field G-type stars. Consequently, a binary system containing such a bright giant star is difficult to detect since the system tends to have a long period and small radial velocity variations.

Figure 1(a) demonstrates this effect for stars in globular clusters, where the horizontal axis is the stellar radius and the vertical axis, the absolute visual magnitude. The plot was made using red giant branch models of Bergbusch & VandenBerg (1992) with [Fe/H] $= -2.26, [\mathrm{O/Fe}] = 0.75$, and an age of 15 Gyr. In Figure 1(a), the solid lines are for three different metallicities with [Fe/H] of 0.7, -1.3 and -2.3. The radii of red giants in a globular cluster brighter than the cluster Horizontal Branch (around M_V of 0.0) are rising rapidly as a function of luminosity, and at the same luminosity the giant stars with higher metallicity are also larger in size. The size of the giant star in a binary system imposes the minimum period which the binary star could possibly have. Figure 1(b) shows the minimum period of a binary system without mass transfer as a function of the absolute magnitude of the primary star. Here for simplicity we only consider binary stars with edge-on circular orbits, in which the primary star mass M_1 was estimated from the catalog of the Revised Yale Isochrones (Green, Demarque & King 1987) and the secondary mass M_2 was assumed to be $0.5M_\odot$. For such a binary system, the minimum semi-major axis is set by the critical Roche lobe radius $R\frac{0.6q^{2/3}+\ln(1+q^{1/3})}{0.49q^{2/3}}$ (Pringle 1984), where R is the stellar radius of the primary star, and $q = M_2/M_1$ is the mass ratio of the binary system. Similarly, Figure 1(c) is the plot of the peak-to-peak radial velocity variation (the maximum velocity variation in a full orbit) versus the luminosity of the primary star.

All of the existing radial velocity surveys for binary stars in globular clusters were carried out among bright giant stars (Gunn & Griffin 1979; Pryor, Latham & Hazen 1988; Côte *et al.* 1994). Table 1 is the summary of all radial velocity surveys carried out in various globular clusters until recently. Note that most surveys in Table 1 are among stars with visual magnitudes of $11-14$, whose radii are as large as $0.1-0.5$ AU. Hence, large velocity variations are generally not expected in the surveys for binary stars among bright giants ($M_v \leq 0$ mag) in globular clusters. Even though peak-to-peak velocity variations up to 50 km/s are allowed, the chance of selecting a

star with a high velocity orbit at a high inclination angle and observing it at phases giving large velocity differences is small. High precision velocity measurement ($\sim$ 1 km s^{-1}) is required.

In 1989, Pryor et al. combined velocity measurements from their own surveys, including unpublished results, with the velocities from other surveys such as that of Mayor et al. (1984) and of Lupton, Gunn & Griffin (1987). They made the first estimate of the globular-cluster binary frequency based on the actual discovery of binaries. The data consisted of 1253 velocities for 393 giants in the globular clusters 47 Tuc, M 71, M 13, M 12 and M 3. With six binary candidates, the estimated frequency of binaries with periods in a range of 0.2−20 years is 5−12%, depending on the eccentricity distribution. In their calculation, they adopted a "flat" logarithmic period distribution function. The most recent large survey was carried out by Côte et al. (1994) in the globular cluster NGC 3201. Among a total of 276 bright giant stars, they discovered 2 strong binary candidates and 13 fair binary candidates. The estimated binary frequency is 6% − 10% and 15% − 18% for circular and eccentric orbits respectively.

The second method for detecting binary stars in globular clusters is to use the analysis of time series photometry technique to look for stars exhibiting periodic photometric variations. This method is only sensitive to short period eclipsing binary systems, whose intensity varies periodically as the systems rotate. Although the first *bona fide* eclipsing binary in a globular cluster was discovered quite a long time ago (Niss *et al.* 1978), only recently did people start to realize the importance of these short period eclipsing binary systems. Their close association with the formation of blue stragglers was revealed for the first time by the discovery of short-period eclipsing binaries among blue stragglers in the globular cluster NGC 5466 (Mateo *et al.* 1990). Since then, many studies have been carried out to increase the number of short-period eclipsing binaries known in various clusters. Table 2 summarizes the present state of our knowledge. In the table, EW and EA denote the W UMa type contact eclipsing systems and the Algol type detached systems respectively. TO, BS, MS and SG indicate the main-sequence turnoff stars, blue stragglers, main-sequence stars and subgiant stars. As shown in Table 2, a few years ago when I started my thesis, there were not many short-period interacting binaries discovered in globular clusters. Since then the number of known short-period binaries has increased dramatically. In §1.2 I will discuss in detail the implications of these

discoveries on the estimate of the overall primordial binary frequency and on the formation process of blue stragglers in globular clusters.

Finally the last method of searching binary systems in globular clusters is to use cluster colour-magnitude diagrams. This method utilizes the fact that a binary system, with two equal mass stars in the extreme situation, is 0.75 magnitude brighter than the single star, *i.e.*, $m(\text{binary}) = \text{constant} + 2.5 \times \log(2 \times \text{L(single)}) = \text{constant} + 0.75 + \text{m(single)}$, where m is magnitude and L is luminosity. Thus a binary system, consisting of two stars with similar brightness, is located off the single star track in the colour-magitude diagram. This method is sensitive to binaries with two nearly equal mass stars. So far due to the crowding problem, this method has not been used successfully in globular clusters from ground-based telescopes. However, this method has been successfully applied to open clusters (Anthony-Twarog *et al.* 1990; Bolte 1991). For example, in the open cluster Praesepe Bolte (1991) found 17 binary candidates from their locations on the HR diagram as shown in Figure 2. The follow-up spectroscopic study confirmed that 11 out of 17 candidates are actually binary systems. The potential use of this method in globular clusters has been further explored by the Hubble Space Telescope (HST) with its high angular resolution. The HST observations of 47 Tuc by De Marchi & Paresce (1995) have revealed a clear sequence of objects running parallel to and brighter than the main sequence. The objects on this sequence are main sequence binary candidates with two equal mass stars. De Marchi & Paresce (1995) estimated that the frequency of main-sequence binaries with two equal mass stars is $\geq 5\%$. Notice their calculation did not consider the accidental overlaps of two or more single stars. In the globular cluster ω Cen., HST observations (Elson *et al.* 1995) also discovered a population of main sequence binary candidates with two equal mass stars, although the sequence of this population is not as clear in its colour-magnitude diagram as in the case of 47 Tuc.

1.2. Motivation and Strategy of This Thesis

This thesis consists of two parts with the purpose of searching for binary stars and determining binary frequency in globular clusters. The first part is based on a radial velocity technique which is sensitive to spectroscopic binary systems with periods of a few days to 10 years, and the second part utilized a different technique

— the analysis of time series photometry — which is efficient in finding short-period eclipsing binaries.

1.2.1. Radial Velocity Survey for Spectroscopic Binaries

As described in §1.1.2, most existing radial velocity surveys for spectroscopic binaries in globular clusters were carried out among bright giant stars. The most recent survey by Côte et al. (1994) went only one magnitude fainter than previous surveys, as shown in Table 1. Consequently, the minimum binary periods imposed by the large radii of these bright giant stars are quite long (see Figures 1), and the possibility of detecting these long period binary systems with a limited amount of telescope time is small. One way to increase the binary detection efficiency is to observe fainter stars. With the advent of the Norris Multi-fiber Spectrograph at the Palomar 200 inch telescope, it became possible for the first time to survey a large number of faint stars with a reasonable amount of telescope time. The sample of our survey consists of 76 cluster member giant and subgiant stars with visual magnitudes of 15−18.6. Our survey went 3 magnitudes fainter than the previous survey (Pryor, Schommer & Olszewski 1991) and sampled almost 3 times as many stars. Of the 76 stars, 65 have multiple velocity measurements with a total number of 223 velocities over a timespan of 3 years. The restriction on the binary periods imposed by the radii of our sample objects is small. Our survey is sensitive to binaries with periods in a range of 4 days to 10 years, and mass ratio larger than 0.125.

To estimate the primordial binary frequency in globular clusters, we chose the cluster NGC 5053. As discussed in section §1.1.1, the spatial distribution as well as the period distribution of binary stars can be significantly modified by stellar encounters. NGC 5053 is an ultra low density cluster, whose half-mass relaxation timescale is comparable to a Hubble timescale. This implies that the primordial binary population in this cluster has not been altered substantially. Note that in Table 1 the majority of the surveys were carried out in the dynamically evolved clusters. Thus the binary frequency inferred from these surveys is really the present-day binary frequency. With increasing number of surveys for spectroscopic binaries in various globular clusters, it will be interesting to investigate if the binary frequency is indeed correlated with the cluster dynamical properties. Although at the present the derived binary frequency in several clusters is still very approximate and may be subject to large errors, it is tempting to compare the actual discovery fractions

in different clusters. As shown in Table 1, it is noticeable that the binary discovery fraction and estimated binary frequency is higher in NGC 5053 than in other clusters. This is perhaps associated with the fact that NGC 5053 is dynamically younger.

1.2.2. Photometric Surveys for Short-period Eclipsing Binaries

The second part of this thesis was designed to be sensitive to a different type of binary stars compared to radial velocity surveys. These binaries are eclipsing systems with periods less than a couple of days. This method generally can sample more than 6000 stars with a single CCD image, and thus is relatively more efficient. One of the motivations of conducting photometric surveys in several globular clusters is, again, to find more binary stars. The discovery of these short-period eclipsing binaries help to constrain the overall binary frequency. More importantly, these surveys were also motivated to achieve a better understanding of the origins of blue stragglers by the first discovery of short-period eclipsing binaries among blue stragglers (Mateo *et al.* 1990).

As shown in Table 2, the photometric surveys in this thesis have discovered almost a dozen short-period eclipsing binaries among main-sequence stars. These results provide, for the first time, strong physical evidence that blue stragglers are closely associated with short-period main-sequence interacting binaries. They strongly support the scenario that blue stragglers in globular clusters were formed by mass transfer/mergers between two stars in short-period interacting binaries. Short-period binaries on the main sequence of a cluster are destined to become blue stragglers when either (a) the primary gains enough mass to push it over the turnoff mass, or (b) the cluster turnoff mass evolves below the mass of the primary or the merged binary remnant.

1.2.3. Outline of the Thesis

The radial velocity survey for spectroscopic binaries in the globular cluster NGC 5053 is presented in Chapter 2. A shorter version of this chapter has been submitted to AJ. Chapters 3 and 4 are the second part of the thesis: photometric surveys for short-period eclipsing binaries in two different clusters M 71 and M 5. The work in M 71 has been published in 1994, AJ, 108, 1810. Chapter 4 has been

accepted for publication by the journal of the Monthly Notice of Royal Astronomical Society. Since Chapters 2, 3 and 4 were written as stand alone articles to be published in journals, parts of the introduction sections in these chapters were repeated in Chapter 1. Finally, a short summary of conclusions and suggestions for future work is given in Chapter 5. In Appendix A, we discussed the throughput efficiency of the Norris Multi-fiber Spectrograph.

REFERENCES

Anthony-Twarog, B.J., Kaluzny, J., Shara, N.M. & Twarog, B.A., 1990, AJ, 99, 1504

Backer, D.C. 1993, in *Planets around Pulsars*, ed. J.A. Phillips et al. (San Fransisco: ASP vol. 36), 11

Backer, D.C., Foster, R.S. & Sallmen, S., 1993, Nature, 365, 817

Bailyn, D.C., Rubenstein, E.P., Girard, T.M., Dinescu, D., Rasio, F.A. & Yanny, B., 1994, ApJ, in press

Binney, J. & Tremaine, S., in *Galactic Dynamics*, 1987 (Princeton University Press), 190

Bolte, M., 1991, ApJ, 376, 514

Côte, P., Welch, D.L., Fischer, P., Da Costa, G.S., Tamblyn, P., Seitzer, P. & Irwin, M.J. 1994, ApJS, 90, 83

De Marchi, G. & Paresce, F., 1995, StSci preprint No. 932

Elson, R.A.W., Gilmore, G.F., Santiago, B.X. & Casertano, S., 1995, preprint

Djorgovski, S. & King, I.R., 1986, ApJL, 305, L61

Gao, B., Goodman, J., Cohn, H. & Murphy, B., 1991, ApJ 370, 567

Gunn, J.E. & Griffin, R.F., 1979, AJ, 84, 752

Harris, H.C. & McClure, R.D., 1983, ApJL, 265, L77

Heggie, D.C., 1980, in *Globular Clusters, NATO Advanced Study Institute*, ed. by D. Hanes and B. Madore, (Cambridge: Cambridge Univ. Press), 281

Heggie, D.C. & Aarseth, S.J., 1992, MNRAS, 257, 513

Hut, P., McMillan, S.L.W., Goodman, J., Mateo, M., Phinney, E.S., Richer, H.B., Verbunt, F. & Weinberg, M., 1992, PASP, 104, 981

Hut, P., McMillan, S.L.W. & Romani, R.W., 1992, ApJ, 389, 527

Kaluzny, J. & Krzeminski, W. 1993, MNRAS, 264, 785

Kulkarni, S.R., Anderson, S.B., Prince, T.A. & Wolszczan, A., 1991, Nature, 349, 47

Lupton, R.H., Gunn, J.E. & Griffin, R.F., 1987, AJ, 93, 1114

Mateo, M., Harris, H.C., Nemec, J.M. & Olszewski, E.W., 1990, AJ, 100, 469

Mateo, M. & Mirabel, N., 1995, preprint

Mayor, M., Imbert, M., Andersen, J., Ardeberg, A., Benz, W., Lindgren , H., Martin, N., Maurice, E., Nordstr öm, B. & Prévot, L., 1984, AA, 134 , 118

McMillan, S.L.W. & Hut, P., 1994, ApJ, 427, 793

McMillan, S.L.W. & Makino, J., 1990, ApJ, 362, 522

McKenna, J. & Lyne, A.G., 1988, Nature, 336, 226

Meylan, G., Dubath, P. & Mayor, M., 1991, ApJ, 383, 587

Niss, B., Jorgensen, H.E. & Lautsen, S., 1978, A&AS, 32, 387

Phinney, E.S., 1992, Phil. Tran. R. Soc. London Ser. A, 341, 39

Phinney, E.S. 1995, in *Binary Stars in Clusters*, ed. by Eugene Milone, in press

Podsiadlowski, P., 1991, Nature, 350, 136

Pringle, J.E., 1984, in *Interacting Binary Stars*, ed. by J.E. Pringle and R.A. Wade, (Cambridge: Cambridge Univ. Press), 1

Pryor, C.P., McClure, R.D., Hesser, J.E. & Fletcher, J.M., 1987, BAAS, 19, 676

Pryor, C.P., Latham, D.W. & Hazen, M.L. 1988, AJ, 96, 123

PryorPryoy, C.P., McClure, R.D., Hesser, J.E. & Fletcher, J.M. 1989, in *Dynamics of Dense Stellar Systems*, ed. D. Merritt (Cambridge Univ. Press), 175

Pryor, C.P., Schommer, R.A. & Olszewski, E.W., 1991, in *The formation and Evolution of Star Clusters*, ed. by K. Janes (San Fransisco: ASP vol. 13), 121

Rubenstein, E. & Bailyn, C.D. 1995, preprint

Stetson, P.B., 1994, PASP, 106, 250

Thorsett, S.E., Arzoumanian, Z. & Taylor, J.H. 1993, ApJ, 412, L33

Vesperini, E. & Chernoff, D.F. 1994, ApJ, 431, 231

Yan, L. & Mateo, M., 1994, AJ, 108, 1810

Yan, L. & Reid, I.N., 1995, MNRAS, in press

TABLE 1

Summary of All Radial Velocity Surveys for Spectroscopic Binaries in Globular Clusters

Cluster	N_{bin}	N_{tot}	N_{rv}	ΔT yrs	Δm_V mag	DM mag	σ kms^{-1}	T_{rh} Gyr	Ref.
NGC 5053	3	28	109	3	12−15.5	16.08	0.9	7	(1)
NGC 5053^2	5	65	223	3	14.2−18.6	16.08	3.0	7	(2)
NGC 3201	2+13	276	786	6	11.5−16.5	14.2	1.1	0.06	(3)
M 3	1	110	504	10	12−14	15.02	1.0	0.6	(4), (5)
NGC 5466	2	36	140	5	12−15.5	15.99	0.9	6	(1)
M 13	1	93	288	5	12−14	14.29	1.0	0.09	(6)
M 71	4	61	≥220	8	12−14	12.96	0.8	0.1	(7), (8)
M 12	2	72	111	4	12−14	15.38	0.8	1.0	(8)
47 Tuc	0	64	124	0.5	11.5−13.5	13.31	0.6	1.5	(9)

Notes: In the table, NGC 5053^2 represents our survey, the second made in the cluster NGC 5053. Because the two surveys in this cluster are different in many aspects, we tabulated their data separately. N_{bin} is the total number of discovered binary candidates, N_{tot} is the total number stars observed in each survey and N_{rv} is the total number of radial velocity obtained in each survey. In the cluster NGC 3201, Côte et al. (1994) discovered 2 good binary candidates together with 13 possible candidates. Δm_V is the visual magnitude range of the sample objects in the survey. DM and T_{rc} represent the distance modulus and the central relaxation time of a cluster respectively. σ is the internal velocity error per measurement. The stars in all surveys are distributed throughout the whole cluster *except* in the case of 47 Tuc. Mayor et al. only sampled the stars from the region beyond 5 core radii in 47 Tuc. The total number of velocities collected for M 71 is not certain because the complete data have not been published. The code for the reference column is as follows:

(1) − Pryor et al. 1991; (2) − this thesis; (3)− Côte et al. 1994;

(4)− Gunn & Griffin 1978; (5)− Pryor et al. 1988; (6)− Lupton et al. 1987;

(7)− Pryor et al. 1992; (8)− Pryor et al. 1987; (9)− Mayor et al. 1984

TABLE 2

Short Period Eclipsing Binaries in Globular Clusters

Cluster	Star	Type	Source
ω Cen	NJL 5	EA BS	Helt et al. 1993
NGC 5466	NH19	EW BS	Mateo et al. 1990
	NH30	EW BS	
	NH31	EA BS	
NGC 4372	V4	EW TO	Kaluzny and Krzeminski 1993
	V5	EW TO	
	V16	EW BS	
	V22	EW BS	
	V30	EA BS	
	V31	EW SG	
	V35	EW SG	
M 71	V1	EW TO	Yan and Mateo 1994
	V2	EW TO	
	V3	EW MS	
	V4	EA TO	
	V5	EW TO	
M 55	V7	EW SG	Mateo and Mirabel 1995
	V8	EW MS	
	V9	EW MS	
M 5	V1	EW BS	Yan and Reid 1995
	V2	EW TO	
	V3	EW MS	
	V4	EW TO	
	V5	EW TO	
	V6	EW TO	

NGC 6397	V1	EW TO	Rubenstein and Bailyn 1995

Notes: In the table, EW stands for W UMa type contact eclipsing binaries, EA for detached eclipsing binaries; TO represents the stars around a cluster main-sequence turnoff, BS blue stragglers, MS main sequence stars and SG sungiant stars.

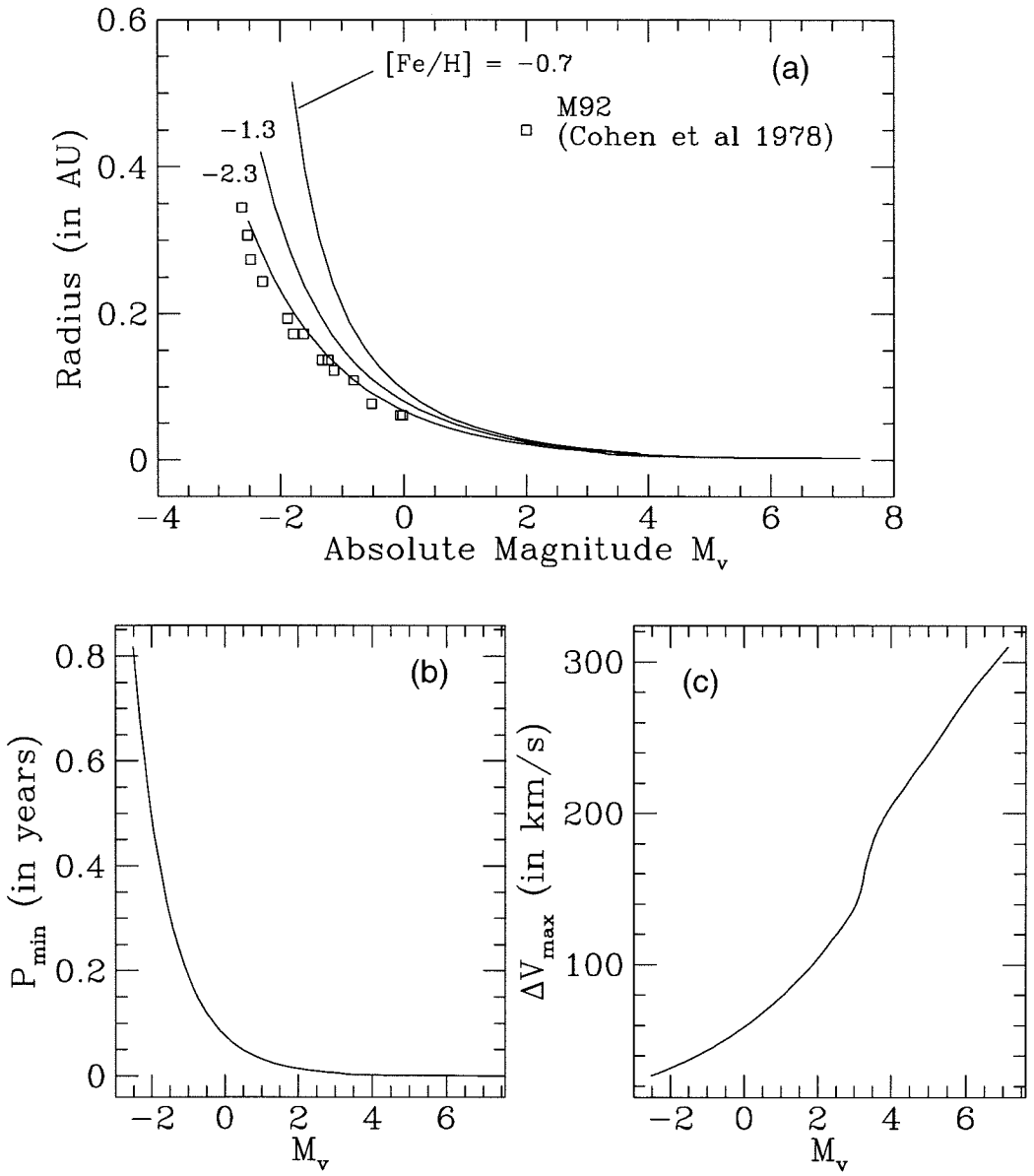

Figure 1.1 Stellar Radius vs. Luminosity

Figure 1.1(a) is a plot of the stellar radius vs. the luminosity for stars in globular clusters. In the figure the curves are generated for three different metallicities using the Revised Yale Isochrones and Luminosity Functions (Green *et al.* 1987) with Y= 0.2 and an age of 15 Gyr. Figure 1.1(b) is the plot of the minimum period of a binary system versus the luminosity of the primary. This minimum period which a binary system could possibly have without undergoing mass transfer is set by the size of the primary star of the binary. Similarly, Figure 1.1(c) plots the maximum radial velocity variations versus the primary star luminosity. For both Figure 1.1(b) and 1.1(c), the calculations were done for binaries on edge-on circular orbits with M_1 derived from the stellar models and an assumed M_2 of $0.5M_\odot$.

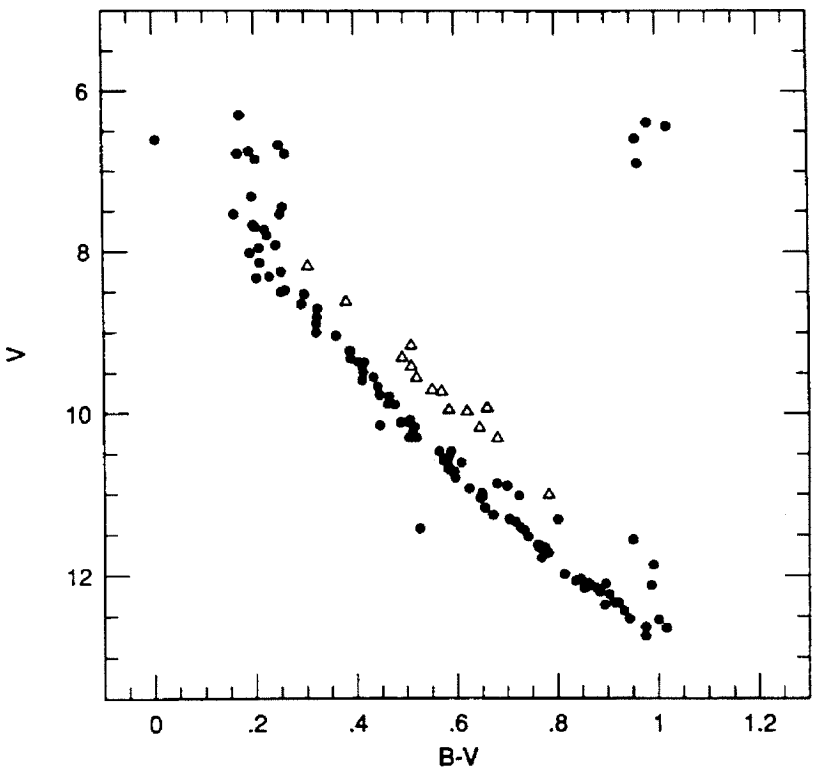

Figure 1.2 Parallel Main-sequence Binaries in Praesepe

The colour-magnitude in the open cluster Praesepe (adopted from Bolte 1991). The open triangles in the figure are the main-sequence binaries which have mass ratios near 1.0. Of these binary candidates, 11 out of 17 were later confirmed as binary systems through subsequent radial velocity studies.

Chapter 2

THE SPECTROSCOPIC SURVEY FOR BINARY STARS IN THE GLOBULAR CLUSTER NGC 5053*

ABSTRACT

We carried out a radial velocity survey for spectroscopic binaries in the low density globular cluster NGC 5053. Our sample contains a total of 76 cluster member giant and subgiant stars with visual magnitudes of 14.5−18.6. Of these 76 stars, 65 stars have an average of 3−4 measurements with a total of 223 velocities. A typical velocity error per measurement is ~3 km s^{-1}. The stars in our sample are spatially distributed from the cluster center out to 10 arcminutes in radius ($4.5r_c$). Among these 65 stars, we discovered 5 spectroscopic binary candidates; and one of these five candidates was discovered as a binary previously by Pryor et al. (1991).

Using a Monte-Carlo simulation method, we estimated the fraction of binary systems which may have been missed from our detection due to unfavourable orbital configurations. With our survey, the binary discovery efficiency is 30% for systems with 4 d $\leq$ P $\leq$ 10 yr, 0.125 $\leq$ q $\leq$ 1.75 and eccentric orbits (0 $\leq$ e $\leq$ 1). This yields a binary frequency of 26%. In the case of circular orbits, the estimated binary frequency is ~24%. The discovery efficiency is higher for binaries with higher mass ratios of 0.3 $\leq$ q $\leq$ 1.75. It reaches 35% and 37% respectively for circular and eccentric orbits. The corresponding binary frequency is 22% and 21%.

* Adapted from a paper entitled "A Spectroscopic Survey for Binary Stars in the Globular Cluster NGC 5053," by L. Yan and J.G. Cohen, submitted to the Astronomical Journal.

The calculations for the binary frequency were also made with an alternative period distribution — the "flat" logarithmic period distribution. Because this type of period distribution produces more short period systems, the resulted binary discovery frequency is higher, 36% for binaries with 4 d $\leq$ P $\leq$ 10 yr, 0.125 $\leq$ q $\leq$ 1.75. The inferred binary frequency is thus 19% and 21% for circular and eccentric orbits respectively.

We also applied Kolmogorov-Smirnov (K-S) tests to the cumulative distributions of maximum velocity variations from the actual measurements and the synthetic velocity data. The results from these tests are consistent with 19−26% binary population with 4 d $\leq$ P $\leq$ 10 yr, 0.125 $\leq$ q $\leq$ 1.75 in NGC 5053. The hypothesis of a binary frequency in NGC 5053 higher than 50% is rejected with a confidence level higher than 90%. The binary frequency in NGC 5053 derived from our survey is somewhat higher than estimates for other clusters by various surveys. This is perhaps related to the fact that NGC 5053 is relatively dynamically young compared to these clusters. We also argue that the binary population in globular clusters is not significantly deficient compared to binaries in other stellar environments such as open clusters, or to field and low metallicity halo stars.

2.1. Introduction

Recently it has been realized that a primordial binary frequency as small as 3% can fundamentally change the dynamical evolution of an entire globular cluster (Heggie & Aarseth 1992). Mass segregation caused by two body relaxation in a cluster essentially transfers "heat" (stellar kinetic energy) from the cluster core to the "cooling" edges, while simultaneously pushing the cluster towards higher central concentration (*gravothermal collapse*). The process of gravothermal collapse can be greatly modified by a binary star population (Gao *et al.* 1991; Heggie & Aarseth 1992; McMillan & Hut 1994; Vesperini & Chernoff 1994). Gravitational binding energy in binary stars can be extracted and converted into kinetic energy during encounters with other stars. The extracted energy can supply a central heat source to stave off or reverse gravothermal collapse.

There is considerable observational evidence that binary stars do exist in globular clusters (see the detailed review by Hut *et al.* 1992). Indisputable evidence came from the discovery of long period binary millisecond pulsars in low density globular clusters during the late 80's and the early 90's. Among a total of ~40 millisecond pulsars in globular clusters, ~12 of them are actually in binary systems. Furthermore, two of these binary millisecond pulsars —discovered in the *low density clusters* M 4 and M 53— have *periods as long as 200–300 days* (McKenna *et al.* 1988; Kulkarni *et al.* 1991). Binaries with such long periods cannot be formed through single star-star tidal capture. They have to be formed by star-binary and binary-binary encounters, or their progenitors are primordial binary stars.

Recent direct searches for spectroscopic and short period eclipsing binaries have discovered many binary systems and binary candidates in globular clusters (Pryor *et al.* 1992; Côte *et al.* 1994; Mateo *et al.* 1990; Yan & Mateo 1994; Yan & Reid 1995). These heroic efforts have been focused on obtaining a better understanding of binary star populations in globular clusters. One of the drivers behind these efforts is to understand many apparently different phenomena in globular clusters which may be

intimately related to binary star population. For example, such phenomena include blue stragglers, colour/stellar gradient in the cores of post-core-collapsed clusters (Djorgovski & King 1986), X-ray sources and numerous "recycled" radio pulsars (Phinney 1992; Phinney 1995). The discovery of short period eclipsing binaries among both blue straggler stars and main sequence stars (Mateo *et al.* 1990; Kaluzny and Krzeminski 1993; Yan & Mateo 1994; Yan & Reid 1995) suggests that the short period binaries may be the progenitors of blue stragglers. Mass transfer/merger among stars in binary systems and stellar encounters involving binary stars are important processes for the formation of blue stragglers. Also, numerous X-ray sources and radio pulsars in globular clusters can be easily explained in terms of binary systems containing degenerate stars.

While mounting evidence, direct or indirect, has suggested the existence of both short and long period binary stars in globular clusters, the binary frequency and binary period distributions are very poorly determined. This has been the major source of uncertainty in the theoretical modeling of globular clusters. The study of binary stars in globular clusters suffers two fundamental limitations: technical limitations and the intrinsic difficulties of the problem itself. For binaries with periods in the range of 10 days to 10 years, the only way to determine the binary frequency is to systematically measure radial velocity variations in individual stars of a globular cluster. Technically, only recently with the advent of high resolution multi-object spectrographs on 4-meter class telescopes did it become possible for the first time to sample a large number of stars and to obtain multi-epoch observations with a reasonable amount of telescope time. With telescopes smaller than the Keck 10-meter telescope, we are limited to bright red giants and subgiants even in the closest globular cluster. These bright low metallicity giant stars have smaller masses and larger radii compared to the field G-type stars. Consequently, a binary system containing such a bright giant star is difficult to detect since the system tends to have a long period and small radial velocity variations. To demonstrate this effect,

we plotted stellar radius versus absolute visual magnitude (Figure 1(a)). The calculations were done using red giant branch models of Bergbusch & VandenBerg (1992) with [Fe/H] $= -2.26$, [O/Fe] $= 0.75$, and an age of 15 Gyr. The same calculations done with the Revised Yale Isochrones (Green, Demarque & King 1987) are in very good agreement with Bergbusch & VandenBerg model. In Figure 1(a), the solid lines are calculated for three different metallicities from the models, the solid triangles represent the stars in our sample with the adopted distance modulus $(m-M)_{V0}$ of 16.08 magnitude and $E(B-V)$ reddening correction of 0.06 mag (Fahlman, Richer & Nemec 1991). Also shown in the figure with the hollow squares are empirical radii for giants in the clusters M 92 found by Cohen, Frogel and Persson (1978) based on broad-band infrared photometry and narrow-band CO and H_2O indices. The globular cluster M 92 has a metallicity [Fe/H] of -2.2, very similar to NGC 5053. In the Zinn & West compilation, NGC 5053 was listed as a very metal-poor cluster with [Fe/H] of -2.58 measured by Bell & Gustafsson (1983). More recent measurements by Sunzteff, Kraft & Kinman (1988) yielded a mean metallicity of [Fe/H] $= -2.2$.

As shown in Figure 1(a) the radii of red giants in a globular cluster brighter than the cluster Horizontal Branch (around M_V of 0.0) are rising rapidly as a function of luminosity, and at the same luminosity the giant stars with higher metallicity are also larger in size. The size of the giant star in a binary system sets the minimum period which the binary star could possibly have. Figure 1(b) shows the minimum period of a binary system without mass transfer as a function of the absolute magnitude of the primary star. Here for simplicity we only consider binary stars with edge-on circular orbits, in which the primary star mass M_1 was estimated from the catalog of the Revised Yale Isochrones (Green *et al.* 1987) and the secondary mass M_2 was assumed to be $0.5M_\odot$. For such a binary system, the minimum semi-major axis is set by the critical Roche lobe radius $R\frac{0.6q^{2/3}+\ln(1+q^{1/3})}{0.49q^{2/3}}$ (Pringle 1984), where R is the stellar radius of the primary star, and $q = M_2/M_1$ is the mass ratio of the binary system. Similarly, Figure 1(c) is the plot of the peak-to-peak radial velocity

variation (the maximum velocity variation in a full orbit) versus the luminosity of the primary star.

All of the existing radial velocity surveys of binary stars in globular clusters generally were done among the bright giant stars (Gunn & Griffin 1979; Pryor, Latham & Hazen 1988; Côte *et al.* 1994). The first radial velocity survey with the high precision was done by Gunn & Griffin (1979) in the globular cluster M 3. They obtained a total of 85 velocity measurements for 33 giant stars with V magnitudes 12−14 (which corresponds to the reddening corrected absolute visual magnitude of ~ -3.0 and -1.0 respectively). They failed to find any binary candidates among the non-pulsating stars and concluded that binaries with separations between 0.3−10 AU (periods between 0.1 years and 30 years) were much rarer in globular clusters than in the field Population I. In 1988, combining Gunn & Griffin's data in M 3, Pryor et al. produced a larger dataset containing 111 giant stars, each with 3 multiple measurements. They found one binary candidate, which later was confirmed as a system with a period of 7.3 years. Recently, Côte et al. (1994) published a similar survey in the globular cluster NGC 3201. A total of 786 velocities were obtained for 276 giant stars with V magnitudes of 11.0−16.5 over a total timespan of 6 years. They found 2 good binary candidates, plus 13 possible candidates. The derived binary frequency from both surveys is roughly 6% − 18% for systems with 0.1 yrs $\leq P \leq$ 10 yrs and $0.1 \leq q \leq 1.0$ depending on orbital eccentricities.

The bright giant stars in these surveys have large radii of 0.1−0.5 AU, which imposes the minimum period of detectable binaries around 0.1 years as indicated in Figures 1(a)−(c). In the case of the edge-on circular orbit, a binary containing $0.8M_{\odot}$ and $0.5M_{\odot}$ stars will have a minimum separation of 0.25 AU, a minumum period of 40 days and a maximum radial velocity change of 52 km/s for the more massive star. Thus, large velocity variations are generally not expected in the surveys for binary stars among bright giants ($M_v \leq 0$ mag) in globular clusters. Even though peak-to-peak velocity variations up to 50 km/s are allowed, the chance of selecting a

star with a high velocity orbit at a high inclination angle and observing it at phases giving large velocity differences is small. High precision velocity measurement ($\sim$ 1 km s^{-1}) is required for the surveys among giants as bright as 13−15 magnitude.

With the advent of the Norris Multi-fiber Spectrograph on the 200 inch telescope at the Palomar observatory, we carried out a radial velocity survey for spectroscopic binary stars in the globular cluster NGC 5053. Our survey was designed to reach much fainter stars than previous surveys. It is thus sensitive to binary systems with much shorter periods, and much larger radial velocity variations. The object sample in our survey consists of 76 cluster member giant and subgiant stars in the globular cluster NGC 5053 with visual magnitudes in the range of 14.2−18.6. We have obtained 6 epochs of observations of these 76 stars in a total timespan of 3 years.

The globular cluster NGC 5053 is an ultra-low density cluster with a half-mass relaxation timescale of $\sim$ 8 Gyr (Djorgovski 1992), comparable to the Hubble timescale. This suggests that NGC 5053 is barely dynamically relaxed, and the spatial distribution of its primordial binary population has not been significantly altered by two-body relaxation processes. Moreover, the long relaxation timescale indicates that in this cluster the binary destruction by star-binary and binary-binary encounters is not important. However, one disadvantage imposed on our survey is that NGC 5053 is a very metal poor cluster with [Fe/H] of −2.2, and thus the spectra from its stars have weaker metal absorption lines than metal rich objects.

In 1991, Pryor, Schommer & Olszewski reported preliminary results of a search for binary stars among 28 giant stars with visual magnitudes of 12−15.5 in the same cluster NGC 5053. They found 3 good binary candidates, with one candidate (star 5) having an estimated period of 0.8 years (Pryor, Schommer & Olszewski 1991). Our survey samples more than twice as many stars as in the Pryor et al. survey and goes almost 3 magnitude fainter. As shown in Figures 1(a)−(c), our survey is sensitive to binary systems with periods as short as 4 days. A maximum radial velocity variation

as large as 116 km s^{-1} is possible for a binary on an edge-on circular orbit with M_1 and M_2 of $0.8M_\odot$ and $0.5M_\odot$ respectively. Our velocity measurement error varies from star to star, but typically is about 3 km s^{-1}, which is somewhat worse than in previous surveys. (We discuss in detail the velocity measurement errors and related problems in §2.2.2.) However, the smaller radii of the stars in our sample compensates for this disadvantage. In addition, our sample stars are less luminous and don't have radial velocity variations on a scale of 8 kms^{-1} caused by intrinsic atmospheric motions found among bright giant stars by previous surveys (Gunn & Griffin 1979; Lupton, Gunn & Griffin 1987; Pryor *et al.* 1987).

2.2. The Survey

2.2.1. Observations

All of the observations were made with the Norris Multi-fiber Spectrograph on the Hale 5.0m telescope at the Palomar observatory. The Norris Spectrograph is a fiber-fed multi-object spectrograph which is mounted at the Cassagrin focal plan of the telescope (Hamilton *et al.* 1993). It has a total of 176 fibers, and each fiber has a 1.6 arcsecond diameter aperture. The small diameter of the fiber aperture implies that the effective throughput of the spectrograph is very sensitive to seeing conditions, especially for stellar objects, as in our case. The fibers are located in two opposing banks of equal number. The minimum separation between two fibers is $\sim$ 16 arcsecond, which is the major limitation for sampling more stars in globular clusters. The spectrograph covers a field of view of 20×20 square arcminutes. Figure 2 shows the layout of the fiber stage.

A fiber-fed multi-object spectrograph has several advantages for doing radial velocity surveys. First it allows us to sample a large number of objects within a confined field such as globular clusters and clusters of galaxies. Second fibers have the characteristic of scrambling the input image resulting in a more stable illumination

of the spectrograph and detector, which produces more stable and accurate radial velocity measurements than can be obtained using standard slit observing techniques (Barden *et al.* 1991).

We obtained a total of 6 epochs of observations of a sample of 76 cluster member stars with a total timespan of 3 years. The summary of all observations is tabulated in Table 1. The first four epochs of observations in 1992 and 1993 were taken with a 1024×1024 pixels CCD and the field of view of 10×10 square arcminutes. The last two epochs of observations in 1994 were taken with a more sensitive and larger CCD with 2048x2048 pixels. These observations therefore had wider wavelength coverage and sampled more stars. Thus some of the stars in our sample have more velocity measurements than others. Also notice that the total exposure time for the primary field in NGC 5053 varies from one epoch to another due to changes in the amount of available observing time and the observing conditions. For some epochs, we could not obtain any observations for the second field in the same cluster. This is one of the causes for the variations of velocity measurement errors for the same star at different epochs.

During all observations, we used a 1200 grove/mm grating centered around 5000 Å. The resulting spectral scale is $\sim$ 0.65 Å/pixel, corresponding to the velocity scale of $\sim$39 km s^{-1}pixel^{-1}. The spectral resolution of the observations is around 2.5−3 Å. With a cross correlation technique, we should be able to measure any velocity shift larger than one-tenth of a pixel, *i.e.*, 4 km s^{-1}. The poor resolution in the April 1994 observing run was due to bad collimator focus caused by a mechanical problem in the spectrograph.

To make accurate velocity measurements, in all our observations we took comparison arc Thorium-Argon spectra both before and after each object exposure to calibrate out any spectrograph flexure. Dome flats were taken immediately after each setup to flatfield the object spectra. We also obtained some exposures of the twilight sky to check the spectrograph velocity zero point shifts between different

nights and also between different observing runs. Depending on the observing conditions and the amount of time we had during each run, we observed at least the primary field and sometimes the secondary field in NGC 5053. Since it is relative velocity variations which we need to measure accurately in the search for spectroscopic binaries, we chose about 10 giant stars brighter than 12 magnitude in the globular cluster M 13 to serve as the velocity standards. These giant stars were chosen from the sample in the radial velocity survey by Lupton, Gunn & Griffin (1987). The typical velocity error in their survey is $\sim$1 km s^{-1}. One advantage of using these stars is that we were able to obtain all their spectra with a single exposure with the Norris Multifiber spectrogragh.

2.2.2. Object Sample

2.2.2.1. Astrometry

Our object sample contains a total of 93 stars with apparent visual magnitudes of 14.2–18.6. Of all sample stars, 76 are cluster member stars and 17 are non-members of the cluster determined from their radial velocity measurements. The small diameter of the fiber aperture on the Norris Multi-fiber spectrograph requires all program objects to have the absolute astrometry accurate to 0.3″. We obtained a mosaic of overlapping images of NGC 5053 with the COSMIC camera mounted at the prime focus of the 5.0m Hale telescope. Each of these CCD images covers a field of view of 10×10 square arcminutes. The basic geometric transformation for obtaining equatorial coordinates from CCD images is the Gnomonic projection (Taff 1981), which serves to project a portion of the celestial sphere onto a tangential plane. This projection transforms an equatorial coordinate (α, δ) to a rectangular coordinate (ξ, η) with the tangent point defined as its zero point. The second transformation is to relate the rectangular coordinate (ξ, η) to the rectangular coordinate (x, y)

measured from a CCD image. Gnomonic projection from (α, δ) to (ξ, η) is well described by the following set of equations.

$$\xi = \frac{\cos\delta \sin(\alpha - \alpha_0)}{\sin\delta \sin\delta_0 + \cos\delta \cos\delta_0 \cos(\alpha - \alpha_0)} \tag{2.1}$$

$$\eta = \frac{\sin\delta \cos\delta_0 - \cos\delta \sin\delta_0 \cos(\alpha - \alpha_0)}{\sin\delta \sin\delta_0 + \cos\delta \cos\delta_0 \cos(\alpha - \alpha_0)} \tag{2.2}$$

Here (α_0, δ_0) is the equatorial coordinate of the tangent point. The second transformation which relates (ξ, η) to the measurable coordinate (x,y) is characterized by the following matrix **A**.

$$\begin{pmatrix} \xi \\ \eta \end{pmatrix} = \begin{pmatrix} a(1) & a(2) \\ a(3) & a(4) \end{pmatrix} \begin{pmatrix} x \\ y \end{pmatrix} + \begin{pmatrix} a(5) \\ a(6) \end{pmatrix} \tag{2.3}$$

Among the six coefficients, a(1) and a(3) represent the scales of CCD images in x & y directions in units of arcsecond per pixel, a(2) and a(4) the rotational angle, and a(5) and a(6) are the offsets between the CCD center and the tangent point in the (ξ, η) plane.

A set of bright stars in CCD images were selected as the reference stars for deriving the transformation matrix **A**. The equatorial coordinates of these reference stars were obtained from *HST Guide Star Catalog*, and the errors in these coordinates are the major source of the inaccuracy in the equatorial coordinates derived for the objects in our survey. Unfortunately, the equatorial positional errors are not well determined in the present version of *HST Guide Star Catalog.* It is not clear how large the position error is on the scale of 20 by 20 square arcminutes. We compared the coordinates (α, δ) of stars in the open cluster M 35 from *HST Guide Star Catalog* with the (α, δ) measured by K. Cudworth (Cudworth 1995 personal communication). The average difference in RA and DEC between the two sets of coordinates are $-0.135''$ and $-0.178''$ with corresponding standard deviations of $0.278''$ and $0.25''$ respectively. In addition, no systematic rotation was found between the two sets of coordinates. Using the computer simulations, we estimated the errors in the derived equatorial coordinates caused by random errors in RA and DEC of the reference

stars. We concluded that the positional errors for stars in our survey sample are less than $0.3''$ if the errors in the equatorial coordinates of the reference stars are random distributed and have 1σ standard deviation less than $0.3''$.

In our astrometry calculation, we did not include the effect of differential refraction across the field of view of 20×20 square arcminutes. Under normal temperature conditions and the pressure of 760 mmHg, the refraction is $R = 58''.3 \tan z - 0''.067 \tan^3 z$, here z is the zenith distance (Allen 1973). From the above equation, the differential refraction is small, especially with small zenith angles. As the 200 inch telescope does not have an atmospheric dispersion compensation system, the Norris Spectrograph is limited to small zenith angles if the majority of the light is to go into the aperture with a small diameter of $1.6''$. The cause of such a limitation is the atmospheric dispersion, i.e., the atmophere refraction index varies as a function of wavelength and thus the refraction of the light at different wavelength is different: $\Delta R = -\tan z \times \delta(n)$, here $\delta(n)$ is the index change between two wavelength (Schroeder 1987). In the wavelength range of 4700−5800Å, the atmospheric refraction is less than $0.3''$ for zenith angle less than 45°; however, for zenith angle larger than 60°, the difference between the atmospheric refraction at 4700Å and 5800Å is larger than $0.6''$ (Cohen & Cromer 1988; Hamilton 1993).

2.2.2.2. Photometry

The selection of stars in our sample is limited by two factors: one is the minimium separation of the two fibers (which is $\sim 16''$), and another is the luminosity limit imposed by the spectrograph sensitivity. The brightness of stars in our sample ranges from V magnitude of 14.2 to 18.6. We have used the colour-magnitude diagram published by Sandage, Katem and Johnson (1977) (thereafter SKJ) to guide us for selecting cluster member stars brighter than V magnitude of 17.3. Unfortunately, for stars fainter than that we had to make our selections without the cluster

HR diagram. This led to some non-members of the cluster being included in our sample.

The photometry of the objects in our sample was obtained from B and V CCD images taken at the Palomar 60 inch telescope. Unfortunately, the data were all taken during non-photometric conditions. Thus, we had to calibrate our data using the photoelectric and photographic photometry reported by SKJ. Figure 3(a) is the colour-magnitude diagram of stars brighter than the main sequence turnoff in the cluster NGC 5053. The solid triangles in the figure represent the sample stars in our spectroscopic survey. The cluster main sequence and the turnoff are more clearly shown in Figure 3(b) (Fahlman *et al.* 1991).

2.2.3. Data Reduction

Our data were reduced using IRAF.[1] After the images were trimmed and corrected for bias, all of the object spectra including sky were identified, traced and extracted using APALL task in the IRAF package SPECRED. An optimal extraction algorithm was used to produce one-dimensional spectra for all stars. The dome-flat spectra from all fibers were extracted and averaged. A lower order polynomial was used to fit the averaged dome-flat spectrum. The flatfield spectra were obtained by normalizing all dome-flat spectra with the single fitted spectrum. The CCD sensitivity variations at small scales in all object spectra were taken out by dividing them with the corresponding flatfield spectra.

Figures 4(a) and 4(b) show spectra of the same star with a typical signal-to-noise ratio taken in 1992 and 1994 respectively. The spectra taken in 1994 have the wavelength coverage of 4700Å−5800Å, and consequently include very strong sky emission lines such as [OI] 5577Å, HgI 5461Å, the Hg doublet 5770, 5791ÅÅ, and the

[1] IRAF is distributed by the National Optical Astronomy Observatories, which are operated by the Association of Universities for Research in Astronomy, Inc., under contract to the National Science Foundation.

NaD doublet 5893Å. To obtain good sky subtraction, we corrected the variations of throughput efficiency from fiber to fiber. The correction for each fiber was estimated by dividing the integrated flux in the sky emission line Hg 5461Å with the average flux of the same line from all fibers. The most useful absorption lines for doing radial velocity cross-correlation, H_β4861Å and the MgI triplet at 5167, 5173 and 5184Å, are outside the strong sky emission line region. Residuals of sky emission lines in the sky-subtracted spectra do not have a big effect on the velocity measurement. In the cases of large residuals from the sky subtraction, we simply mask off the regions with sky lines. Throughput correction was not necessary for spectra taken in 1992 since there are not many strong sky emission lines in the range of 4710Å−5300Å. Figure 4(c) shows the spectrum of the radial velocity standard II-76 in the globular cluster M 13.

Wavelength calibrations were done with the Thorium-Argon comparison spectra taken before and after each object exposure with the same fiber setup as was used for the cluster observations. The spectrum of Thorium-Argon has a large number of lines in the wavelength range of 4700 Å to 5800 Å. At a spectral resolution of 2−3 Å, many lines are blended. Using the CCD Atlas of Thorium-Argon Hollow Cathode Comparison Spectra (NOAO 1987) taken with a high resolution echelle spectrograph, we identified 20 to 27 strong and isolated features usable for wavelength calibrations. All wavelength calibrations were consequently done only with this set of isolated lines. Typically, we used 3rd order polynomial fitting and obtained an rms error in the dispersion solution less than 0.04 Å, which corresponds to a velocity error of less than 2 kms^{-1}. Each star spectrum was wavelength calibrated with its own comparison arc spectra which were taken through the same fiber before and after the star exposure. To make sure spectra taken through different fibers and in different nights have the same wavelength scale, we cross-correlated every wavelength calibrated thorium-argon spectrum against all the other Th-Ar spectra. With care in the calibration procedure, we were able to keep the relative shift between all Thorium-Argon spectra under 2 kms^{-1}.

The object spectra were dispersion corrected and binned into linear logarithmic scale. Radial velocities for all stars in the sample were obtained with a cross-correlation technique (Tonry & Davis 1979). Each object spectrum was cross-correlated with the template spectra of radial velocity standards. We used the task FXCOR in RV package of IRAF to obtain radial velocity measurements. The basic idea of the cross-correlation procedure FXCOR is as follows. The input spectra, both the object and the template, were continuum subtracted using a 3rd-order polynomial fit. An endmasking of 10% from each end of the spectrum by multiplication with a cosine bell removed the discontinuity between the beginning and end of the spectra. The spectra were then transformed into Fourier space. A ramp filter (cutting on at 10 wavenumbers, reaching full value at 20, beginning to cut off at 256 and reaching zero at 512) was applied to both object and template spectra to filter out high frequencies (which are just noise in the spectra) and low frequencies (which represent the large scale fluctuations of the spectra after continuum subtraction). After two spectra were cross-correlated, we used a Gaussian function to fit the cross-correlation peak. The points used in fitting are weighted by a power of the distance from the center as weight = 1 - $(\frac{\text{distance}}{0.5\text{width}})^x$ with $x = 1$ for all cross-correlations.

2.2.4. Radial Velocities

We have obtained a total of 234 new radial velocities for 76 cluster member giant and subgiant stars in the globular cluster NGC 5053. Of the 76 cluster member stars, 65 stars have multiple radial velocity measurements and are suitable for the binary search study. Therefore, we will concentrate only on these 65 stars with a total of 223 radial velocity measurements. Table 2 lists photometry, astrometry and 223 radial velocities for all 65 stars in NGC 5053. The columns record, from left to right, the star's identification names, right ascension and declination in the epoch of 1950.0, the radial distance from the cluster center in arcseconds, the heliocentric Julian date (plus 244000 in days) of the observation, the heliocentric radial velocity

at the date and its corresponding uncertainty in kms^{-1}, the total number of observations, the weighted mean radial velocity and the external velocity error in a single measurment estimated from the dispersion about the mean, the chi-square for the observations and the probability of obtaining a chi-square at least this large purely due to measurement errors. The final two columns give the star's magnitude and (B − V) colour. To distinguish the stars originally identified in the SKJ paper from the new stars we selected, we combined the same names SKJ used with the prefix S.

The chi-square for the combined set of velocities and the weighted mean were calculated as follows:

$$\chi^2 = \sum_{i=1}^{n} \frac{(v_i - \bar{v})^2}{\sigma_i^2}, \qquad \bar{v} = \frac{\sum(v_i/\sigma_i^2)}{\sum 1/\sigma_i^2}$$

where σ_i is the internal estimate of radial velocity error, and χ^2 represents the radial velocity variability over the timespan of three years. The second and any subsequent lines under each object report the radial velocities and the internal errors at the corresponding heliocentric Julian dates. To evaluate the significance of the velocity variations represented by χ^2 for a set of radial velocity measurements, we calculated the probability of having a χ^2 at least this large purely due to chance fluctuations with a Gamma function $Q(0.5\nu,\ 0.5\chi^2)$, here ν is the number of the degree of freedom. Reasonable limits of χ^2 probability for identifying significant variations are 0.01− 0.001. One underlying assumption with these calculations is that the velocity measurement errors are normally distributed.

Making a realistic estimate of the internal error for each radial velocity measurement is crucial for identifying the radial velocity variables. As shown in Table 1, we usually took multiple exposures of the same set of stars in a single observing run, which consisted of 2 or 3 nights. For the majority of stars in our sample, the spectra from a single exposure yield enough signal for measuring the radial velocities using cross-correlation. These stars have several repeated velocity measurements at each epoch. The internal errors of the mean radial velocities at each epoch for these

stars were represented simply by the dispersion around the mean. However, for some stars the spectra from a single 3000 second exposure are too noisy to be usable for measuring radial velocities. Summation of all exposures within a single observing run is required to measure velocities for these stars.

One underlying problem in the above procedure is that it works fine for almost all types of potential binaries in our sample *except* binaries with periods of a few days. As discussed in section §2.1 (Figure 1), the shortest period for a binary allowed by the sizes of stars in our sample is $\sim$4 days. In the case of an edge-on circular orbit with $M_1 = 0.8M_\odot, M_2 = 0.5M_\odot$, the expected peak-to-peak radial velocity variation is $\sim$113 km s^{-1}. Obviously the binaries with such orbital configuration can be easily identified by inspecting the velocities measured during the same observing run. We found one binary candidate ST with radial velocity (individual measurements) variations larger than 30 km s^{-1} over two days. This star is a strong candidate for a short period spectroscopic binary (see §2.3.1 for detailed discussion of this system). This implies that in our sample all potential binaries except star ST are not systems with periods of a few days and near edge-on orbits. However, the binaries with periods of a few days and *near face-on* orbits will not show large radial velocity variations during a single observing run. Summation of spectra will smear out velocity variations of this type of binaries and we cannot distinguish them from single stars. The problem is partly inherent for this type of binaries, and partly due to the noisy spectra of the faint stars in our survey. Fortunately, the probability of having this particular type of binaries in our sample is very small ($\leq \sim 2\%$). The final result of the survey should not be significantly affected by this limitation.

The internal velocity errors are estimated from the repeated measurements for a large fraction of the stars in our sample. However, a small fraction of the stars have only one measurement per epoch. The velocity errors for these stars can be

evaluated as follows. The quality of a cross-correlation can be characterized by a quantity R (Tonry & Davis 1979):

$$R = \frac{H}{\sqrt{2}\sigma_{cc}} \tag{2.4}$$

Here σ_{cc} is the antisymmetric noise of the cross correlation function and the H is the height of a cross correlation peak. It is obvious from the definition that the larger R is, the more accurate the velocity is. The value of R reflects the signal-to-noise ratio of the object spectrum as well as how well the object spectrum matches with the template spectrum. With this definition of R, the internal error is calculated as

$$\sigma = \frac{\sigma_0}{1+R} \tag{2.5}$$

Here σ_0 is a constant which can be calculated from the theoretical formula (Tonry & Davis 1979). A better way is to estimate σ_0 from our data.

There are two kinds of errors which contribute to the uncertainty of the velocity change. One is systematic errors such as the residual of the spectrograph flexure correction, bad collimator focus and the errors of the wavelength calibration. The second is the photon statistics errors, which can be described by the Tonry and Davis error σ in equation (2.5). For those stars with very high signal spectra, the first kind of error should be the dominant one, which can be characterized by the repeatibility error. The photon statistics error will be the dominant one for those stars with low to median signals. Almost all of the spectra in our sample have moderate signal-to-noise ratio, except two very bright stars S36 and S72 which were excluded from the calculation of σ_0 below. To estimate σ_0, we used two methods. One is to take the velocity difference Δv between each pair of velocities for those stars with multiple measurements. Then

$$\sigma_0 = \frac{\Delta v}{[(1+R_1)^{-2} + (1+R_2)^{-2}]^{1/2}} \tag{2.6}$$

Here R_1 and R_2 are the Tonry & Davis values for velocity v_1 and v_2 respectively. If velocity errors have a Gaussian distribution, σ_0 is equal to the standard deviation

of a normal distribution produced by the equation (2.6). The second method is to calculate the weighted mean velocity for each star with multiple velocities. Then for the given velocity measurement v_i, we can compute the velocity difference Δv, and σ_0 is

$$\sigma_0 = \frac{(v_i - \bar{v})}{[(1+R_i)^{-2} + (\sum(1+R_i)^{-2}]^{1/2}}. \tag{2.7}$$

Figure 5 shows the σ_0 distribution calculated with the equation (2.6). It is roughly gaussian and the standard deviation σ_0 is 44.7 kms^{-1} for the April 1992 observation. For all observed objects, Figure 6 is the plot of the internal velocity error versus R of each velocity measurement. A separate σ_0 was estimated for each observing run. With the derived σ_0, we got a total χ^2 of 185.1 for 196 degrees of freedom for all velocities in our sample excluding non-members and potential variables. The probability of a χ^2 larger than this is 0.68, which is acceptable.

As tabulated in Table 2, the velocity error of a single measurement varies substantially from star to star. A typical value is ~3 km s^{-1}, but the worst is as large as 10 km s^{-1}. This is partly due to the instrinsic luminosity differences between stars in our sample, and partly because some stars were observed more frequently than others. In addition, the accuracy of fiber positioning is different from star to star and from one observing run to another. With non-uniform velocity measurement errors, it is dangerous to use only the velocity variations between different epochs to represent the true velocity variabilities due to orbital motion of binary stars. The more effective way of selecting binary candidates is to calculate χ^2 of all velocity measurements and the probability of obtaining a χ^2 value larger than that observed by chance.

The velocity zero-point shifts between different epochs were examined by cross-correlating spectra of bright stars in M 13. The twilight spectra taken in several epochs were also used to estimate the velocity zero-point shifts. We didn't find any significant velocity zero-point shifts between different epochs.

2.3. Results

2.3.1. Spectroscopic Binary Candidates

Using the criterion that a binary candidate must have a velocity χ^2 such that the probability of obtaining a χ^2 larger than this value by chance is less than 0.01, we identified 5 spectroscopic binary candidates among a sample of 65 cluster member stars. The χ^2 probabilities of these five binary candidates indicate that their radial velocity variations are significant over the timespan of 3 years. Of these 5 binary candidates, one star S5 was previously found as a binary candidate in the Pryor et al. survey (1991). Figure 7 is a cluster colour-magnitude diagram, in which the solid triangles represent the five binary candidates discovered by our survey and the hollow circles show the three brighter binary candidates discovered in the Pryor et al. (1991) survey. Notice that one binary candidate in Pryor et al.'s survey may be a field star according to its location in the cluster colour-magnitude diagram. Figures 8(a)−(d) are the detailed finding charts of the 5 binary candidates.

The velocities tabulated in Table 2 are the radial velocities of stars in NGC5053 relative to star II-76 in M 13. The globular clusters M 13 and NGC 5053 have cluster systematic velocities of about -246.4 km s^{-1} and 43 kms^{-1} respectively (Pryor & Meylan 1993). Figure 9 shows the histogram of all relative velocities tabulated in Table 2 including non-cluster member velocities. With only cluster members and excluding the variable stars, the mean relative velocity is 291.0 kms^{-1} and the standard deviation is 3.7 kms^{-1}.

In addition, we discovered one strong short period spectroscopic binary, star ST. Table 3 shows the radial velocities obtained for this star over three years. The internal velocity error for each measurement was estimated using the Davis & Tonry parameter R as described in §2.2.4. Over two days star ST has a velocity variation as large as 45 kms^{-1}. In fact, the absorption lines from this star are broader than these from the standard star. Together with the large velocity variations, this suggests

that star ST is a short period spectroscopic binary. The star is 318.1″ away from the cluster center and located in a isolated environment as shown in the finding chart (Figure 10). In the cluster colour-magnitude diagram (Figure 7) the solid square represents star ST, whose (B-V) colour and V magnitude are fairly consistent with those of the cluster member stars.

To determine if star ST is a cluster member, we measured the absorption line strength for the Mgλ5177 triplet, which is defined as the equivalent width in the range of 5162.00−5193.25Å (Faber *et al.* 1985). As described in detailed studies by Faber et al. (1985) and Gorgas et al. (1993), the Mgλ5177 line strength is determined by the metallicity, the effective temperature and the surface gravity. Figure 11(a) is taken from Gorgas et al. (1993). It shows the equivalent width measured in the range of 5162.00−5193.25Å versus the (V-K) colour, and the different symbols represent field K giants, G dwarfs, stars from very metal poor and metal rich globular clusters and stars from various open clusters, as explained in the figure. It is clearly shown that most stars in metal poor globular clusters have much weaker Mgb lines than field K giant and G dwarfs as well as stars in metal rich globular clusters and open clusters. We should point out here that NGC 5053 and M 92 have similar metallicities. For all stars in our sample including non-cluster members, we constructed a similar plot of the Mgλ5177 equivalent width versus the (B - V) colour, as shown in Figure 11(b). The solid dots in the figure are non-cluster member stars identified from their radial velocities, the crosses are the cluster stars in our sample and the open circle represents star ST. Thus we concluded that star ST is probably a dwarf which doesn't belong to the cluster NGC 5053. It is definitely a strong candidate for a short period spectroscopic binary system. In the following analyses of the binary frequency in NGC 5053, we did not include this star.

2.3.2. Modeling the Binary Frequency[2]

In any spectroscopic survey for binary stars, the probability of detecting a binary depends not only on the binary frequency, but also on a set of unknown binary orbital parameters such as period, eccentricity, mass ratio, orbital phase and inclination angle of the binary system. Unfavourable binary orbital configurations would cause a fraction of binary systems to be missing from our detection sample. Thus, to properly interpret the measurements in our survey, we use Monte-Carlo simulation methods to generate a large number of simulated radial velocity data sets and compare them with the measured radial velocities. A simple straightforward method of estimating the true binary frequency is to calculate from the synthetic data sets the fraction of binaries we might have missed in our survey, and then correct the observed binary frequency. The second method is to compare the number of detected binaries in the simulated data to the number of actually detected binaries in the survey. As described in detail below, the number of binaries detected in the sythetic data depends on the assumed binary frequency. We applied the same criterion used in the survey to the sythetic data for identifying binary candidates. This criterion is that the probability of obtaining a χ^2 larger than observed by chance has to be less than 0.01.

An additional statistical method is to use a Kolmogorov-Smirnov (K-S) test to compare the cumulative distributions of maximum velocity differences for the real data to the mean distribution determined from a large number of simulated data sets. This method has been used in several surveys, such as Harris & McClure (1983), Pryor et al. (1988) and Côte et al. (1994). We will discuss in detail the applicability of this method to our data later in section §2.4.3.

[2] Here the binary frequency is defined as the ratio of the number of binary candidates to the total number of "stars," here "stars" includes both single stars and binary stars; and a binary is counted as "one star."

Because all stars in our survey sample are giants and subgiants in NGC 5053, the primaries of the binary candidates among these stars should have masses of $\sim 0.8 M_{\odot}$, which is what we assumed in our simulations.

2.3.2.1. The Binary Models

To generate synthetic radial velocities for binary systems, we used the following models. For a binary star with a mass ratio of $q = M_2/M_1$, an orbital period P, semi-major axis a, eccentricity e, the inclination i of the orbital plane to the line of sight and the orbital longitude ω, the radial velocity V_r of the primary star M_1 is (Taff 1985)

$$V_r = \frac{2\pi a M_2 \sin(i)}{(M_1 + M_2) P \sqrt{(1-e^2)}} [e\cos(\omega) + \cos(v+\omega)]; \tag{2.8}$$

here the true anomaly v is associated with the eccentricity anomaly E, and the mean anomaly $M = n(t-T)$, with $n = 2\pi/P$ by the following equations:

$$E - e\sin(E) = n(t-T) = M \tag{2.9}$$

$$\tan\left(\frac{v}{2}\right) = \left(\frac{1+e}{1-e}\right)^{1/2} \tan\left(\frac{E}{2}\right). \tag{2.10}$$

Here t is the heliocentric julian date of the actual observations, and T is the starting time, thus nT is the initial orbital phase. ω and $\cos(i)$ were randomly drawn from uniform distributions between 0 and 2π, and 0 and 1 respectively. The true anomaly v was obtained by solving Kepler's equation (2.9) numerically with a starting value of $M + e\sin M$. In this equation, the initial orbital phase was chosen randomly from 0 and 2π with a uniform distribution. The distribution functions of binary orbital parameters q, e, P were assumed to have the similar forms as what Duquennoy and Mayor (thereafter DM) (1991) have measured for dwarf-type stars in the solar neighbourhood. Of course, the orbital parameter distribution functions may be very different in globular clusters than in the field. It remains the ultimate goal for surveys such as ours to actually measure them in globular clusters. However, at the present they are the major uncertainty for the modeling of binary populations.

The DM survey found that the logarithmic period distribution for field G-dwarf type stars shown in Figure 12, can be approximately characterized as a Gaussian function

$$f(\log_{10} P) = constant \times \exp\left(\frac{-(\log_{10} P - \mu)^2}{2\sigma^2}\right)$$

where $\mu = 4.8, \sigma = 2.3$, and P is in days. Also shown in Figure 13(a) and 13(b) are the eccentricity distributions for binaries with $P \geq 1000$ days and $P_{circular} < P < 1000$ days respectively. Here the circularization period is ~ 11 days. The mass ratio distribution is shown in Figure 14, which is roughly described by

$$f(q) = constant \times \exp\left(\frac{-(q - \mu)^2}{2\sigma^2}\right)$$

and $q = M_2/M_1, \mu = 0.23, \sigma = 0.42$. The solid line in Figure 14 is the Salpeter power law mass function with the power index of -2.35 ($\xi(m) \propto m^{-2.35}$). This plot clearly indicates that G-dwarf type binaries in the solar neighbourhood have fewer systems with mass ratio q ≤ 0.4 compared to what is predicted by the Salpeter power law mass function.

Notice in Figures 12 and 14 that the period and mass ratio distribution functions were plotted over wide ranges. However, our survey is only sensitive to binary systems with periods and mass ratios within much narrower windows. All observations in our survey spread out over a total of 3 years. For a binary with a period of 10 years, an edge-on circular orbit and $M_1 = 0.8M_\odot M_2 = 0.5M_\odot$, the expected maximum velocity variation over 10 years is $\sim$16 km s^{-1}. Thus our survey is not sensitive to binaries with orbital periods longer than 10 years. As discussed in section §2.1, the shortest period for a binary allowed in our sample is ~ 4 days. Thus 4 days $\leq$ P $\leq$ 10 years is the period window to which our survey is sensitive. Similarly, our survey is not sensitive to binaries with mass ratio less than 0.125.

The effect of mass transfer was considered in our simulations by eliminating the binary system whenever the two stars get closer than the critical Roche lobe radius.

Mass transfer from the primary to the secondary would take place if the periastron distance of the binary $a(1-e)$ is equal to or less than (Pringle 1984)

$$a_{crit} = R/h(q) = R\frac{0.6q^{2/3} + \ln(1+q^{1/3})}{0.49q^{2/3}},$$

where R is the radius of the giant. Typically, $h^{-1}(q)$ is in the range of 4.5 to 2.7 for the mass ratio q of 0.125 to 1.75, as shown in Figure 15. This equation is exact for circular orbits and gives the approximate separation needed for mass transfer to occur in the case of elliptical orbits. The critical Roche lobe radius was then obtained by calculating the stellar radius of the giant star in a binary system as discussed in detail in section §2.1 (See Figure 1(a)).

If a star is on the asymptotic giant branch, then it has already evolved through the giant branch tip at some time in the past. While it was doing so, it probably experienced a more severe Roche lobe overflow constraint than its current radius would suggest. According to the standard stellar evolutionary models, 19% of the stars above the Horizontal Branch in our sample have already gone through the AGB phase. However, since in our sample fewer than 24% of the stars are above the Horizontal Branch, we ignore the effect of AGB population in our simulations.

2.3.2.2. The Binary Frequency

We discovered 5 spectroscopic binary candidates among a total of 65 cluster member stars in the globular cluster NGC 5053. To convert this discovery fraction of 0.077 to the true binary frequency f_b, we estimate the incompleteness correction using Monte-Carlo simulations. This correction is also called the binary discovery efficiency D_b, which is defined as the fraction of the "discovered" binaries in the synthetic velocity data if we assume all 65 stars as binary systems. Radial velocities of each binary were calculated using the binary models described in §2.3.2.1 at the actual observation dates. Velocity noises were drawn randomly from Gaussian distributions with the mean of zero and standard deviations of the real velocity

measurement errors. By applying the same binary identifying criterion used in the survey, we obtained the fraction of "discovered" binaries in the simulated data. Figures 16(a)−(b) show the binary discovery efficiency D_b as a function of period P in days for the binary models with circular orbits and with eccentricity distribution $f(e) = 1.5\sqrt{e}$ respectively. Notice that each data point in the plots is the mean of 1000 simulation tries. Here we assume the primary star in a binary system to have $0.8M_\odot$, and a mass ratio q in the range of 0.125 to 1.75. This implies that the secondary could be anything from a $0.1M_\odot$ low mass star to a $1.4M_\odot$ heavy neutron star. In both figures, the solid triangles and dots represent simulations with and without the effect of mass transfer respectively. It is clearly shown in the figures that the biasing of the discovered binary orbits by the size of the giants is significant at the short period end. This bias is higher for stars with brighter magnitudes, which is the major reason that the previous surveys could not detect any binary with period shorter than 40 days.

In the case of non-zero eccentricity orbits, the average binary discovery efficiency is about 30% for binaries with 4 days $\leq P \leq$ 10 years and $0.125 \leq q \leq 1.75$. For binaries with the same period and mass ratio range, the inferred true binary frequency f_b is $0.077/D_b$, i.e., 26%. In the case of circular orbits, the corresponding binary frequency for systems with periods and mass ratios in the same ranges is 24%. The discovery efficiency varies as the limits of binary period and mass ratio change. A binary with a very low mass companion is usually difficult to detect even if the period is short. For instance, the primary star in a binary with a period of 100 days shows a maximum radial velocity change of 10 km s^{-1} in the case of an edge-on circular orbit and $M_1 = 0.8M_\odot, M_2 = 0.1M_\odot$. If we choose the sensitivity limits of our survey as 4 days $\leq P \leq$ 10 years and $0.3 \leq q \leq 1.75$, the binary discovery efficiency is 35% and 37% for the binary models with non-circular and circular orbits respectively. The corresponding binary frequency f_b in the cluster is 22% and 21% respectively.

Another way of utilizing the simulated radial velocity data for estimating true binary frequency is to simply compare the number of "discovered" binaries in the synthetic data with the number of binary candidates discovered in the actual survey. A grid of models corresponding to different binary frequencies were generated for various ranges of P and q. Simulations were carried out with f_b from 0.0 to 40% in a 5% interval for four different cases: (1) $e = 0$, 4.0 d $\leq P \leq$ 10 yr and $0.125 \leq q \leq 1.75$; (2) $e \neq 0, f(e) = 1.5\sqrt{e}$, 4 d $\leq P \leq$ 10 yr and $0.125 \leq q \leq 1.75$; (3) $e = 0$, 4 d $\leq P \leq$ 10 yr and $0.3 \leq q \leq 1.75$; (4) $e \neq 0, f(e) = 1.5\sqrt{e}$, 4 d $\leq P \leq$ 10 yr and $0.3 \leq q \leq 1.75$. In Table 4, we tabulated the numbers (each number is an average of 1000 simulation tries) of "discovered" binaries with the χ^2 probability P less than 0.01 and 0.001 in the synthetic data. Here we keep the mean numbers of "discovered" binaries as real instead of integer in order to show the small differences in the four different cases. Table 4 should be compared with the actual results from our survey. From Table 2 there are a total of 5 binary candidates with χ^2 probabilities P($< \chi^2$) less than 0.01 and only 4 less than 0.001. By matching the actual results with the simulations, we indicate in the bottom line of Table 4 the likely binary frequencies in the cluster using binary selection criteria P($< \chi^2$) $\leq$ 0.01 and P($< \chi^2$) $\leq$ 0.001. For binaries with periods and mass ratios in the ranges of 4 d $\leq$ P $\leq$ 10 yr and $0.125 \leq$ q ≤ 1.75, the estimated binary frequency in NGC 5053 is close to 25%. The frequency of a binary population with $0.3 \leq$ q ≤ 1.75 is around 20−25% depending on the adopted orbital eccentricities.

2.4. Discussion

2.4.1. An Alternative Period Distribution Function in Globular Clusters

The binary frequency estimated above depends on the adopted period distribution in the simulations. An alternative period distribution, that of Abt & Levy (1976), has a constant number of binaries per unit logarithmic period interval, the

so called "flat" period distribution. The "flat" distribution produces more short period binaries and less long period ones for 4 d $\leq P \leq$10 yr than the DM period distribution. Obviously, it also gives a somewhat higher binary discovery efficiency for our survey. Specifically, with an average discovery efficiency of 36% derived from the "flat" distribution, we obtained a binary frequency of 21% for systems with 4 d $\leq P \leq$10 yr, $0.125 \leq q \leq 1.75$ and $f(e) = 1.5\sqrt{e}$. Similarly in the case of circular orbits, the inferred binary frequency is 19%. Similar to Table 4, Table 5 shows the detailed comparison between the real data and the synthetic velocity data generated with the "flat" period distribution and with four sets of orbital parameter combinations. Thus, the derived binary frequency is close to 20% for binaries with 4 d $\leq$ P $\leq$ 10 yr and $0.125 \leq$ q ≤ 1.75. This is smaller than using the DM period distribution in the simulations.

Period distributions of binaries in open clusters and among Pop. II low metallocity halo stars share perhaps more similarities with ones in globular clusters. The first published period distribution in the Hyades cluster by Griffin (1985) was approximately flat in the logarithmic period interval between 0 and 4 with period in days. Many extensive programs of studying binary stars in open clusters and among low metallicity halo stars are being carried out at the Center for Astrophysics (CfA) (Carney & Latham 1987; Latham *et al.* 1988, 1992). Although almost 200 spectroscopic binaries (Latham *et al.* 1995) with the known orbital solutions have been found in the old open cluster M 67, the period distribution has not been determined using an unbiased sample. Similarly, among low metallicity halo stars, $\sim$ 80 spectroscopic binaries have been discovered but no effort has been made to measure the halo binary period distribution. The completion of these long term surveys will shed light on the period distribution functions in clusters and among halo stars.

2.4.2. The Effect of Stellar Encounters

One effect, which we did not take into account in our calculations, is that the star-binary and binary-binary encounters can alter the shape of the primordial

distributions of binary orbital elements in globular clusters. As briefly discussed in §2.1, this effect is not significant in very low density clusters such as NGC 5053 since the cluster half-mass relaxation timescale T_{rh} is comparable to a Hubble timescale T_h. However, of the eight globular clusters in which radial velocity surveys for binary stars have been carried out by various groups (Hut *et al.* 1992), six have cluster central relaxation timescales T_{rh} much shorter than T_h of 14 Gyr. These six clusters include M 3, M 13, 47 Tuc, M 12, M 71 and NGC 3201, where T_{rh} is in the range of 10^8 to 10^9 yrs. NGC 3201 and M 71 have particularly short T_{rh} of only 300 and 100 million years in spite of their apparent low central densities.

It is a rather complicated problem to characterize quantitatively the change in the primodial period distribution due to dynamical evolution. A tremendous amount of theoretical computations have been devoted to this subject (Phinney & Sigurdsson 1991; McMillan & Hut 1994; Sigurdsson & Phinney 1995). Generally, due to mass segregation the initial binary spatial distribution is changed and binary stars are more concentrated towards the cluster core after a couple of half-mass relaxation timescales. "Soft binaries"[3] are quickly disrupted during star-binary and binary-binary encounters whereas "hard binaries" are made to have even shorter periods (Binney & Tremaine 1987). Eventually, a hard binary is destroyed by a collision with an even harder system. The detailed N-body simulations (McMillan, Hut & Makino 1991) show that binary-binary encounters are a very effective binary-destruction process. Binary-destruction starts around the time of core collapse, t_{coll}; and almost all primordial binaries are destroyed by the time of $\sim 30t_{coll}$. Here t_{coll} is several hundred of the cluster central relaxation timescale. Most binary destruction occurs within a few core radii of the cluster center. In addition, some binaries can be ejected to the outer parts of a cluster due to large recoil during binary-binary encounters

[3] Soft binaries are systems whose orbital kinetic energy is less than the kinetic energy of the cluster single stars; and hard binaries are systems whose kinetic energy is larger than the kinetic energy of the cluster single stars.

in the core. Thus, in dynamically evolved clusters such as M 71, it is perilous to assume the field period distribution since the actual number of binaries compared to the primordial number will decrease with increasing periods.

Although it is premature to draw any comprehensive conclusions about the binary frequency dependence on the dynamical properties of globular clusters, it is illuminating to compare the results from various surveys for binary stars in different globular clusters. Table 6 provides the basic statistics of eight surveys carried out in globular clusters with different dynamical properties. From Table 6 the binary discovery rate in NGC 5053 is notably higher than any other cluster. Using only his survey results in NGC 5053 and NGC 5466, Pryor (Pryor *et al.* 1991; Hut *et al.* 1992) calculated that the hypothesis that the binary frequency in NGC 5053 is as the same as that in the denser clusters can be rejected at the 85% −97% confidence level. The result of our survey appears to further support Pryor's conclusion. This is perhaps associated with the fact that NGC 5053 and NGC 5466 are dynamically young clusters, in contrast to the rest of clusters in Table 6.

2.4.3. Kolmogorov-Smirnov (K-S) Tests

Harris & McClure (1983) first pointed out that in estimating the frequency of binary populations in globular clusters, it is important to consider two effects: one is small number statistics, and another is that low metallicity giant stars have smaller masses and larger radii compared to field K giants. They compared statistically simulated radial velocity data containing 54% binary stars with the real data taken in M 3 by Gunn & Griffin (1979), and demonstrated that Gunn & Griffin's failure to detect any spectroscopic binaries among 33 giants is *not inconsistent* with the high value of binary frequency as in the field, contrary to what Gunn & Griffin previously concluded.

Subsequently, a more sophisticated and quantitative statistical method —the Kolmogorov-Smirnov test— has been employed in many surveys for binary stars in

globular clusters. K-S tests were applied to the cumulative distributions of maximum velocity difference obtained from both simulated and real data. A K-S statistic is useful for *rejecting* the null hypothesis that two data sets are drawn from the same parent distribution.

We applied K-S statistics to our measured velocities and the simulated data. Figure 17 compares the cumulative distribution of maximum velocity change from the real dataset with the distribution from the 1000 simulated datasets. In the figure, solid dots represent the actual measurements, and the solid lines from left to right indicate the simulated datasets containing binary frequency of 0%, 5%, 10%, 15%, 20%, 25%, 30%, 35% and 40% respectively. The binary model used in generating this figure has 4 d $\leq$ P $\leq$ 10 yr, 0.125 $\leq$ q $\leq$ 1.75, the eccentricity distribution of $f(e) = 1.5\sqrt{2}$ and the DM type period distribution.

To clearly present the results of K-S tests for various binary frequency f_b, in Table 7 we tabulated the confidence level at which the null hypothesis of the simulated data and real data drawn from the same distribution is accepted. K-S tests show that the binary frequency in NGC 5053 is close to 25%, and the hypothesis that the binary frequency is higher than 50% is rejected with confidence higher than 85%. However, it is noticed in Table 7 that with our data K-S tests are not effective in *rejecting* the cases with different binary frequencies. For instance, the cases with binary frequencies of 0% and 40% are rejected only at a confidence level of $\sim$ 55%. This problem results from the large errors in our velocity measurements. As described previously, the synthetic data are generated using the actual velocity errors. The corresponding cumulative distribution of maximum velocity variation is primarily controlled by a few large errors. K-S tests have been applied more effectively by Pryor et al. (1989) and Côte et al. (1994) to their data with the radial velocity errors as small as 1 kms^{-1}. They have derived a binary frequency in the range of 10% to 20% for binaries with 0.1 yr $\leq$ P $\leq$ 20 yr.

2.4.4. Binary Frequencies in Different Stellar Environments

How does the frequency of binary stars in globular clusters compare to that of the field stars, in open clusters and of the low metallicity halo stars?

With an unbiased sample of G-dwarf type stars, the DM survey (1991) found the binary frequency of $\sim 40\%$ for systems with P $\leq 10^7$ yr in the solar neighbourhood. The earlier survey by Abt & Levy (1976) among the same type field stars yielded a slightly higher frequency of 52% for binaries with the similar period range. These two results are essentially consistent considering the fact that the AL sample may contain some spurious spectroscopic binaries (Morbey & Griffin 1987; Abt 1987). From the DM survey, we derived a binary frequency of $\sim 16\%$ for systems with P $\leq$ 2000d. Among halo low metallicity stars and open clusters, extensive surveys of spectroscopic binaries are being carried out at the CfA (Carney & Latham 1987; Stefanik & Latham 1992; Latham *et al.* 1992). The published preliminary results indicated that for binaries with P $\leq$ 2000 days, the frequency appears to be close to 20% in both the halo and open clusters (Latham 1992). The survey by Griffin et al. (1988) in Hyades yielded a binary frequency of ~30%. These results suggest that the binary frequency in open clusters, among low metallicity halo stars and among the field solar-type stars, may be very similar.

Among giant stars in the dynamically relaxed globular clusters (including M 3, M 13, 47 Tuc, M 2, M 71 and NGC 3201), the binary frequency was estimated to be roughly in the range of $5\% - 18\%$ for systems with 40 d $\leq$ P $\leq$ 7000 d (Pryor *et al.* 1992; Hut *et al.* 1992; Côte *et al.* 1994). Our survey among giant and subgiant stars in the ultra-low density globular cluster NGC 5053 yields a binary frequency roughly $20\% - 26\%$ for systems with 4 d $\leq$ P $\leq$ 4000 d depending on the distribution of binary orbital elements. For field binaries in the similar period range, the estimated frequency in the DM survey is $\sim 12\%$. Considering the large uncertainties, it is perhaps too early to draw any definitive conclusion about the frequency of binary populations in globular clusters compared to other different stellar environments. However, with current observational evidence, at least we can argue that binary

stars are not as deficient in globular clusters as originally thought (Gunn & Griffin 1979) when compared to the field stars.

2.5. Conclusions

In this section, we summarize briefly the results from our survey and discuss the future improvements in this field.

We carried out a radial velocity survey among 65 cluster member giant and subgiant stars in the globular cluster NGC 5053. We obtained a total of 223 velocities over a timespan of 3 years. Among these 65 stars, we discovered 5 spectroscopic binary candidates and the derived binary frequency in NGC 5053 is 20−26% depending on the period distribution function and orbital eccentricities. Compared with previous surveys in other globular clusters, the binary frequency and binary discovery fraction are higher. This is probably due to the fact that NGC 5053 is dynamically young and the primordial binary population has not yet been significantly altered by stellar encounters. Thus, our estimated binary frequency should represent the frequency of the primordial binary population in NGC 5053. Furthermore, our result once again demonstrates that binary populations in galactic globular clusters are not significantly deficient compared to stars in other stellar environments, and perhaps are equally abundant.

However, studies of spectroscopic binaries in globular clusters are still in their infancy. Among a handful of spectroscopic binary candidates, we have orbital solutions for only one or two systems. Long-term surveys dedicated to searching for spectroscopic binaries will provide us with a more complete picture of binary populations — their period distributions and their effect on the evolution in globular clusters.

We would like to thank The Kenneth T. and Eileen L. Norris Foundation and especially Kenneth Norris for their generous support in building the Norris spectrograph. Michael Doyle, John Henning and Juan Carrasco of the Palomar Observatory

staff are thanked for providing excellent service during the observations. We wish to thank Tad Pryor for useful discussions on many occasions. The Norris Spectrograph was built by Bev Oke, Judith Cohen and Donald Hamilton; we thank Don Hamilton for his help during our initial observing runs. We appreciate the help from Todd Small during the observations and useful discussions concerning the data reduction.

REFERENCES

Abt, H.A., 1987, ApJ, 317, 353

Abt, H.A. & Levy, S.G., 1976, ApJS, 30, 273

Allen, C.W., 1973, in *Astrophysical Quantities* (University of London, The Athlone Press), 124

Binney, J. & Tremaine, S., 1987, in *Galactic Dynamics* (Princeton University Press), 534

Bell, R.A. & Gustafsson, B., 1983, MNRAS, 204, 249

Bergbusch, P.A. & VandenBerg, D.A., 1992, ApJS, 81, 163

Barden, S., Elston, R., Armandroff, T. & Pryor, C., 1991, in *Fiber Optics in Astronomy*, ed. by Peter M. Gray (San Fransisco: ASP vol. 37), 223

Carney, B.W. & Latham, D.W., 1987, AJ, 93, 116

Cohen, J.G. & Cromer, J., 1988, PASP, 100, 1582

Cohen, J.G., Frogel, J.A. & Persson, S.E., 1978, ApJ, 222, 165

Côte, P., Welch, D.L., Fischer, P., Da Costa, G.S., Tamblyn, P., Seitzer, P. & Irwin, M.J., 1994, ApJS, 90, 83

Djorgovski, S., 1992, in *Structure and Dynamics of Globular Clusters*, ed. by S.G. Djorgovski and G. Meylan (San Fransisco: ASP volume 50), 357

Djorgovski, S. & King, I.R., 1986, ApJL, 305, L61

Duquennoy, A. & Mayor, M., 1991, A&A, 248, 485

Faber, S.M., Friel, E.D., Burstein, D. & Gaskell, C.M., 1985, ApJS, 57, 711

Fahlman, G.G., Richer, H.B. & Nemec, J., 1991, ApJ, 380, 124

Gao, B., Goodman, J., Cohn, H. & Murphy, B., 1991, ApJ, 370, 567

Gorgas, J., Faber, S.M., Burstein, D., Gonzalez, J.J., Courteau, S. & Prosser, C., 1993, ApJS, 86, 153

Green, E.M., Demarque, P. & King, C.R., 1987, *The Revised Yale Isochrones and Luminosity Functions*, Yale University Observatory

Griffin, R.F., Gunn, J.E., Zimmerman, B.A. & Griffin, R.E.M., 1988, AJ, 96, 172

Gunn, J.E. & Griffin, R.F., 1979, AJ, 84, 752

Kaluzny, J. & Krzeminski, W. 1993, MNRAS, 264, 785

Kulkarni, S.R., Anderson, S.B., Prince, T.A. & Wolszczan, A., 1991, Nature, 349, 47

Hamilton, D., Oke, J.B., Carr, M.A., Cromer, J., Harris, F.H., Cohen, J.G., Emery, E. & Blakee, L. 1993, PASP, 105, 1308

Harris, H.C. & McClure, R.D., 1983, ApJL, 265, L77

Heggie, D.C. & Aarseth, S.J., 1992, MNRAS, 257, 513

Hut, P., McMillan, S.L.W., Goodman, J., Mateo, M., Phinney, E.S., Richer, H.B., Verbunt, F. & Weinberg, M., 1992, PASP, 104, 981

Latham, D.W., 1992, in *Complementary Approaches to Binary and Multiple Star Research*, Edited by Harold McAlister & William H. Hartkopf (San Fransisco: ASP), 110

Latham, D.W. et al., 1995, in *Binary Stars in Clusters*, ed. Eugene Milone, in press

Latham, D.W., Mazeh, T., Stefanik, R.P., Davis, R.J., Carney, B.W., Krymolowski, Y., Laird, J.B., Torres, G. & Morse, J.A., 1992, AJ, 104, 774

Latham, D.W., Mazeh, T., Carney, B.W., McCrosky, R.E., Stefanik, R.P. & Davis, R.J., 1988, AJ, 96, 567

Lupton, R.H., Gunn, J.E. & Griffin, R.F., 1987, AJ, 93, 1114

The CCD Atlas of Thorium-Argon Hollow Cathode Comparison Spectra, 1987, published by National Optical Astronomy Observatories

Mateo, M., Harris, H.C., Nemec, J., and Olszewski, E.W., 1990, AJ, 100, 469

Mayor, M., Imbert, M., Andersen, J., Ardeberg, A., Benz, W., Lindgren, H., Martin, N., Maurice, E., Nordström, B. & Prévot, L., 1984, AA, 134, 118

McKenna, J. & Lyne, A.G., 1988, Nature, 336, 226

McMillan, S.L.W. & Hut, P., 1994, ApJ, 427, 793

McMillan, S.L.W., Hut, P. & Makino, J., 1991, ApJ, 372, 111

Morbey, C.L. & Griffin, R.F., 1987, AJ, 352, 709

Phinney, E.S., 1995, in *Binary Stars in Clusters*, ed. Eugene Milone, in press

Phinney, E.S., 1992, Philos. Trans. R. Soc. Lond., A, 341, 39

Phinney, E.S. & Sigurdsson, S., 1991, Nature, 349, 220

Press, W.H., Flannery, B.P., Teukolsky, S.A. & Vetterling, W.T. 1987, in *Numerical Recipes* (Cambridge University Press), 165

Pringle, J.E., 1984, in *Interacting Binary Stars*, ed. by J.E. Pringle and R.A. Wade (Cambridge: Cambridge Univ. Press), 1

Pryor, C.P. & Meylan, G. 1993, in *Struncture and Dynamics of Globular Clusters*, ed. by S.G. Djorgovski and G. Meylan (San Frabsisco: ASP), 50, 357

Pryor, C.P., Hesser, J.E., McClure, R.D., Krismer, M. & Fletcher, J.M., 1992, BAAS, 24, 775

Pryor, C.P., Schommer, R.A. & Olszewski, E.W. 1991, in *The Formation and Evolution of Star Clusters*, ed. Janes (San Fransisco: ASP), 121

Pryor, C.P., McClure, R.D., Fletcher, J.M. & Hesser, J.E., 1989, in *Dynamics of Dense Stellar Systems*, ed. D. Merritt, (Cambridge: Cambridge University Press), 175

Pryor, C.P., Latham, D.W. & Hazen, M.L., 1988, AJ, 96, 123

Pryor, C.P., McClure, R.D., Hesser, J.E. & Fletcher, J.M., 1987, BAAS, 19, 676

Sandage, A.R., Katem, B. & Johnson, H.L., 1977, AJ, 82, 389

Schroeder, D.J., 1987, in *Astronomical Optics* (Academic Press, Inc.), 26

Sigurdsson, S. & Phinney, E.S., 1995, ApJS, 99, 609

Stefanik, R.P. & Latham, D.W., 1992, in *Complementary Approaches to Binary and Multiple Star Research*, Edited by Harold McAlister & William H. Hartkopf, (San Fransisco: ASP), 173

Sunzteff, N.B., Kraft, R.P. & Kinman, T.D., 1988, AJ, 95, 91

Taff, L.G., 1981, in *Computational Spherical Astronomy* (Wiley-Interscience Publication), 115

Taff, L.G., 1985, in *Celestial Mechanics* (Wiley-Interscience Publication), 481

Tonry, J. & Davis, M., 1979, AJ, 84, 1511

Vesperini, E. & Chernoff, D.F., 1994, ApJ, 431, 231

Yan, L. & Mateo, M. 1994, AJ, 108, 1810

Yan, L. & Reid, N. I. 1995, MNRAS, in press

TABLE 1

Summary of Observing Log

Date (UT)	Object	Exp. Time (sec)	$\Delta\lambda$ (Å)	Resolution (Å)	Weather Conditions
7/4/1992	NGC 5053	3×3000	4710–5310	2.5	clear, 1.3″ seeing
7/4/1992	M 13	1×900	4710–5310	2.5	clear, 1.3″ seeing
8/4/1992	NGC 5053[2]	3×3000	4710–5310	2.5	cloudy, 1.3″ seeing
8/4/1992	M 13	1×900	4710–5310	2.5	cloudy, 1.3″ seeing
25/5/1992	NGC 5053	2×3000	4710–5310	2.5	cloudy, 1.5″ seeing
26/5/1992	NGC 5053	3×3000	4710–5310	2.5	clear, 1.5″ seeing
26/5/1992	M 13	1×900	4710–5310	2.5	clear, 1.5″ seeing
16/4/1993	NGC 5053	1×3000	4710–5310	2.5	cloudy, 1.5″ seeing
16/4/1993	M 13	1×900	4710–5310	2.5	cloudy, 1.5″ seeing
21/5/1993	NGC 5053	1×2515	4710–5310	2.5	cloudy, 1.5″ seeing
21/5/1993	M 13	1×900	4710–5310	2.5	cloudy, 1.5″ seeing
11/4/1994	NGC 5053	3×3000	4700–5800	3.0	clear, 1.2″ seeing
11/4/1994	M 13	2×700	4700–5800	3.0	clear, 1.2″ seeing
12/4/1994	NGC 5053	3×3000	4700–5800	2.5	cloudy, 1.5″ seeing
12/4/1994	M 13	3×900	4700–5800	3.0	cloudy, 1.5″ seeing
12/4/1994	NGC 5053[2]	4×3000	4700–5800	3.0	cloudy, 1.5″ seeing
8/5/1994	NGC 5053	3×3000	4700–5800	2.5	cloudy, 1.3″ seeing
8/5/1994	M 13	1×600	4700–5800	2.5	cloudy, 1.3″ seeing
10/5/1994	NGC 5053	2×3000	4700–5800	2.5	clear, 1.2″ seeing
10/5/1994	M 13	3×600	4700–5800	2.5	clear, 1.5″ seeing
10/5/1994	NGC 5053[2]	2×3000	4700–5800	3.0	cloudy, 1.5″ seeing
10/5/1994	M 13	1×900	4700–5800	2.5	clear, 1.3″ seeing

Notes: NGC 5053[2] is the second field we observed in the same cluster. In M 13 several bright giant stars were observed to serve as the radial velocity standards. The radial velocities of these stars have been accurately measured by Lupton, Gunn and Griffin (1987). The observations taken in 1994 were made with a 2048×2048 pixels CCD, and the rest of the observations were done with a 1024×1024 pixels

CCD. The third column in the table gives the number of exposure times the time of a single exposure, *i.e.*, the total exposure time. The spectral resolution in April 1994 is larger than other runs due to problems with the collimator focus in the Norris spectrograph during that observing run. The CCD spectral scale is 0.65 Å pixel^{-1} for all of the observations.

TABLE 2

Relative radial velocities of stars in N5053

ID	RA (1950)	DEC (1950)	R ($''$)	HJD (+244000days)	V_r kms^{-1}	σ kms^{-1}	n	$\bar{V}_r$ kms^{-1}	σ kms^{-1}	χ^2	$P(<\chi^2)$	V_0	$(B-V)_0$
S35	13:14:29.803	18:01:17.816	450.4	8719.777	296.7	9.9	5	291.1	3.7	1.355	0.8519	16.69	0.75
				8768.330	291.8	1.1							
				9093.791	286.4	6.4							
				9454.247	290.3	2.0							
				9481.533	290.8	3.7							
LY014	13:14:20.325	18:04:06.804	498.8	8719.777	292.3	3.1	6	291.5	3.5	2.512	0.7746	17.12	0.63
				8768.330	291.3	4.7							
				9093.791	289.2	3.2							
				9128.754	287.6	5.1							
				9454.247	297.7	5.4							
				9481.533	291.9	2.5							
LY012	13:14:19.169	17:58:08.904	220.8	8719.777	279.0	8.1	4	291.6	8.1	3.589	0.3090	17.20	0.32
				8768.330	292.0	1.0							
				9093.791	285.5	6.1							
				9454.247	291.4	2.1							
S33	13:14:19.468	17:57:54.244	219.2	9481.533	291.3	1.3	2	291.9	1.1	0.529	0.4669	16.06	0.72
				9454.247	292.8	1.6							
S37	13:14:14.123	18:03:22.185	424.3	9454.247	291.6	1.7	2	291.0	0.9	0.165	0.6850	15.28	0.81
				9481.533	290.8	1.0							
LY019	13:14:13.245	17:58:17.772	153.5	8719.777	285.8	12.4	4	294.1	6.7	1.393	0.7072	18.54	0.65
				8768.330	297.1	5.5							
				9093.791	301.6	11.3							
				9454.247	292.1	4.4							
S38	13:14:11.189	18:01:03.399	279.4	8719.777	291.4	1.7	5	289.8	5.0	5.322	0.2558	17.33	0.60
				8768.330	289.9	3.6							
				9093.791	284.4	8.3							
				9454.247	289.4	3.5							

				9481.533	281.4	4.2							
LY116	13:14:11.950	17:57:36.648	114.4	8719.777	289.4	4.3	4	289.4	1.7	0.205	0.9768	17.57	0.63
				8768.330	288.8	2.3							
				9454.247	290.5	4.6							
				9481.533	290.7	4.6							
S45	13:14:10.314	17:58:55.271	156.3	8719.777	292.7	4.2	6	292.3	4.5	5.069	0.4076	16.48	0.68
				8768.330	290.8	2.5							
				9093.791	295.0	3.6							
				9128.754	301.6	5.0							
				9454.247	290.2	3.0							
				9481.533	291.0	3.0							
S41	13:14:09.486	17:59:24.254	177.8	8719.777	289.6	2.9	6	290.0	3.0	1.421	0.9220	16.54	0.74
				8768.330	290.6	3.7							
				9093.791	292.7	4.4							
				9128.754	284.0	6.7							
				9454.247	290.6	1.8							
				9481.533	289.5	1.7							
LY022	13:14:8.497	17:56:40.615	49.0	8719.777	290.5	3.2	5	289.6	2.0	1.673	0.7957	17.49	0.61
				8768.330	292.3	3.0							
				9093.791	291.8	5.8							
				9454.247	288.7	4.8							
				9481.533	288.2	1.8							
S28	13:14:07.689	17:57:10.948	49.8	8719.777	292.2	4.0	5	289.8	3.5	5.831	0.2119	17.04	0.66
				8768.330	294.1	2.6							
				9093.791	285.0	3.2							
				9454.247	289.8	3.2							
				9481.533	288.4	2.0							
S40	13:14:06.045	18:00:12.435	214.9	8719.777	290.2	3.5	5	297.4	6.2	10.02	0.0400	16.47	0.60
				9093.791	288.8	6.3							
				9128.754	296.6	10.3							
				9454.247	298.7	4.9							
				9481.533	302.5	2.6							
S26	13:14:04.983	17:56:53.106	15.2	9454.247	296.4	4.5	2	293.2	3.8	0.846	0.3577	17.01	0.68
				9481.533	291.1	3.6							

S25	13:14:05.104	17:56:58.405	20.4	8719.777	291.5	5.7	3	291.4	2.1	0.307	0.8570	16.53	0.42
				8768.330	292.0	2.5							
				9128.754	288.6	5.6							
S54	13:14:04.168	17:57:53.199	76.3	8719.777	277.1	2.3	6	290.7	9.5	59.133	0.0000	16.63	0.65
				8768.330	292.2	2.0							
				9093.791	295.4	3.2							
				9128.754	281.0	4.7							
				9454.247	294.0	1.8							
				9481.533	302.6	3.2							
S55	13:14:02.892	17:57:26.260	57.4	8719.777	290.1	1.7	5	290.4	6.9	4.058	0.3980	16.44	0.58
				8768.330	291.0	1.7							
				9093.791	304.0	7.4							
				9128.754	292.5	4.7							
				9454.247	289.6	1.4							
LY'37	13:14:03.277	17:59:45.181	188.9	9481.533	293.4	5.7	1	293.4	5.7	-	-	18.14	0.56
LY'22	13:14:01.636	17:58:15.147	108.8	8719.777	290.1	4.4	3	292.2	3.4	0.851	0.6533	17.60	0.57
				8768.330	294.9	4.1							
				9128.754	288.8	7.8							
LY31	13:14:01.777	18:0:12.363	219.5	9454.247	296.5	5.8	2	294.6	7.8	0.529	0.4669	18.55	0.55
				9481.533	287.0	11.7							
S56	13:14:02.381	17:57:14.604	53.0	9454.247	290.2	2.1	2	290.9	1.7	0.361	0.5480	16.58	0.73
				9481.533	292.4	3.0							
S60	13:14:0.900	17:59:11.026	49.8	8719.777	287.0	5.1	5	291.3	4.8	2.443	0.6548	16.68	0.67
				8768.330	290.9	3.7							
				9093.791	297.2	5.3							
				9454.247	290.5	2.1							
				9481.533	293.1	3.1							
LY'28	13:14:0.052	17:59:47.882	202.9	8791.777	293.4	2.5	4	292.1	4.7	2.219	0.5282	17.86	0.65
				8768.330	291.9	5.4							
				9454.247	284.1	6.5							
				9481.533	293.2	5.2							
S66	13:13:59.098	17:59:26.701	189.0	8791.777	288.7	3.0	5	290.2	2.3	2.282	0.6840	16.79	0.67
				8768.330	289.0	2.4							

				9093.791	286.7	4.6								
				9454.247	290.5	4.7								
				9481.533	292.5	2.1								
S84	13:13:57.296	17:58:01.991	139.1	8791.777	293.8	1.6	4	293.3	1.2	0.559	0.9057	15.94	0.72	
				8768.330	293.6	2.4								
				9093.791	293.2	2.5								
				9454.247	291.3	3.0								
S90	13:13:57.740	17;56:55.873	106.1	9481.533	289.7	2.8	1	289.7	2.8	-	-	15.98	0.76	
LY52	13:13:56.530	17:57:06.575	125.2	9454.247	291.4	4.7	1	291.4	4.7	-	-	17.93	0.61	
LY21	13:13:56.983	17:56:33.690	xxxx	9454.247	290.3	2.2	2	291.0	1.8	0.336	0.5620	17.89	0.55	
				9481.533	292.6	3.3								
LY042	13:13:55.074	17:58:18.612	174.6	9481.533	290.7	6.8	1	290.7	6.8	-	-	17.82	0.57	
LY043	13:13:54.012	17:58:09.566	182.4	8719.777	287.0	3.4	3	290.0	4.3	3.348	0.1875	17.14	0.60	
				8768.330	288.8	2.5								
				9454.247	295.2	3.4								
LY1	13:13:52.698	17:56:28.824	176.8	8719.777	288.7	5.1	4	288.0	4.5	3.162	0.3674	17.19	0.64	
				8768.330	293.1	4.1								
				9454.247	288.2	5.1								
				9481.533	288.1	4.4								
S80	13:13:51.521	17:58:41.187	229.3	8719.777	293.4	1.9	6	292.1	3.0	2.352	0.7986	16.95	0.74	
				8768.330	290.0	2.5								
				9093.791	295.1	3.8								
				9128.754	286.8	8.0								
				9454.247	293.1	4.7								
				9481.533	291.7	1.5								
LY065	13:13:49.572	17:58:0.164	235.9	8719.777	287.0	9.6	2	295.7	9.0	1.042	0.3075	18.60	0.61	
				8768.330	298.0	4.9								
S102	13:13:48.913	17:58:18.160	251.4	9454.247	294.6	3.2	2	292.2	5.0	1.560	0.2113	17.24	0.66	
				9481.533	287.8	4.4								
SAH	13:13:48.259	17:59:25.503	292.6	8719.777	288.8	2.5	5	290.5	2.9	3.989	0.4075	17.04	0.59	
				8768.330	292.1	1.5								
				9093.791	287.7	2.4								

				9128.754	295.0	4.6							
				9481.533	290.1	1.5							
LY7	13:13:47.502	17:56:52.114	251.1	9454.247	286.6	7.2	1	286.6	7.2	-	-	18.06	0.62
S109	13:13:46.654	17:57:27.460	267.4	8719.777	288.3	0.7	6	291.0	9.4	72.79	0.0000	16.02	0.75
				8768.330	291.6	1.2							
				9093.791	288.6	4.1							
				9128.754	304.9	4.9							
				9454.247	300.2	1.9							
				9481.533	303.2	2.4							
S72	13:13:45.530	18:02:11.898	435.0	9454.247	294.6	1.5	2	294.1	0.8	0.151	0.6978	14.18	1.13
				9481.533	293.9	1.0							
SU	13:13:45.018	17:56:54.485	286.6	8719.777	289.8	3.3	3	292.1	4.2	1.479	0.4775	16.40	0.72
				8768.330	292.8	4.1							
				9093.791	297.5	5.5							
LY004	13:13:43.928	18:02:07.887	447.0	8719.777	289.3	2.0	4	290.2	2.4	1.867	0.6004	17.86	0.61
				8768.330	293.0	2.5							
				9093.791	287.3	5.0							
				9454.247	289.6	2.2							
SW	13:13:37.452	17:58:13.463	405.5	9454.247	293.4	6.2	2	289.1	4.4	0.575	0.4481	16.52	0.50
				9481.533	288.3	2.6							
S108	13:13:45.230	17:57:14.148	285.4	9454.247	292.9	3.4	2	290.1	2.8	0.753	0.3857	16.44	0.72
				9481.533	289.8	1.1							
S106	13:13:35.905	17;57:18.472	418.2	9454.247	301.9	4.8	2	296.9	5.8	1.742	0.1868	17.27	0.58
				9481.533	293.9	3.7							
LY009	13:13:32.497	18:00:17.104	513.9	9481.533	289.0	8.8	1	289.0	8.8	-	-	16.21	0.20
SX	13:14:19.553	17:53:35.426	275.8	8719.777	290.8	1.8	5	291.9	4.7	5.849	0.2107	16.56	0.74
				8768.330	300.9	4.0							
				9093.791	292.0	5.9							
				9454.247	289.9	3.3							
				9481.533	291.0	4.2							
SS	13:14:18.787	17:54:27.594	235.2	8719.777	289.5	2.4	3	288.9	3.4	0.966	0.6168	16.21	0.77
				9454.247	288.2	1.7							

			9481.533	293.7	5.6									
SAB	13:14:16.837	17:53:18.761	260.6	8719.777	291.5	1.7	6	294.0	6.7	21.20	0.0007	16.76	0.66
				8768.330	295.2	1.4							
				9093.791	306.1	4.9							
				9128.754	291.2	9.2							
				9454.247	300.3	2.5							
				9481.533	289.2	2.0							
LYV5	13:14:14.407	17:53:59.234	207.3	8719.777	306.1	18.3	2	291.0	15.1	0.707	0.4000	16.61	0.43
				8768.330	290.4	3.7							
SP	13:14:13.679	17:56:14.145	125.1	8719.777	292.7	4.0	5	289.8	3.3	9.552	0.0487	15.61	0.80
				8768.330	295.1	2.0							
				9128.754	291.7	4.3							
				9454.247	288.3	1.5							
				9481.533	288.9	1.0							
LY88	13:14:12.704	17:55:37.984	124.4	8719.777	285.2	4.1	3	288.1	4.1	1.486	0.4757	18.65	0.65
				8768.330	286.7	8.8							
				9454.247	283.0	5.0							
S21	13:14:10.278	17:56:18.829	76.8	8719.777	294.7	5.4	3	288.6	4.6	1.915	0.3839	17.18	0.63
				9454.247	287.3	2.0							
				9481.533	290.6	4.3							
S23	13:14:07.463	17:56:08.401	45.2	8719.777	292.2	1.9	5	290.7	2.8	2.006	0.7347	16.40	0.78
				8768.330	288.3	4.1							
				9093.791	289.6	5.1							
				9128.754	295.4	5.6							
				9454.247	290.0	1.3							
SV	13:14:08.588	17:55:52.247	67.9	9454.247	290.4	2.7	2	290.9	1.0	0.049	0.8250	16.50	0.54
				9481.533	291.0	1.0							
SAI	13:14:04.116	17:56:08.155	32.8	8719.777	290.4	2.7	3	289.7	3.0	0.705	0.7027	17.11	0.66
				9454.247	293.2	6.8							
				9481.533	287.5	3.6							
LY17	13:14:03.031	17:52:57.642	222.3	8719.777	288.0	4.3	4	289.0	2.6	0.350	0.9505	18.15	0.62
				8768.330	292.7	8.0							
				9454.247	287.7	5.3							

				9481.533	290.1	4.7							
LY15	13:14:1.653	17:55:18.040	93.7	8719.777	293.9	3.0	4	290.2	5.6	6.600	0.0858	17.32	0.60
				8768.330	298.4	5.2							
				9454.247	286.5	2.3							
				9481.533	290.0	3.6							
S2	13:13:59.996	17:56:13.925	76.3	9454.247	287.9	2.9	2	288.8	1.9	0.169	0.6812	16.04	0.8
				9481.533	289.5	2.6							
S4	13:14:0.241	17:55:17.243	106.2	8719.777	291.4	3.5	4	290.3	3.3	0.392	0.9419	16.81	0.72
				8768.330	289.5	3.1							
				9128.751	284.7	12.0							
				9454.247	290.7	4.2							
LY18	13:13:58.283	17:52:58.351	240.1	8719.777	290.2	2.9	4	291.3	4.5	1.673	0.6429	18.20	0.65
				8768.330	299.0	6.4							
				9454.247	291.6	3.7							
				9481.533	290.2	4.0							
S91	13:13:57.385	17:56:08.211	144.2	8719.777	291.5	1.0	4	292.4	11.3	13.03	0.0046	16.97	0.70
				8768.330	310.9	5.9							
				9454.247	291.8	3.8							
				9481.533	298.4	3.9							
S5	13:13:56.001	17:54:56.196	164.7	8719.777	304.3	1.8	5	296.2	10.2	46.41	0.0000	15.67	0.74
				8768.330	294.5	2.2							
				9093.791	280.3	6.0							
				9454.247	287.5	2.1							
				9481.533	300.9	4.0							
S94	13:13:55.155	17:55:48.676	149.8	8719.777	291.1	1.3	3	290.2	5.0	1.022	0.5999	16.38	0.75
				8768.330	289.8	1.0							
				9128.754	283.3	11.1							
S93	13:13:55.122	17:56:12.750	144.2	9454.247	294.5	2.3	2	295.9	2.4	0.866	0.3522	16.56	0.67
				9481.533	297.8	2.7							
LY85	13:13:54.297	17:51:27.686	346.3	8719.777	293.0	3.9	4	289.9	4.1	1.295	0.7302	18.05	0.65
				8768.330	287.3	4.6							
				9454.247	289.0	5.7							
				9481.533	281.3	11.4							

LY02	13:13:52.945	17:54:47.363	205.4	9454.247	291.8	3.0	2	292.2	2.2	0.039	0.8427	17.58	0.64
				9481.533	292.7	3.4							
LY76	13:13:49.573	17:53:49.279	278.2	9454.247	291.2	6.0	1	291.2	6.0	-	-	17.80	0.62
LY08	13:13:47.715	17:56:17.018	248.5	9454.247	289.7	6.0	2	292.5	4.3	0.436	0.5088	17.57	0.66
				9481.533	295.4	6.2							
LY109	13:13:43.670	17:55:55.426	308.3	9454.247	297.6	4.0	2	294.3	4.2	1.232	0.2670	17.80	0.64
				9481.533	291.7	3.5							
LY015	13:13:43.993	17:52:9.349	403.3	9454.247	290.0	2.3	2	290.7	5.4	0.757	0.3842	17.48	
				9481.533	296.0	6.5							
LY068	13:13:49.262	17:56:14.973	226.8	9454.247	292.5	9.4	1	292.5	9.4	-	-	19.09	0.55
LY03	13:13:52.346	17:55:8.680	202.4	9454.247	289.6	2.1	2	291.2	6.0	2.683	0.1014	17.73	0.55
				9481.533	297.0	4.0							
LY87	13:14:11.701	17:55:26.597	118.5	9454.247	290.5	3.5	2	289.5	3.1	0.315	0.5745	18.32	0.66
				9481.533	286.6	6.0							
LY40	13:14:7.288	17:58:39.484	125.5	9454.247	289.5	3.0	2	290.7	3.6	0.578	0.4469	17.26	0.67
				9481.533	294.0	5.1							
S27	13:14:4.453	17:57:4.988	28.4	9454.247	299.7	4.0	2	294.8	6.3	2.735	0.0982	17.10	0.67
				9481.533	290.8	3.6							
LY65	13:14:3.539	17:56:38.914	21.9	9454.247	285.7	3.0	2	289.0	3.7	1.806	0.1789	17.71	0.59
				9481.533	290.7	2.2							
LY9	13:14:1.330	18:0:48.993	256.6	9454.247	290.2	1.0	1	290.2	1.0	-	-	18.04	0.68
LY11	13:13:59.635	18:0:32.094	246.6	9454.247	289.0	3.7	2	290.1	5.0	0.493	0.4820	17.92	0.66
				9481.533	295.0	7.7							
LY016	13:14:12.485	17:59:59.227	227.4	9454.247	287.7	5.1	1	287.7	5.1	-	-	18.18	0.56
LY017	13:14:13.332	18:2:30.144	371.4	9454.247	294.8	5.0	2	291.0	8.9	1.779	0.1823	18.29	0.55
				9481.533	283.0	7.3							
S70	13:13:57.481	18:0:25.807	252.2	9454.247	289.6	2.8	2	290.8	2.2	0.448	0.5033	17.22	0.65
				9481.533	292.6	3.5							
LYAC	13:13:55.012	17:56:21.794	144.4	9454.247	290.9	3.4	2	289.1	3.3	0.693	0.4050	17.35	0.62
				9481.533	286.4	4.2							

LY13	13:13:51.659	18:0:9.043	284.9	9454.247	292.2	1.1	2	292.1	2.5	0.268	0.6046	17.41	0.70
				9481.533	289.6	5.4							
LY5	13:13:50.600	17:59:2.148	251.8	9454.247	288.6	1.2	2	289.2	1.4	0.692	0.4054	17.45	0.68
				9481.533	290.4	1.8							
LY024	13:13:46.049	18:0:3.952	340.7	9454.247	291.8	6.3	1	291.8	6.3	-	-	18.41	0.60

Notes: The objects with the prefix S in their names were identified in Sandage, Katem & Johnson (1977), and the rest are newly identified. The third column is the distance of a star in unites of arcsecond relative to the position RA (1950) =13:14:5.070 and DEC (1950)=17:56:38.00. The fourth column records the heliocentric julian dates (plus 244000 in days) of the observations. The eighth and ninth columns are the weighted mean radial velocity and the external velocity error in a single measurement estimated from the dispersion about the mean. The tenth and eleventh columns are the χ^2 estimated for all observations and the probability of obtaining a χ^2 at least this large purely due to consequence of measurement errors. The final two columns give the star's visual magnitude and (B − V) colour.

TABLE 3

Relative radial velocities and properties of star ST

ID	RA	DEC (1950)	R ($''$)	HJD (+244000days)	V_r kms^{-1}	σ kms^{-1}	n	$\bar{V}_r$ kms^{-1}	σ kms^{-1}	χ^2	P($<\chi^2$)	V_0	(B - V)$_0$
ST	13:14:26.180	17:58:20.081	318.1	8719.7347	247.9	4.1	14	299.2	40.9	3938	0.0	16.36	0.81
				8719.7769	235.9	3.4							
				8719.8184	252.1	2.9							
				9453.8303	338.1	2.2							
				9453.8850	336.7	2.4							
				9453.9424	337.0	2.2							
				9454.7627	295.6	2.4							
				9454.8137	291.3	2.0							
				9454.8649	287.7	2.6							
				9480.6831	337.6	2.0							
				9480.7310	338.7	2.1							
				9480.7857	335.4	2.3							
				9482.7090	254.2	1.7							
				9482.7564	254.7	1.8							

Notes: The third column is the distance of a star in unites of arcsecond relative to the position RA(1950) =13:14:5.070 and DEC(1950) =17:56:38.00. The fourth column records the heliocentric julian dates (plus 244000 in days) of the observations. The eighth and nineth columns are the weighted mean radial velocities and the external velocity error in a single measurement estimated from the dispersion about the mean. The tenth and eleventh columns are the χ^2 estimated for all observations and the probability of obtaining a χ at least this large purely due to consequence of measurement errors. The final two columns give the star's visual magnitude and (B $-$ V) colour.

TABLE 4

Mean Number of Discovered Binaries with P($< \chi$) $\leq$ (0.01,0.001) per Artificial Data Set

	$0.6 \leq \log_{10}$P ≤ 3.56 $0.125 \leq$q ≤ 1.75		$0.6 \leq \log_{10}$P ≤ 3.56 $0.3 \leq$q ≤ 1.75	
f_b	$e = 0.0$	$f(e) = 1.5\sqrt{e}$	$e = 0.0$	$f(e) = 1.5\sqrt{e}$
0.00	(0.6, 0.06)	(0.6, 0.06)	(0.6, 0.06)	(0.6, 0.06)
5%	(1.5, 0.8)	(1.4, 0.6)	(1.7, 0.9)	(1.5, 0.8)
10%	(2.4, 1.5)	(2.2, 1.3)	(2.7, 1.8)	(2.5, 1.6)
15%	(3.4, 2.3)	(3.2, 2.2)	(3.9, 2.7)	(3.5, 2.4)
20%	(4.3, 2.9)	(3.9, 2.7)	(4.9, 3.7)	(4.5, 3.2)
25%	(5.2, 3.7)	(4.7, 3.3)	(6.1, 4.5)	(5.6, 4.1)
30%	(6.2, 4.6)	(5.7, 4.1)	(7.3, 5.6)	(6.5, 4.9)
35%	(7.1, 5.2)	(6.5, 4.8)	(8.3, 6.4)	(7.6, 5.8)
40%	(8.1, 6.1)	(7.3, 5.4)	(9.4, 7.4)	(8.4, 6.5)
f_b	**(24%, 27%)**	**(26%, 30%)**	**(21%, 22%)**	**(22%, 25%)**

Notes: The period distribution used in the simulation is the DM distribution. Period P in the table is in days. Mass ratio q is M_2/M_1, where M_1 is the primary star with a mass of $0.8M_\odot$. The number of discovered binaries for each entry in the table is an average of 1000 simulation tries, and is recorded as real instead of integer in order to show the small differences in different cases. The last line in the table indicates the binary frequency inferred by comparing the number of discovered binaries in synthetic data with the number of binary candidates in real data. Notice in Table 2 that there are a total of 5 binary candidates whose χ^2 probabilities are less than 0.01, but only 4 less than 0.001.

TABLE 5

Mean Number of Discovered Binaries with P($< \chi$) $\leq$ (0.01,0.001) per Artificial Data Set (with the "Flat" Period Distribution)

	$0.6 \leq \log_{10}$P ≤ 3.56 $0.125 \leq$q ≤ 1.75		$0.6 \leq \log_{10}$P ≤ 3.56 $0.3 \leq$q ≤ 1.75	
f_b	$e = 0.0$	$f(e) = 1.5\sqrt{e}$	$e = 0.0$	$f(e) = 1.5\sqrt{e}$
0.00	(0.61, 0.06)	(0.61, 0.06)	(0.65, 0.07)	(0.63, 0.06)
5%	(1.65, 0.94)	(1.49, 0.79)	(1.87, 1.14)	(1.64, 0.95)
10%	(2.71, 1.84)	(2.36, 1.43)	(3.09, 2.14)	(2.70, 1.86)
15%	(3.72, 2.66)	(3.39, 2.29)	(4.37, 3.28)	(3.79, 2.75)
20%	(4.85, 3.62)	(4.27, 3.07)	(5.64, 4.37)	(4.85, 3.64)
25%	(5.93, 4.43)	(5.36, 3.92)	(6.91, 5.40)	(6.15, 4.74)
30%	(7.02, 5.35)	(6.21, 4.63)	(8.11, 6.48)	(7.26, 5.72)
35%	(8.27, 6.38)	(7.16, 5.36)	(9.55, 7.65)	(8.33, 6.53)
40%	(9.26, 7.26)	(8.34, 6.37)	(10.8, 8.79)	(9.60, 7.72)
f_b	**(21%, 23%)**	**(23%, 26%)**	**(18%, 18%)**	**(21%, 22%)**

Notes: The "flat" period distribution was used in the simulations for this table. Period P in the table is in days. Mass ratio q is M_2/M_1, where M_1 is the primary star with a mass of $0.8M_\odot$. As the same in Table 3, the number of discovered binaries for each entry is an average of 1000 simulation tries, and is real instead of integer. The last line in the table indicates the binary frequency inferred by comparing the number of discovered binaries in synthetic data with the number of binary candidates in real data. Notice in Table 2 that there are a total of 5 binary candidates whose χ^2 probabilities are less than 0.01, but only 4 less than 0.001.

TABLE 6

Summary of All Radial Velocity Surveys for Spectroscopic Binaries in Globular Clusters

Cluster	N_{bin}	N_{tot}	N_{rv}	ΔT yr	Δm_V mag	DM mag	σ kms^{-1}	T_{rh} Gyr	Ref.
NGC 5053	3	28	109	3	12–15.5	16.08	0.9	7	(1)
NGC 5053^2	5	65	223	3	14.2–18.6	16.08	3.0	7	(2)
NGC 3201	2+13	276	786	6	11.5–16.5	14.2	1.1	0.06	(3)
M 3	1	110	504	10	12–14	15.02	1.0	0.6	(4), (5)
NGC 5466	2	36	140	5	12–15.5	15.99	0.9	6	(1)
M 13	1	93	288	5	12–14	14.29	1.0	0.09	(6)
M 71	4	61	$\geq$220	8	12–14	12.96	0.8	0.1	(7), (8)
M 12	2	72	111	4	12–14	15.38	0.8	1.0	(8)
47 Tuc	0	64	124	0.5	11.5–13.5	13.31	0.6	1.5	(9)

Notes: In the table, NGC 5053^2 represents our survey, the second made in the cluster NGC 5053. Because the two surveys in this cluster are different in many aspects, we tabulated their data separately. N_{bin} is the total number of discovered binary candidates, N_{tot} is the total number of stars observed in each survey and N_{rv} is the total number of radial velocity obtained in each survey. In the cluster NGC 3201, Côte et al. (1994) discovered 2 good binary candidates together with 13 possible candidates. Δm_V is the visual magnitude range of the sample objects in the survey. DM and T_{rc} represent the distance modulus and the central relaxation time of a cluster respectively. σ is the internal velocity error per measurement. The stars in all surveys are distributed throughout the whole cluster *except* in the case of 47 Tuc. Mayor et al. only sampled the stars from the region beyond 5 core radii in 47 Tuc. The total number of velocities collected for M 71 is not certain because the complete data have not been published. The code for the reference column is as follows:

(1) – Pryor et al. 1991; (2) – this survey; (3)– Côte et al. 1994;

(4)– Gunn & Griffin 1978; (5)– Pryor et al. 1988; (6)– Lupton et al. 1987;

(7)– Pryor et al. 1992; (8)– Pryor et al. 1987; (9)– Mayor et al. 1984

TABLE 7

KOLMOGOROV-SMIRNOV PROBABILITIES FOR MODEL ACCEPTANCE

	$4\text{d} \leq \text{P} \leq 10\text{yr}$ $0.125 \leq \text{q} \leq 1.75$	
f_b	$e = 0.0$	$f(e) = 1.5\sqrt{e}$
0%	0.47	0.48
10%	0.69	0.72
20%	0.88	0.89
25%	0.92	0.92
30%	0.81	0.82
40%	0.46	0.45
50%	0.14	0.16

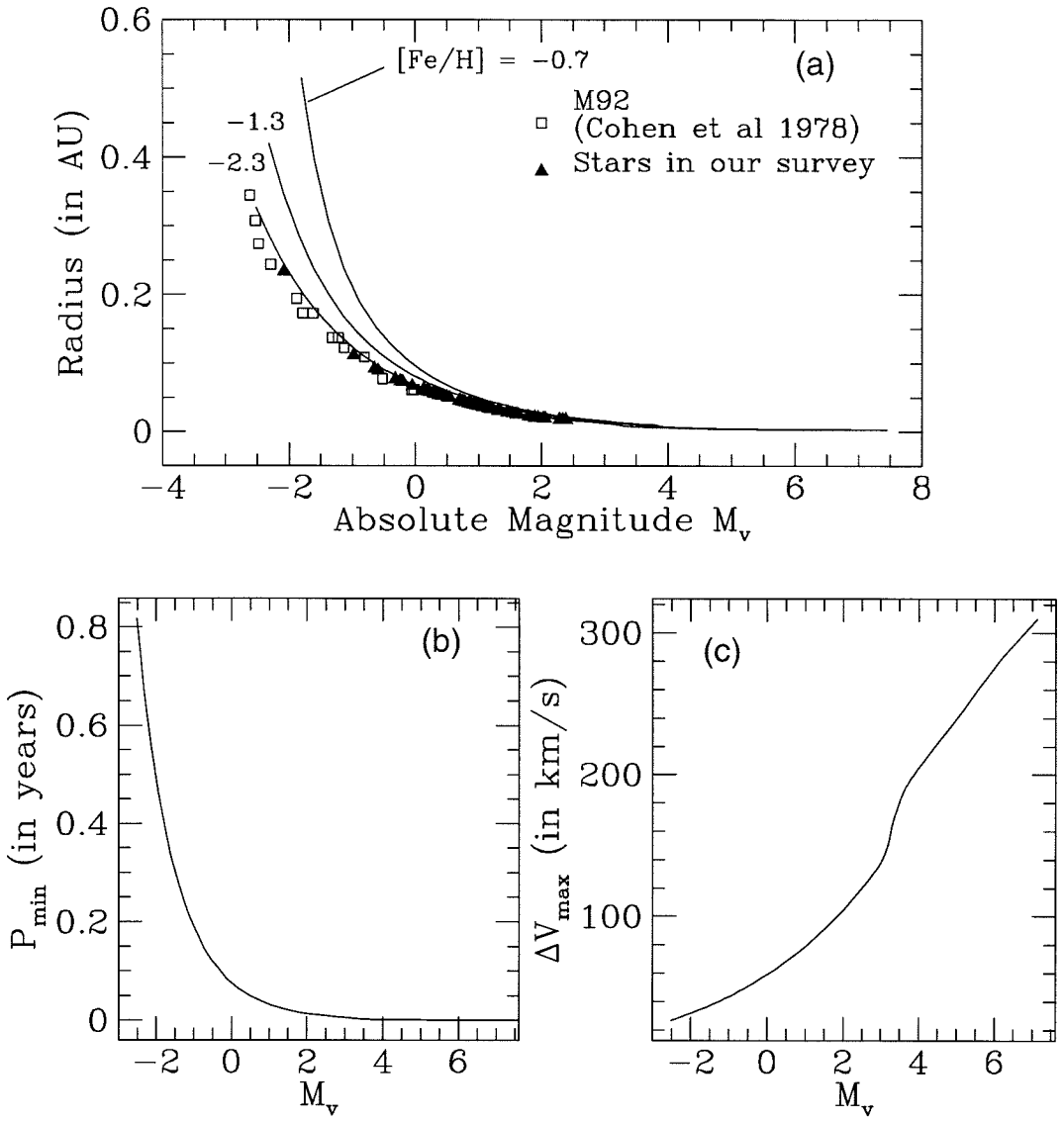

Figure 2.1: Stellar Radius vs. Luminosity for Stars in Globular Clusters

Figure 2.1(a) is a plot of the stellar radius vs. the luminosity for stars in globular clusters. In the figure the curves are generated for three different metallicities using the Revised Yale Isochrones and Luminosity Functions (Green *et al.* 1987) with Y= 0.2 and an age of 15 Gyr. Figure 2.1(b) is the plot of the minimum period of a binary system versus the luminosity of the primary. This minimum period which a binary system could possibly have without undergoing mass transfer is set by the size of the primary star of the binary. Similarly, Figure 2.1(c) plots the maximum radial velocity variations versus the primary star luminosity. For both Figure 2.1(b) and 2.1(c), the calculations were done for binaries on the edge-on circular orbits with M_1 derived from the stellar models and assumed M_2 of $0.5M_\odot$.

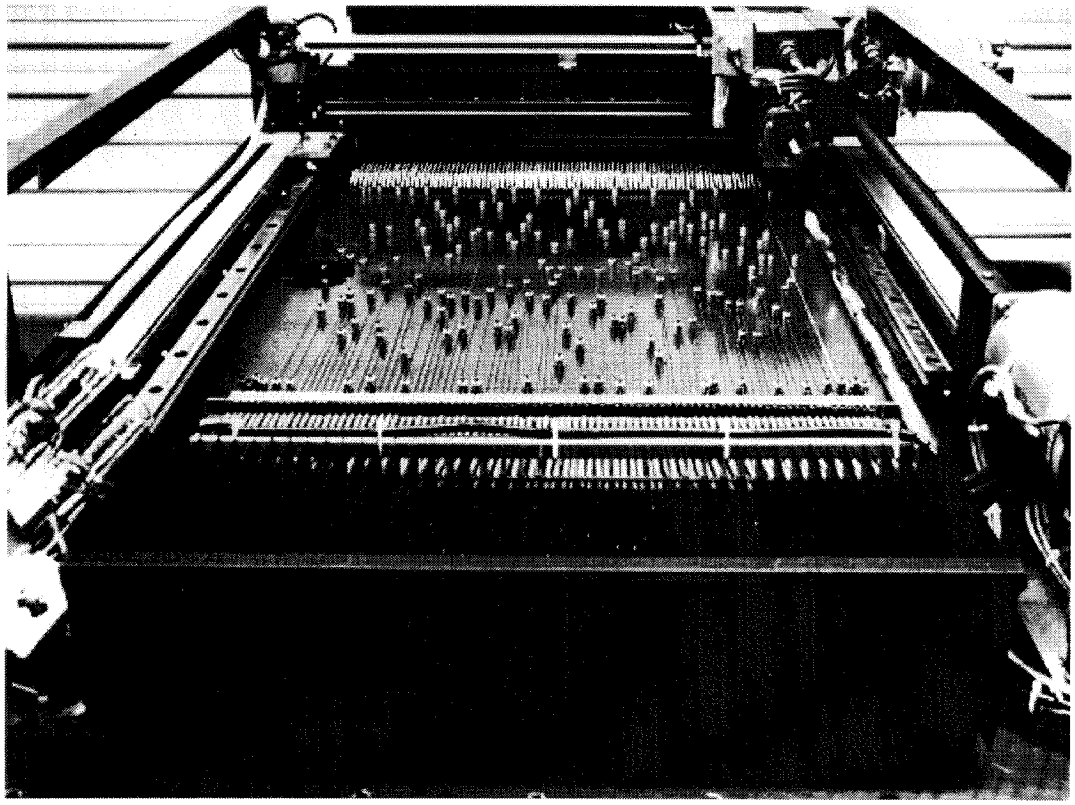

Figure 2.2: The Layout of the Fiber Stage

The layout of the fiber stage of the Norris Multi-object Spectrograph on the Hale 5.0m telescope.

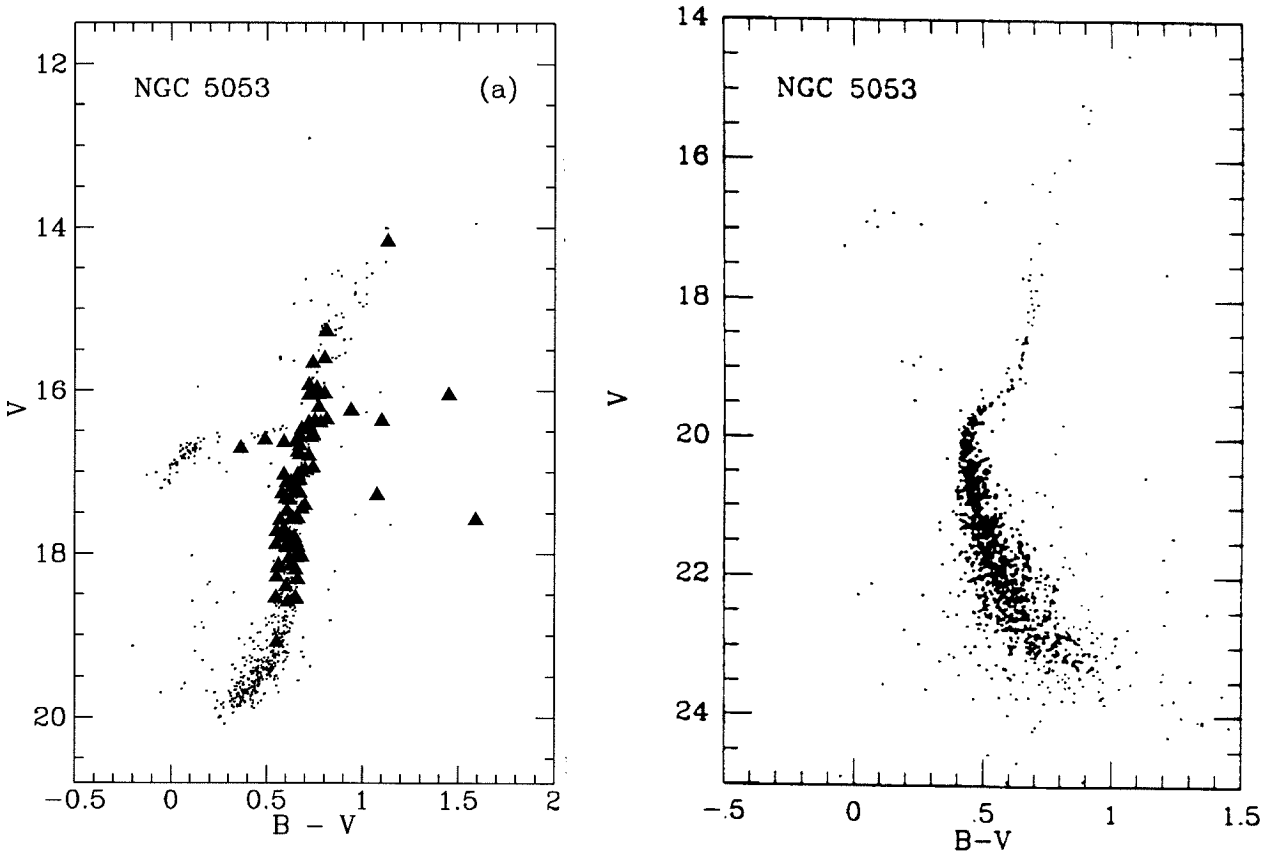

Figure 2.3: The Colour-Magnitude Diagram

The colour-magnitude diagrams of the cluster NGC 5053. In Figure 2.3(a), the solid triangles represent the stars in our sample including both cluster member and non-member stars. Figure 2.3(b) is a deeper HR diagram of the cluster showing a well-defined main sequence turnoff.

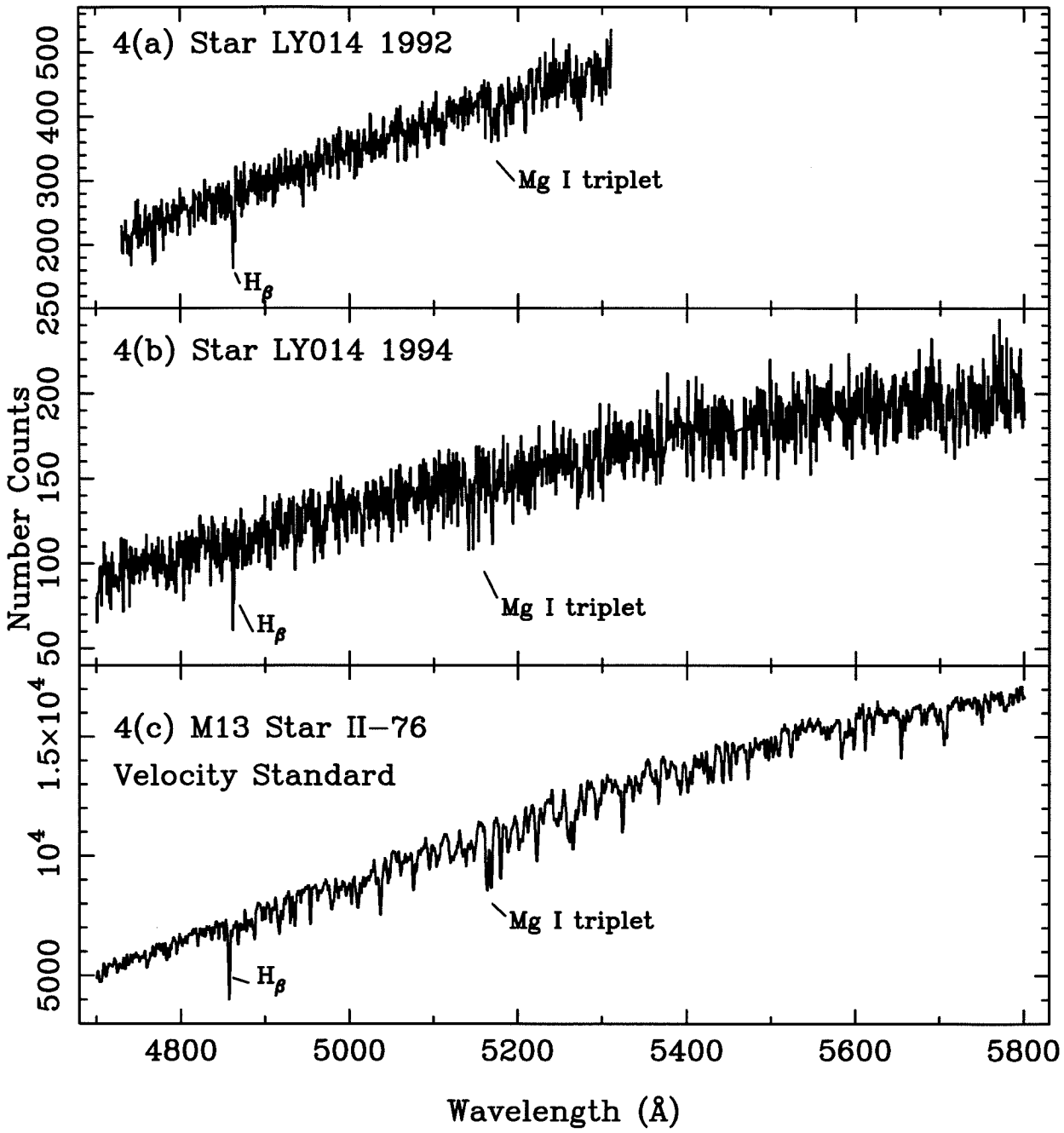

Figure 2.4: Exmaples of Spectra

Figures 2.4(a) and 2.4(b) show spectra of star LY014 with a typical signal-to-noise ratio taken in 1992 and 1994. Figure 2.4(c) is the spectrum of star II-76 in M 13 which serves as a radial velocity standard.

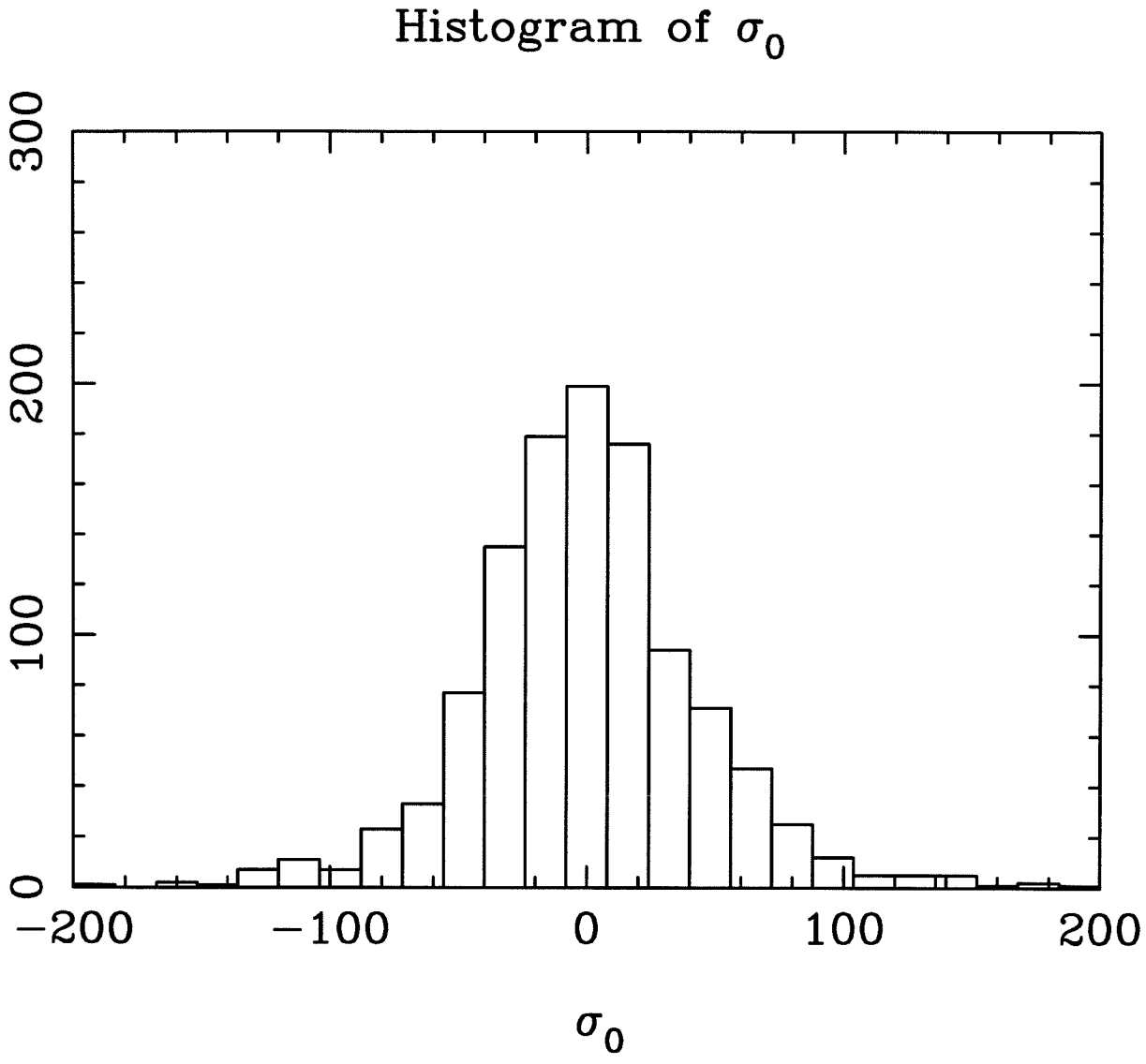

Figure 2.5: The Distribution of σ_0

The distribution of σ_0 (See the equation (2.6) in the text) derived from our data.

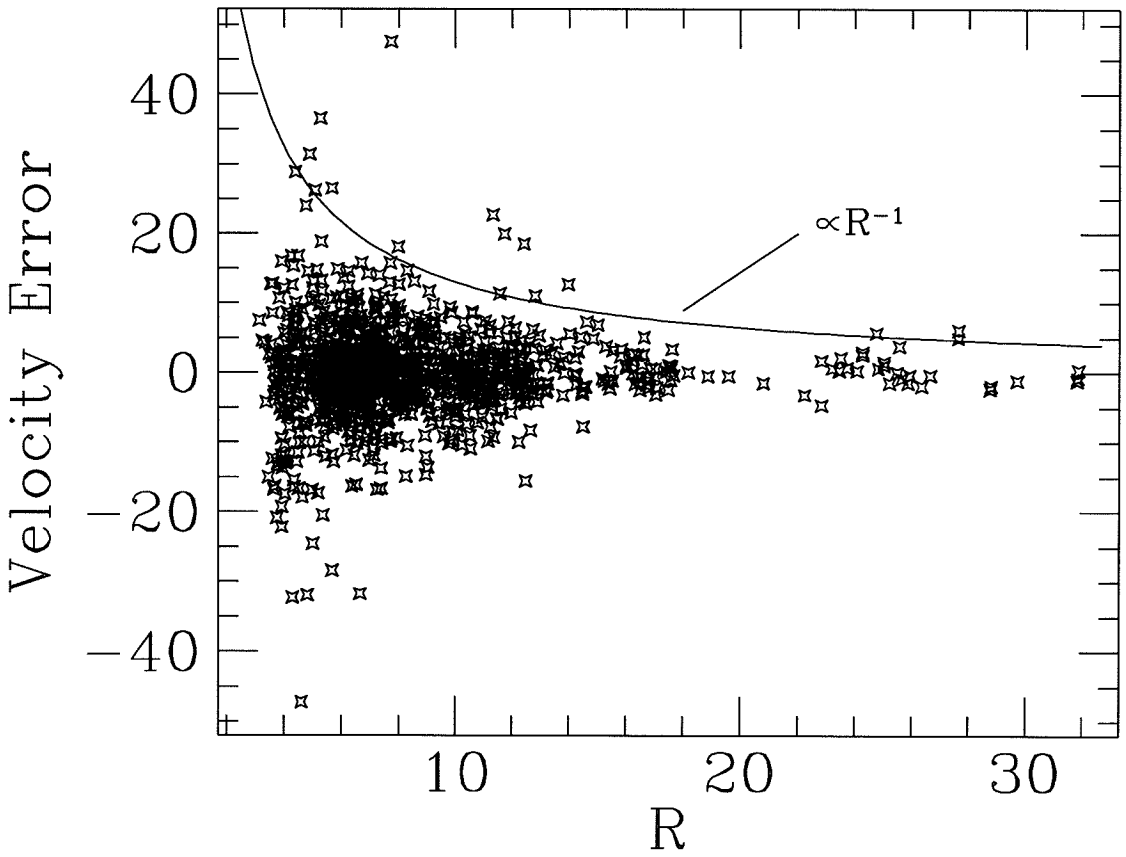

Figure 2.6: Velocity Error versus the Tonry & Davis Value R

The plot shows the velocity error versus the Tonry & Davis value R. The envelope of the velocity errors in the figure is roughly proportional to $\propto R^{-1}$, as described in Tonry & Davis (1979).

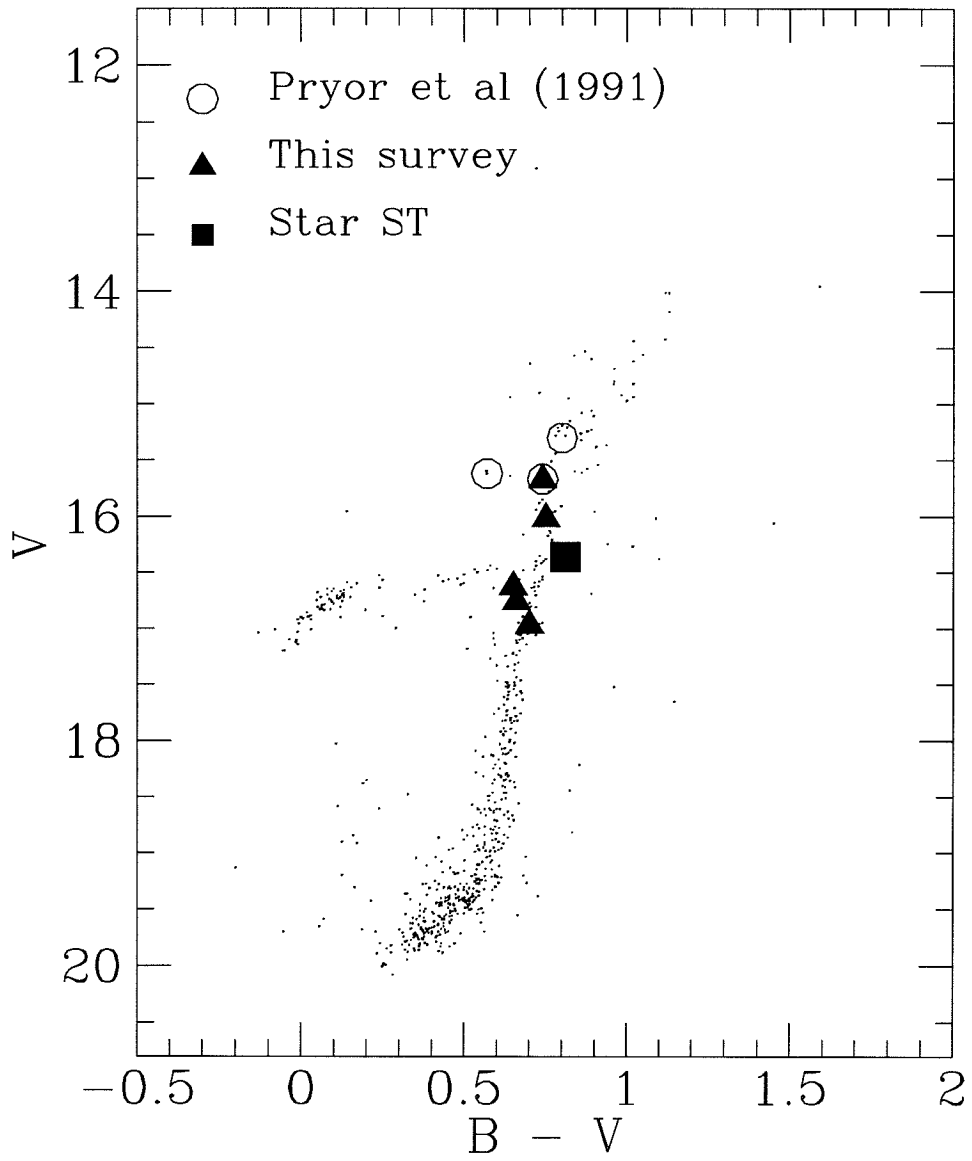

Figure 2.7: Colour-Magnitude Diagram

In this cluster colour-magnitude diagram, the solid triangles show the locations of the five binary candidates discovered in this survey, the solid square indicates the short period binary candidate ST, and the open circles represent the candidates found previously by Pryor et al. (1991).

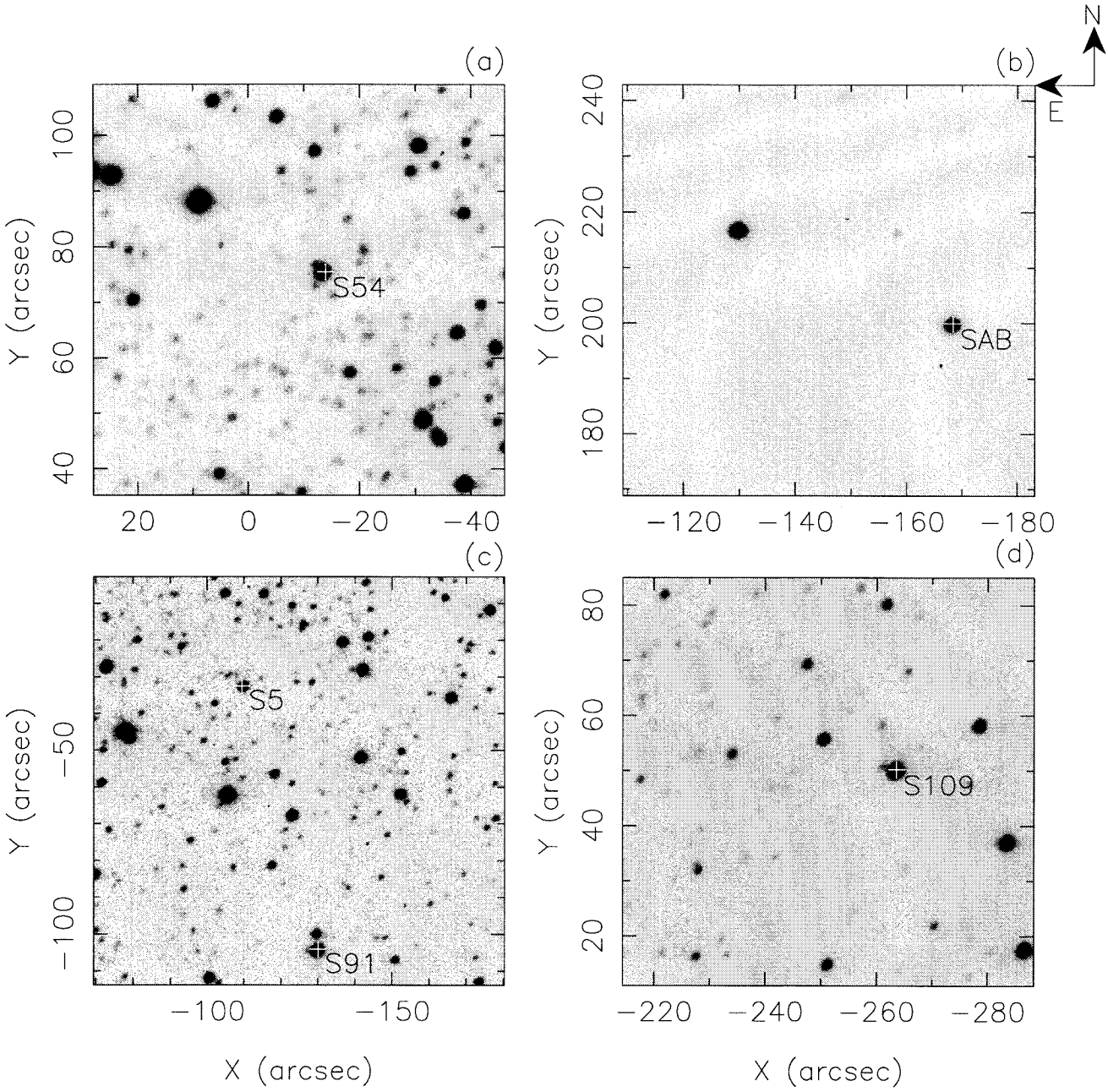

Figure 2.8: Finding Charts

The detailed finding charts for the five binary candidates. All objects are plotted relative to the position with RA (1950)=13:14:5.070 and DEC (1950)=17:56:38.00. The axes are in units of arcsecond and the north and the east are indicated in the plot.

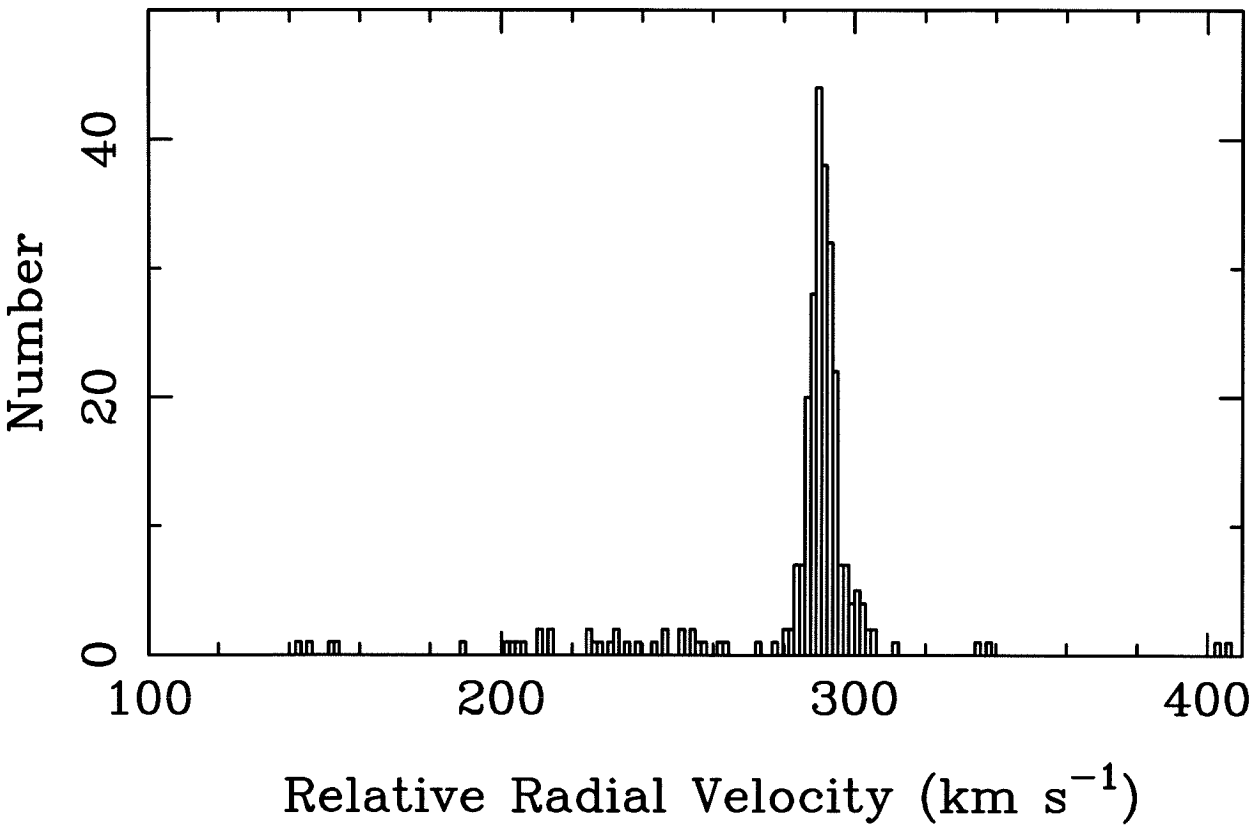

Figure 2.9: Histogram of Relative Radial Velocities

The histogram of all relative radial velocities measured in our survey including non-members of the cluster stars. Each bin is 1.55km s^{-1} wide. The majority of the stellar radial velocities distributed around the cluster relative velocity. Non-members of the cluster stars are clearly distinguished from the member stars by their radial velocities. Also notice that the dispersion around the mean radial velocity is only 3.7 kms^{-1} excluding the measurements from non-member stars and binary candidates.

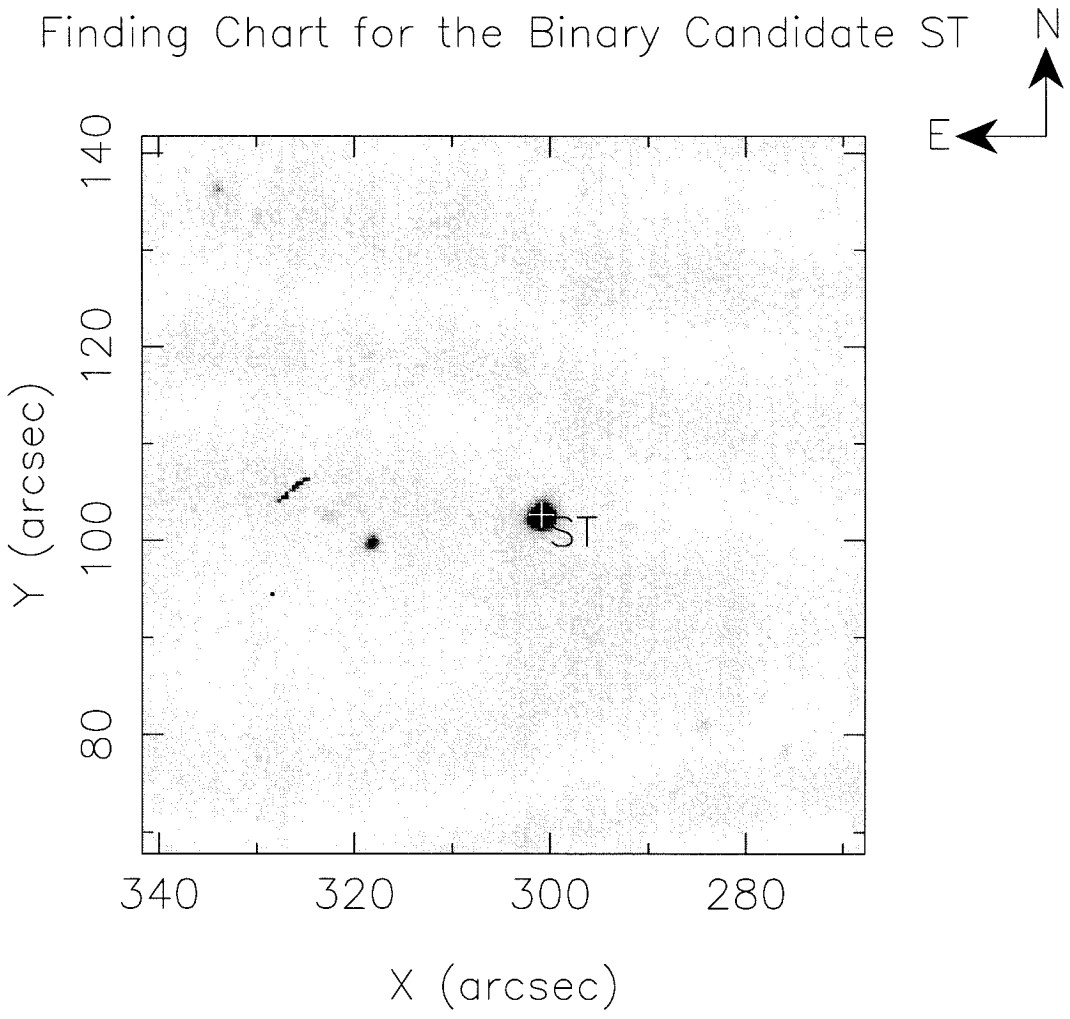

Figure 2.10: Finding Chart for Star ST

The detailed finding chart for the short period candidate ST.

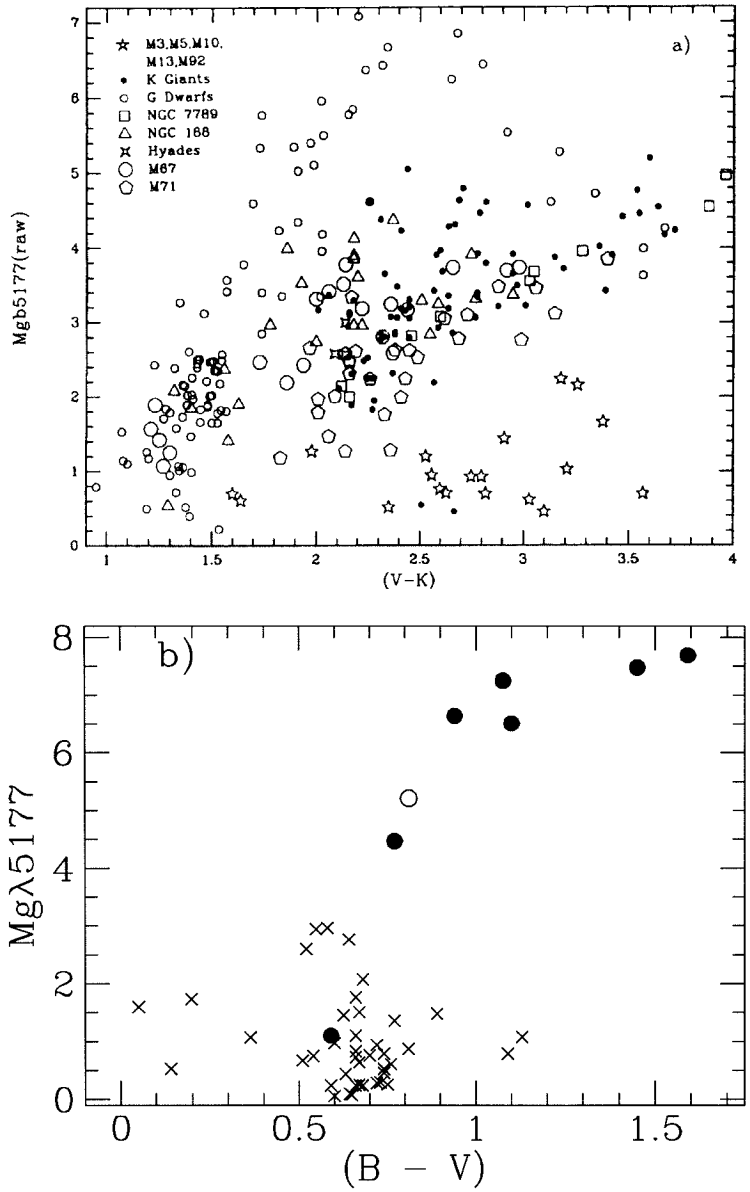

Figure 2.11: The Mgb Equivalent Width Versus Colour

Figure 2.11(a) is a plot of the equivelant width of the Mgb triplet versus (V - K) colour, taken from Gorgas et al. (1993). The different symbols represent stars from field, metal poor and rich globular clusters and open clusters, as explained in the figure. The stars from metal poor globular clusters are clearly segregated from others in the plot. Figure 2.11(b) is a similar plot of Mgλ5177 strengths versus (B - V) colours for all stars in our survey including non-cluster member stars. In the figure, the solid dots are for stars identified as non-cluster member stars using radial velocities, the crosses, the cluster member stars in our survey, and the open circle represents star ST.

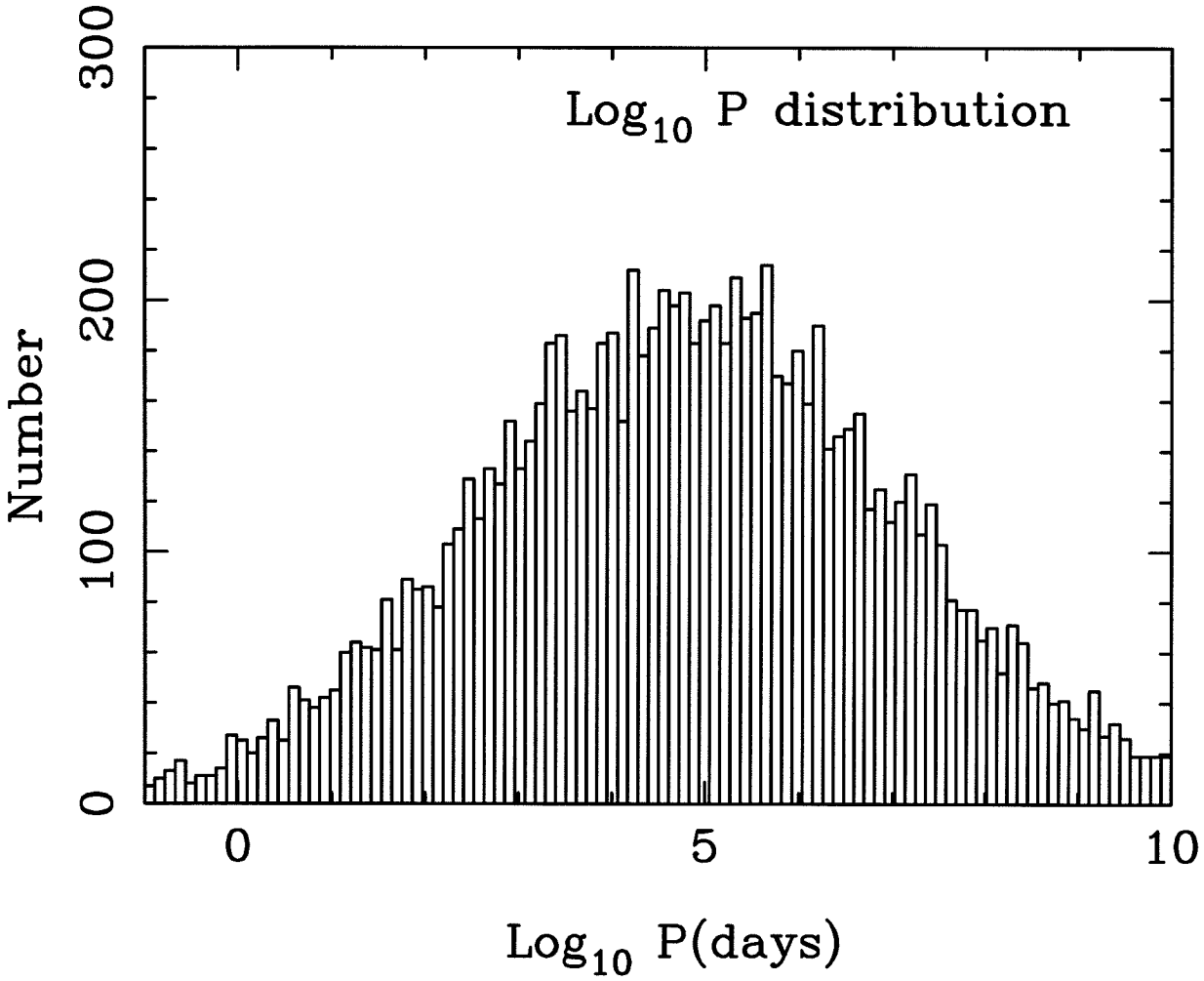

Figure 2.12: The Period Distribution

The logarithmic period distribution used in the simulations. Notice that the 1000 periods in the figure were generated using the function $f(\log_{10} P) = constant \times \exp\left(\frac{-(\log_{10} P - \mu)^2}{2\sigma^2}\right)$, here $\mu = 4.8, \sigma = 2.3$, and 0.1 d $\leq P \leq 10^{10}$ d. However, our survey is only sensitive to binaries which have periods between 4 days and 10 years.

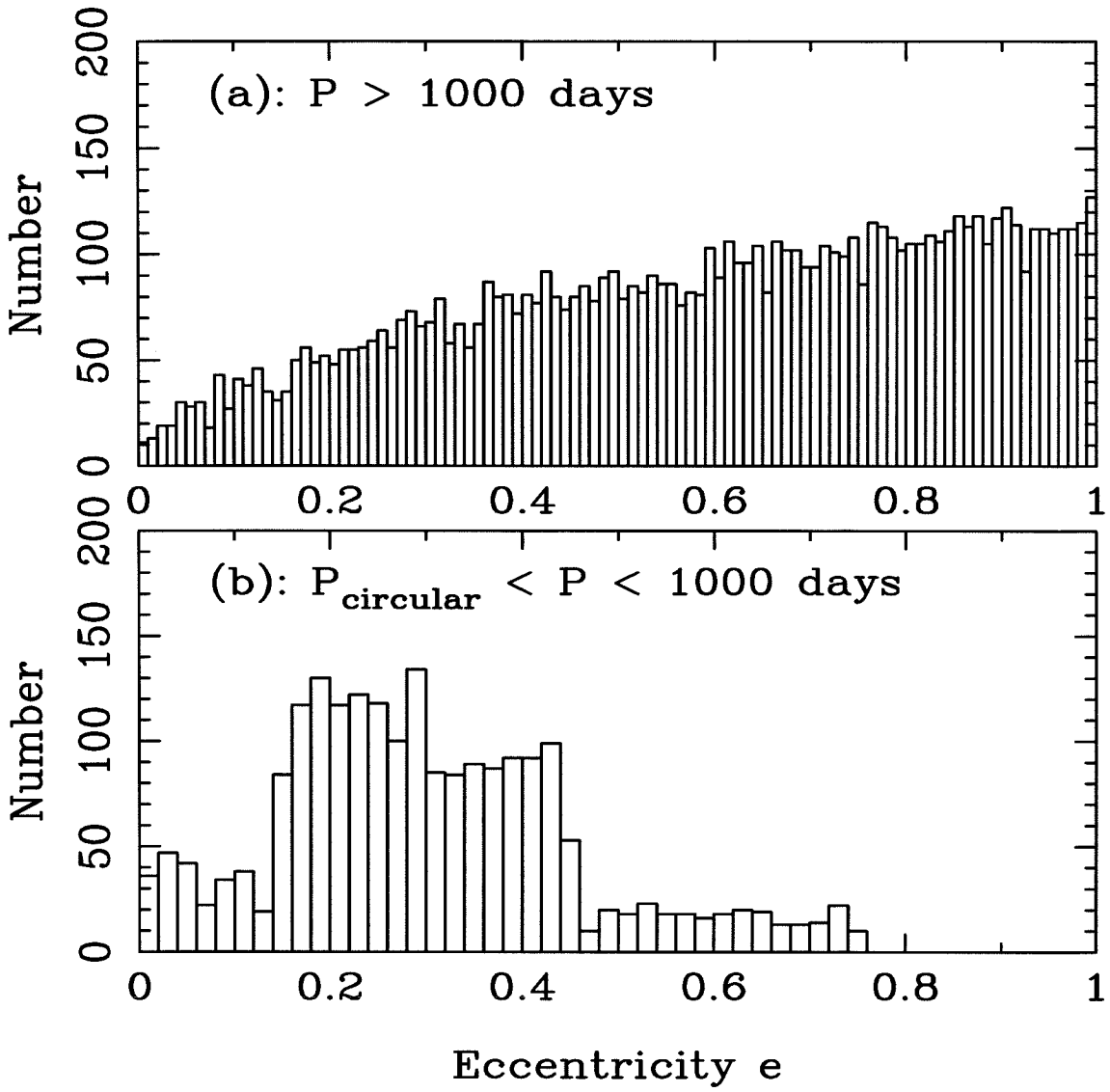

Figure 2.13: The Eccentricity Distribution

The eccentricity distribution used in the simulations. Here Figure 2.13(a) is for binary systems with periods longer than 1000 days, and Figure 2.13(b), for P_{circ} <P< 1000 days, with P_{circ} of ~11 days found among field G-dwarf type stars (Duquennoy & Mayor 1991). Figure 13(a) was produced using the function described in the text, and Figure 13(b) was generated numerically to match what was found in Duquennoy & Mayor 1991.

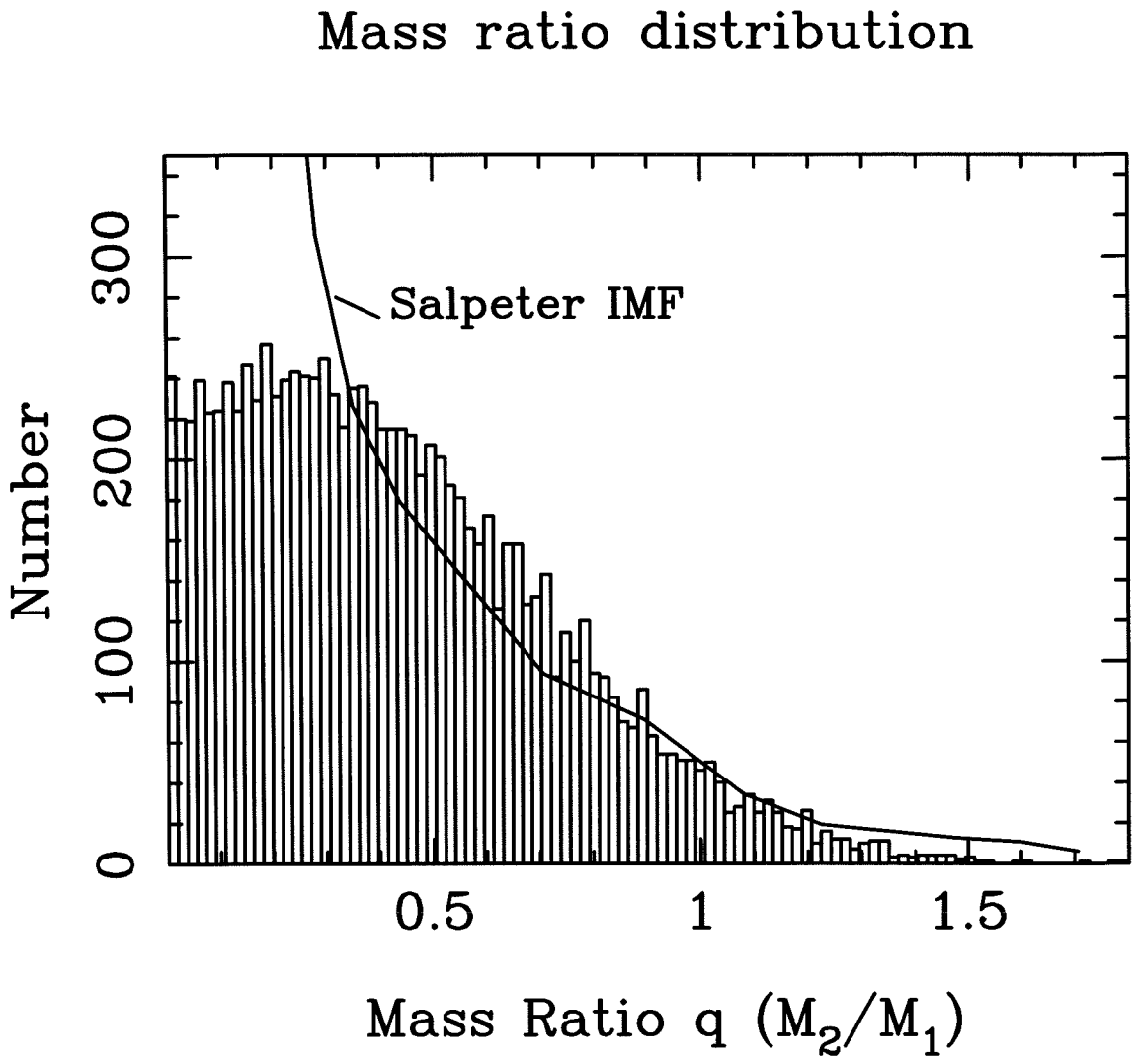

Figure 2.14: The Mass Ratio Distribution

The mass ratio distribution used in the simulations. The data in the figure were generated using the function $f(q) = constant \times \exp(\frac{-(q-\mu)^2}{2\sigma^2})$, where $q = M_2/M_1$, $\mu = 0.23, \sigma = 0.42$. In the plot the solid line indicates the Salpeter power law mass function with the power index of -2.35 ($\xi(m) \propto m^{-2.35}$). Notice that our survey is only sensitive to binary systems with mass ratios in the range of $0.125 \leq q \leq 1.75$.

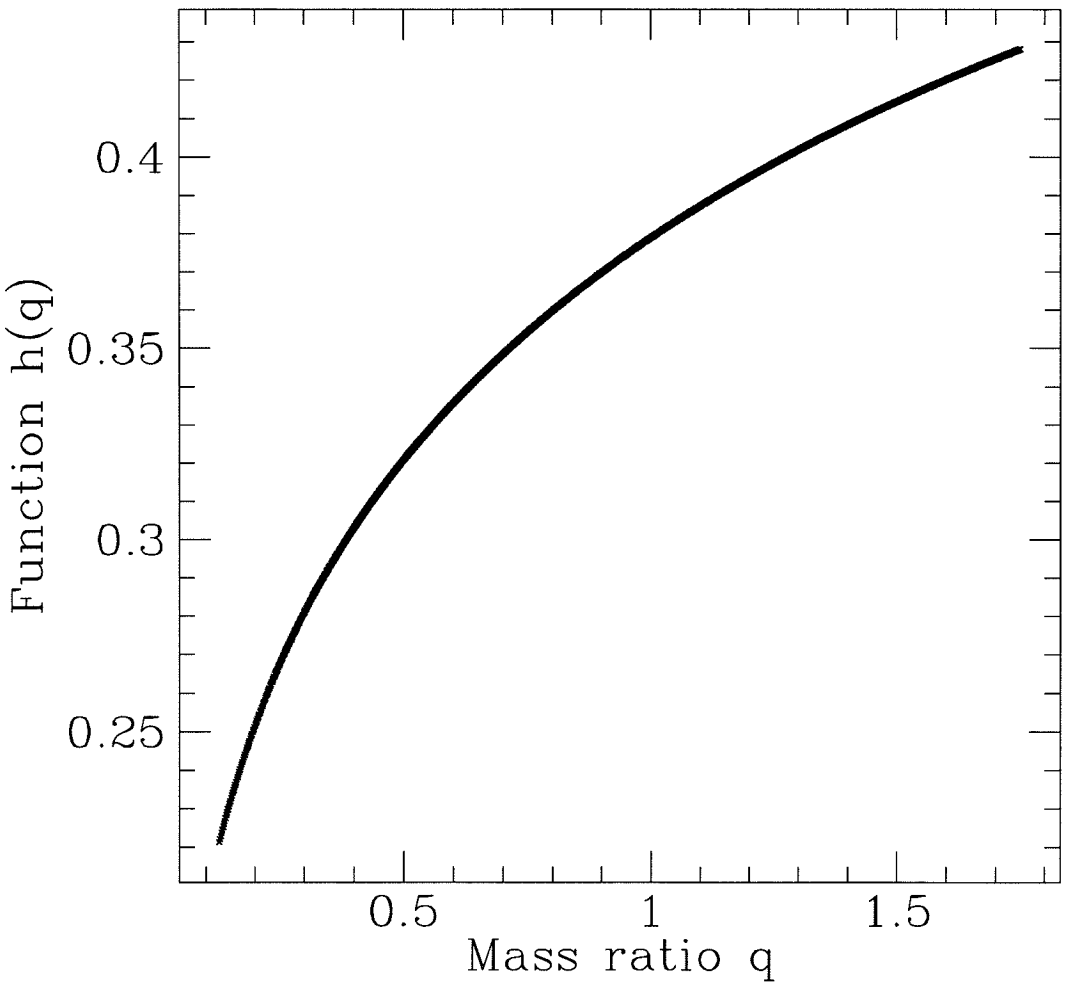

Figure 2.15: Critical Roche-lobe Radius Versus Mass Ratio

The critical Roche-lobe radius $a_{crit} = R/h(q)$; here R is the stellar radius. The plot shows the value h(q) as a function of mass ratio q. See the text for the definition of h(q).

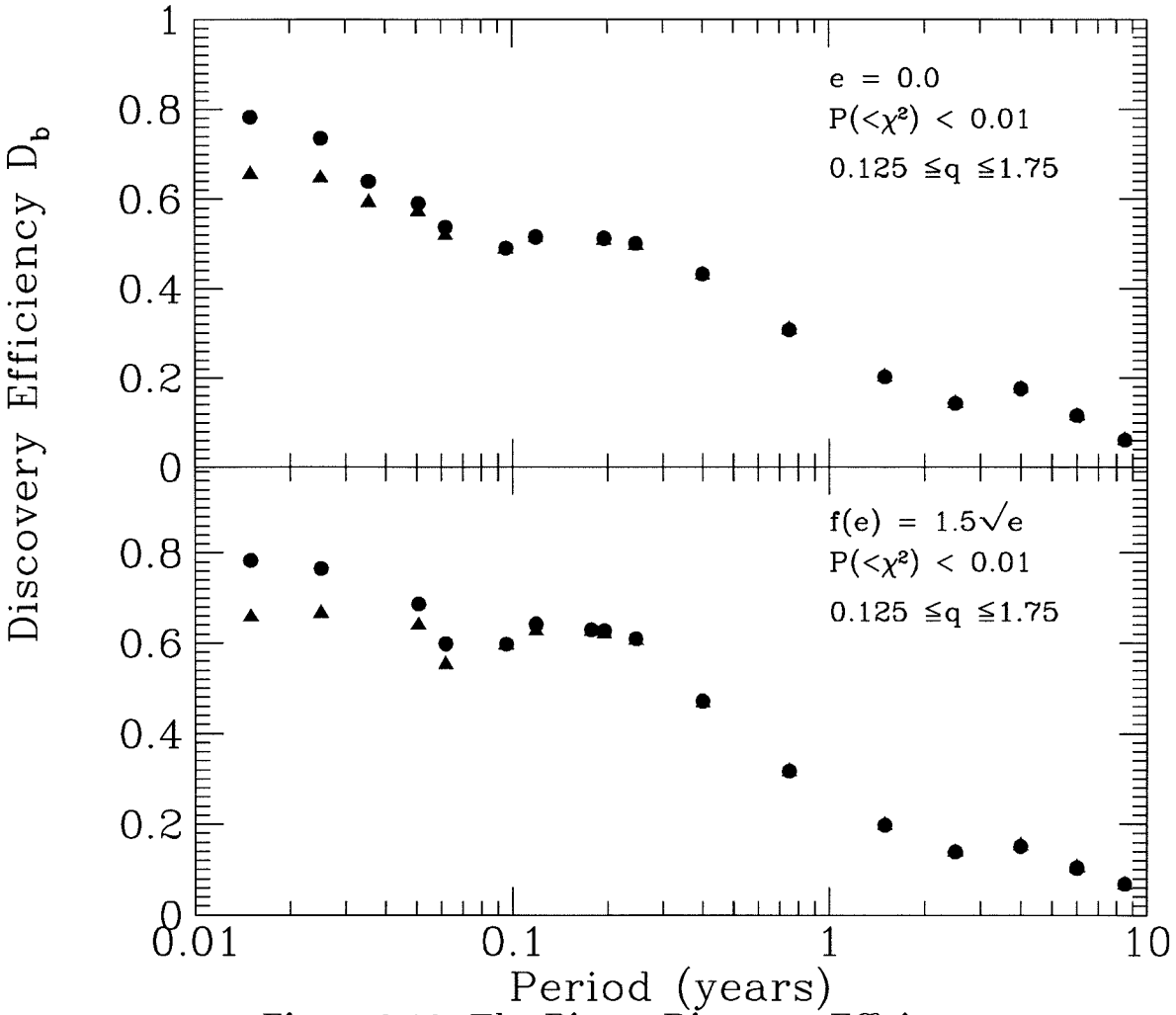

Figure 2.16: The Binary Discovery Efficiency

Figures 2.16(a) and 2.16(b) show the binary discovery efficiency D_b as a function of period P (in days) for two different binary models with circular orbits and with the eccentricity distribution $f(e) = 1.5\sqrt{e}$. In both figures the solid triangles and the solid dots represent the simulations with and without considering the mass transfer effect respectively. Clearly the effect of mass transfer is significant at the short period end. Note that each data point in the plots is the mean of 1000 simulation tries.

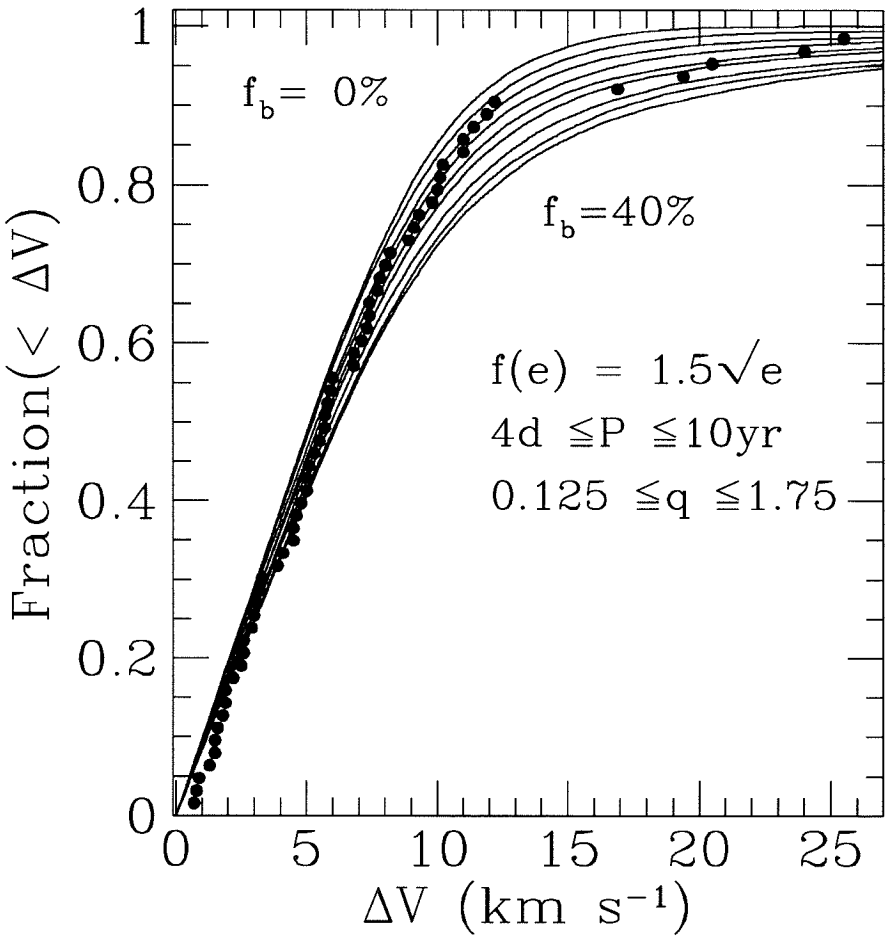

Figure 2.17: Cumulative Distributions of the Maximum Velocity Variations

Kolmogorov-Smirnov tests applied to both the synthetic velocity data and the actual data. The solid lines in the plot represent the cumulative distributions of the maximum velocity differences drawn from the synthetic data generated with binary frequency from 0% to 40% with a 5% interval. The solid dots are from the actual data.

Chapter 3

THE IMAGING SURVEY FOR SHORT PERIOD ECLIPSING BINARIES IN THE GLOBULAR CLUSTER M 71[†]

ABSTRACT

We report the identification of five short-period variables near the center of the metal-rich globular cluster M71. Our observations consist of multi-epoch VI CCD images centered on the cluster and covering a $6.3' \times 6.3'$ field. Four of these variables are contact eclipsing binaries with periods between 0.35 to 0.41 days; one is a detached or semi-detached eclipsing binary with a period of 0.56 days. Two of the variables were first identified as possible eclipsing binaries in an earlier survey by Hodder *et al.* (1992). We have used a variety of arguments to conclude that all five binary stars are probable members of M71, a result that is consistent with the low number (0.15) of short-period field binaries expected along this line of sight. Based on a simple model of how contact binaries evolve from initially detached binaries, we have determined a lower limit of 1.3% on the frequency of primordial binaries in M71 with initial orbital periods in the range 2.5-5 days. This implies that the overall primordial binary frequency, f, is 22% assuming $df/d\log P = const$ (the 'flat distribution'), or $f = 57\%$ for $df/d\log P = 0.032\log P + const$ as observed for G-dwarf binaries in the solar neighborhood (the 'sloped' distribution). Both estimates of f correspond to binaries with initial periods shorter than 800 yrs since any longer-period binaries would have been disrupted over the lifetime of the cluster. Our

[†] Adapted from a paper entitled "Primordial main sequence binary stars in the globular cluster M 71," by L. Yan & M. Mateo, published in 1994, AJ, 108, 1810.

short-period binary frequency is in excellent agreement with the observed frequency of red-giant binaries observed in globulars if we adopt the flat distribution. For the sloped distribution, our results significantly overestimate the number of red-giant binaries. All of the short-period M71 binaries lie within 1 mag of the luminosity of the cluster turnoff in the color-magnitude diagram despite the fact we should have easily detected similar eclipsing binaries 2−2.5 magnitudes fainter than this. We discuss the implications of this on our estimates of the binary frequency in M71 and on the formation of blue stragglers.

3.1. Introduction

Considerable recent effort has been devoted to understanding two issues intimately related to the binary star population in globular clusters. The first is the realization that a primordial binary frequency as small as 3% can fundamentally change the dynamical evolution of an entire globular cluster (Heggie and Aarseth 1992). The existence of binaries, and in particular primordial binaries, has been conclusively demonstrated by a number of direct observational techniques in many globular clusters (see the detailed review by Hut *et al.*, 1992). For a number of other clusters, theoretical modeling of their structural parameters has provided more indirect, but nonetheless compelling evidence for a significant primordial binary population. For example, Drukier *et al.* (1992) were unable to simultaneously explain the high degree of mass segregation and centrally flat surface density profile of M71 (Richer & Fahlman 1989) using dynamical models which did not include primordial binaries. These authors concluded that unaccounted effects associated with stellar evolution and, more importantly, primordial binaries are probably required to understand the dynamical evolution of M71.

The second important issue related to binary stars in globular clusters is the problem of the origin of blue stragglers. A variety of mechanisms have been proposed to explain how blue stragglers are formed in star clusters (see recent reviews by Stryker 1993, and Livio 1993). One mechanism – mass transfer between the components of short-period main sequence binary stars – is directly supported by observations. The discovery of short period eclipsing binaries among blue stragglers in the ultra-low density globular cluster NGC 5466 (Mateo *et al.* 1990) provides evidence that the progenitors of at least some globular cluster blue stragglers are short-period interacting binary stars. Short-period binaries on the main sequence of a cluster are destined to become blue stragglers when either a) the primary gains enough mass to push it over the turnoff mass, or b) the cluster turnoff mass evolves below the mass of the primary or the merged binary remnant.

In this paper we present results of a new survey for faint variable stars in the field of M71. The primary goal of the survey is to significantly increase the number of main sequence globular cluster stars that have been surveyed for short-period binaries (the meager data available are described in section 5.1 and Hut *et al.* 1992). A photometric search for binary stars in M71 was reported by Hodder *et al.* (1992) who concluded that the cluster may contain two short-period binaries among its most luminous main sequence stars. The Hodder *et al.* (1992) database was limited in both time and area coverage and they were unable to determine periods for these two suspected binaries. This paper reports a much more extensive photometric survey for main sequence stars in M71. The results of this paper supersede an earlier report in Hut *et al.* (1992).

We specifically chose M71 for our study for several reasons. First, the cluster is known to contain an abundant population of blue stragglers (Richer and Fahlman 1988), as well as the two candidate main sequence binaries identified by Hodder *et al.* (1992). A long-term radial velocity study of red giants in M71 (by C. Pryor and collaborators; see Hut *et al.* 1992 for details) has uncovered direct evidence for longer-period binaries among the evolved stars in the cluster. Second, M71 has a central density of 630 $M_{\odot}/\mathrm{pc}^{-3}$ and a concentration parameter $c \equiv \log(r_t/r_c) = 1.3$, values that qualify it as a 'low-density' globular cluster (Djorgovski, 1993). Third, the low central surface density ($\Sigma_V = 18.9$ mag arcsec^{-2}) of M71 permits us to obtain high quality photometry even near the cluster core. Finally, M71 is one of the closest globular clusters, an important consideration for a search for main sequence photometric binaries in the cluster. The one serious disadvantage of M71 is that it lies close to the Galactic plane and field-star contamination is potentially a significant problem.

3.2. Observations and Data Reduction

We obtained 362 Johnson V and Gunn i CCD images of M71 with the the Palomar 1.5m telescope during 4 nights in 1991, and 11 nights in 1993 (see Table 1). Of these frames, 328 were of sufficiently high quality to be useful for this study. Two different Tektronix 1024×1024 CCDs were used during the course of this study. Every image covers an area of $6.3' \times 6.3'$ with a scale of 0.37 arcsec per pixel and was centered on the cluster. Exposure times were either 300 or 600 sec in V and i, depending on the brightness of the sky and amount of cloud cover. We typically spent about 4 hours taking sequential images of M71, alternating between V and i. The seeing was typically $1.3''$, though some of the best frames contain $0.9''$ images. A summary of the observation log is shown in Table 1. A complete log listing the times of every exposure is provided in Table 2 which is available in the CD-ROM supplement to this journal.

The processing of the raw data was performed using IRAF. All frames were trimmed and bias-subtracted using standard procedures. Median-averaged sky flats were used to flatfield the data. The processed images typically exhibit much less than 1% sky background variations across the whole chip. The stellar photometry was performed using the two-dimensional photometry reduction program DoPHOT (Schechter *et al.* 1993). This program uses an analytic, position-independent point spread function (PSF) to determine relative photometry of stars on a CCD image; this is appropriate for our purpose since there is no significant PSF variation across any of our cluster frames. For each CCD image, DoPHOT determines the positions, magnitudes and errors of all the stars it finds. Some of these 'stars' do not correspond to actual objects in the sky, but rather regions excess flux, diffraction spikes or scattered light in the wings of bright stars, cosmic rays, unflattened CCD defects, *etc.* We designed a simple algorithm to efficiently filter out such objects. This algorithm identified 'false' detections as objects with significantly larger errors than the mean error of other stars of similar brightness. We monitored a grand total of about 7000 stars in our M71 field.

The following steps were used to search for variable stars in our data set. First, we transformed the positions of the stars measured on every CCD image to a common CCD coordinate system. One good-seeing frame was chosen to define this master coordinate system and transformations were determined using the positions of numerous bright stars common to most of the frames. These transformations typically consisted of small shifts in both axes for CCD frames obtained during the same run as the master frame. For frames acquired during other runs, a small rotation was also needed. The typical rms of the transformations was less than 0.01 pixel in both coordinates.

Second, we transformed all of the photometry to a common photometric system. Because the photometric conditions differed significantly from night to night, and because we used two different CCDs, our data are not photometrically homogeneous. We therefore chose the best-seeing frames in each band to define a master photometric reference system (hereafter the master frame). For every star we then identified a set of "local comparison stars" consisting of nearby isolated stars with good-quality photometry. The photometric offset for any star was the median magnitude difference calculated for its local comparison stars relative to the photometry of the same stars on the master frame. We had originally devised this method of calculating photometric offsets in order to handle data with a significantly varying PSF. Although a significantly variable PSF was *not* seen in the present data, this procedure appeared to work well and provided consistent photometric offsets for most frames.

Third, we compiled lists of the instrumental V and i magnitudes for each star in the field where each entry corresponds to the observed instrumental magnitude (on a common system) at each epoch. We used only the positions of stars to match objects from different frames. A matching tolerance of about 0.3 arcsec effectively avoided all false matches.

Fourth, candidate variables were identified using the reduced chi-squared, which is defined as $\chi^2_\nu = (1/\nu)\sum_i (m_i - \overline{m})/\sigma_i^2$, where ν is the number of degrees of freedom, m_i is the measured magnitude at epoch i, $\overline{m}$ is the mean magnitude of the star, and σ_i is the Dophot-supplied formal error of the ith observation. Figure 1 shows a plot of χ^2_ν as a function of I magnitude; every star with $\chi^2_\nu \geq 5.0$ was checked for variability. We also demanded that every candidate was measured on at least 40% of frames in each color (Figure 1 only includes stars that fulfill this criterion). Most of the stars with $\chi^2_\nu > 5.0$ turned out to be non-variable; their large values of χ^2_ν generally resulted from just one or two spurious measurements.

We further restricted our candidate variables to those with strong evidence for *periodic* variability. To do this, we used the period-finding algorithm described by Lafler and Kinman (1965) and determined possible periods for every candidate variable in the range 0.02-5 days. We then visually examined the phased light curves to confirm periodicity and the adopted period. All *bona fide* variables were required to show evidence for variability at the same period in both colors. We identified five variables discovered in our M71 field that satisfied these criteria. The phased V and I light curves for these stars are shown in Figures 2 and 3, respectively. Stars M71-V3 and M71-V4 were identified as possible eclipsing systems by Hodder *et al.* (1992), though they were unable to derive periods.

Our procedure to identify variables was sufficiently stringent that we may have missed some variables with amplitudes comparable to the variables plotted in Figure 2. To quantify this we performed a series of experiments in which we added a set of false variable stars into one quadrant of 70 I-band images (43 frames from the run during July 5 to 12, 27 frames from the run during July 20 to 24) from our dataset. We added 20 false variables in three narrow magnitude ranges (I = 17.3, 18.3, and 20.3; we shall refer to these as sets A, B, and C, respectively). Each variable was assumed to have a light curve similar to V3, the star with the smallest photometric amplitude. Our recovery rates were 90%, 85%, and 50% for sets A, B, and C,

respectively, where a 'recovery' corresponds to the unambiguous detection of the variable with a light curve and period identical (to within the observational errors) to the input values. These recovery rates are probably slightly underestimated since we did not use all of the frames in the false-star tests, and we restricted ourselves to just one color. We conclude that our search is complete for all periodic variables with periods in the range 0.05 - 5 days, V and i amplitudes $\gtrsim$ 0.25 mag, and I $\lesssim$ 19.5, and 50-75% complete to I $\sim$ 20.5. The 5-day upper limit is an estimate based on the fact that eclipsing systems with periods longer than this become *much* harder to detect in surveys such as ours (see Mateo 1994 for a more detailed discussion of this point). Not surprisingly, crowding is a major factor in variable detectability. For each set of false variables, we primarily missed the stars located closest to the cluster center.

We calibrated the photometry by observing 18 standards (Landolt 1992) during a photometric night of the 1993 July 5-12 run. The following equations were derived from these observations to transform that night's instrumental magnitudes to the Cousins VI system:

$$V = V_{inst} - 0.058(V - i)_{inst} - 0.24X - 0.336 \tag{3.1}$$

$$(V - I) = 1.058(V - i)_{inst} - 0.10X + 0.261. \tag{3.2}$$

Here X is the airmass, and the instrumental magnitude in the equation is normalized to the magnitude of 1 second exposure. All of the coefficients in equation 3.1 were derived from our observations; no mean extinction coefficients or transformation slopes were assumed. The rms of the photometric transformation equation is less than 0.015 mag.

The master frames were not obtained on the same night that the standards were observed. Thus, we transformed the photometry of the master frames by using the now-calibrated photometry of a number of bright, uncrowded stars in the M71 field. This allowed us to transform the light curves of the variables to the standard Cousins

system. In this last step we did not assume the colors of the variables were constant. Rather, we used the light curves to determine the (V−I) color at the appropriate phases. For example, for a given V-band observation we estimated the instrumental i-band magnitude by interpolating that light curve at the corresponding phase. We were able to determine the instrumental colors precisely because of the excellent sampling of the light curves of all the variables.

The V and I light curves in Figures 2 and 3 were all calibrated using this procedure and a complete listing of the photometry for each variable can be found in Table 2, which is available in the CD-ROM supplement to this journal. A wide-field identification chart showing the locations of the variables is shown in Figure 4, while detailed charts of each variable star are presented in Figure 5. Table 3 provides the ephemerides for the five eclipsing systems.

3.3. Results

Figure 6 shows the CM diagram of M71 derived from our data. For $I \gtrsim 17$, the points were derived by averaging the photometry from the 20 best-seeing Vi CCD pairs in our data set. Brighter stars are saturated on good-seeing frames, so the data plotted in Figure 6 for $I \lesssim 17$ were measured on a single poor-seeing pair of Vi images. The main sequence turnoff is visible in Figure 6 at $I \sim 16.8$, while brighter than this a split is seen between the redder M71 subgiants, and blue field stars and blue stragglers. The filled squares in Figure 6 show the locations of the five eclipsing binary stars. The magnitudes and colors for each variable plotted in Figure 6 correspond to the maximum-light values derived from the phased light curves (Figures 2 and 3).

Star M71-V3, with a period of 0.37386(5) days, and star M71-V4, with a period 0.55615(6) days, were previously identified as possible eclipsing binaries and designated H3 and H4, respectively, by Hodder *et al.* (1992), though these authors

were unable to obtain periods for either stars. The two other variables discovered by Hodder *et al.* (1992) were either too bright (H1) or were located too close to a saturated star (H2) to be reliably measured on our CCD images.

Four of the variables have light curves typical of W UMa type contact eclipsing binaries. Such systems are composed of components that both fill their critical Roche surfaces, forming a common envelope of approximately constant temperature. The shape and depths of the two eclipses of a W UMa type binary are typically similar despite having mass ratios far from unity. M71-V3 shows a strong O'Connell effect, widely believed to be due to an uneven distribution of starspots over the surfaces of the two stars in the binary (Davidge and Milone 1984). The light curve of M71-V4 is qualitatively different from the other eclipsing binaries. Although it is clearly an eclipsing system, the two eclipses have very different depths, indicating that the two components have unequal effective temperatures. M71-V4 is almost certainly a detached or semi-detached Algol-type eclipsing binary system.

Table 3 lists the fundamental properties of the five new variables in M71. In this table, I_{Amp} is the maximum I-band amplitude, $\langle I \rangle$ is the I magnitude at maximum light, $\langle V - I \rangle$ is the intensity-weighted mean color, $\langle I_0 \rangle$ is the reddening-corrected value of $\langle I \rangle$, and $\langle (V - I)_0 \rangle$ is the extinction-corrected mean color. We have adopted E(B−V) = 0.28 (Hodder *et al.* 1992) and the reddening relations of Cardelli *et al.* (1989) for $R = A_V/E(B - V) = 3.1$. For this value of R, $A_I = 0.61 A_V = 0.53$ mag, and E(V−I) = 1.20 E(B−V) = 0.34 mag. The equatorial coordinates of the five variables have been tied to the system defined by Cudworth (1985) and are listed in Table 3.

3.4. Cluster Membership

Without proper motion or radial velocity data we cannot definitively determine whether the variable stars in our sample are members of M71 (the Cudworth 1985

proper motion study does not reach to faint enough magnitudes to include any of these variables). Even with velocities, the relatively low heliocentric velocity of M71 (22 km s^{-1}; Peterson and Latham 1986) would make it difficult to unambiguously assign cluster membership. Because of the limited telescope time, we were not able to obtain comparable observations of a control field to measure the number of eclipsing binaries along the line of sight near the cluster. However, we have identified two indirect ways to estimate how many of the variables might be field stars.

A first test of membership involves estimating the absolute magnitude of each binary using the method described by Mateo *et al.* (1990). For the contact binaries, the procedure involves estimating the mass ratio and orbital inclination from the observed light curve of a given binary. This can be done rather precisely for our well-sampled light curves using the Fourier analysis described by Rucinski (1993). Because the stars fill (or even slightly overfill) their critical Roche surfaces, we can calculate their radii from the Roche criterion, Kepler's third law, and the orbital period for an assumed total binary mass. Since the surface temperatures of both components are similar (due to efficient energy transfer through the 'neck' connecting the two stars at the inner Lagrangian point; see Rucinski 1985), we can directly estimate the total luminosity of the system using the relation $L_{tot} = \sigma T_{eff}^4 4\pi(R_1^2 + R_2^2)$, where σ is the Stefan-Boltzmann constant.

The most uncertain parameter in this procedure is the total binary mass. We have taken the range in the mass to be $M_{MS} \leq M_{tot} \leq M_{max}$, where M_{MS} is the mass of a single star in M71 that has the same luminosity as the binary, and $M_{max} = M_{MS}(1+q)$, where $q = M_2/M_1$ is the binary mass ratio, and $M_1 \geq M_2$. We used the models of VandenBerg and Bell (1985) to estimate M_{MS} from the cluster CM diagram (Figure 6). For a fixed orbital period the total luminosity scales as $M_{tot}^{2/3}$; thus we do not need an extremely precise estimate of the total binary mass. Finally, we used the VandenBerg and Bell (1985) models to estimate the temperatures of the binaries using their (V−I) colors. Our results agree well

with the temperatures derived using the Böhm-Vitense (1981) temperature scale for $\log Z/Z_{\odot} = -0.7$ after correcting the (V−I) colors to (B−V) with the VandenBerg and Bell (1985) models. The precision of the photometric transformations (0.015 mag; section 3.2) and the color variations exhibited by each contact system (0.01-0.03 mag in (V−I)) implies that the uncertainties in our temperature estimates are about ±3%, or ±0.15 mag in the distance modulus.

Table 4 lists the various parameters used and derived in this analysis. The most important result for this discussion is the estimate of the distance modulus of *each* contact binary. It is clear that for all four stars the moduli derived in this manner are consistent with cluster membership (the distance modulus of the cluster is 12.8 ± 0.3; Richer and Fahlman 1988).

A more involved process is needed to estimate the distance for M71-V4. Because this star is an Algol binary, we cannot make the simplifying assumption that its components have similar effective temperatures. Again, we follow the procedure outlined by Mateo *et al.* (1990) to analyze the light curve of the Algol system in NGC 5466. In summary, there are two possible scenarios that can account for the light curve of M71-V4. Either the primary eclipse results from a transit eclipse (in which case the larger star is the hotter star), or it is due to an occultation eclipse (the smaller star is the hotter component in this case). The high-quality light curve of M71-V4 allows us to directly calculate the radii of the stars if we assume a total mass. Again, the luminosity scales as $M_{tot}^{2/3}$ so our mass estimate does not have to be very precise. We adopted the range M_{tot} = 0.7-1.4 $M_{\odot}$. In all other respects the present analysis is the same as in Mateo *et al.* (1990). Table 5 lists the various parameters used and derived to estimate the luminosity of M71-4. Both the transit and occultation geometries result in distance moduli for M71-V4 which are fully consistent with cluster membership.

A second method of determining cluster membership is to use the recent calibration of the absolute magnitudes of contact binaries (Rucinski 1994) to estimate

the luminosities of the four contact systems in our sample. Table 6 lists the absolute magnitudes and distance moduli derived in this way. These results are perfectly consistent with cluster membership for each contact binary.

How are these distance estimates affected by the fact that M71 is somewhat more metal-poor than the stars used by Rucinski (1994) to establish his calibration? From the colors of VandenBerg's (1985) models we estimate $\Delta(\mathrm{V}-\mathrm{I})/\Delta \log Z \sim 0.15$ for main sequence stars with $Y = 0.25$. This means that the M71 binaries (for which we assume $\log(Z/Z_{\odot}) \sim -0.7$) are about 0.1 mag bluer in (V−I) compared to identical binaries with solar metallicity. This translates into absolute magnitudes that are 0.3 mag too luminous using Rucinski's (1994) calibration. The final column in Table 6 lists the distance moduli of the M71 binaries corrected for metallicity in this manner. Once again, we find that the distance estimates are consistent with cluster membership for each of these binaries.

We conclude that the individual properties of the five M71 binaries imply that they are all members of the cluster. Moreover, the expected number of binaries in our M71 field is sufficiently low that it is reasonable to suppose that *none* of the binaries in our sample are field stars.

3.5. Discussion

3.5.1. The Distribution of the Binaries in the CM Diagram

The most striking feature of the distribution of binaries in the CM diagram of M71 (Figure 6) is that they are all located within 1 mag of the main sequence turnoff (*i.e.*, $\mathrm{I} \lesssim 17.8$). This is puzzling because our false star tests indicate that we should have easily detected similar binaries to $\mathrm{I} \sim 20$. This implies that some physical mechanism concentrates short-period systems near the cluster turnoff luminosity. We shall refer to this phenomenon as the 'crowding effect'.

One possible explanation of the crowding effect is that the present locations of the binaries in the CM diagram are considerably different than their original locations, possibly due to binary mass exchange. Consider M71-V5 ($q \sim 0.2$). If it first came into contact when it was a binary with a mass ratio of unity, the present-day primary is about 70% more massive than before (assuming no mass loss). For $Z = 0.003$ and $Y = 0.23$, $\Delta \log L / \Delta \log M = 5.4$ along the main sequence (VandenBerg and Bell 1985). If this relation applies to the primary in V5, then the system was about $0.5 \times 1.7^{5.4} = 2.5$ magnitudes fainter before mass transfer commenced (the factor 0.5 takes into account the equal luminosities of the two stars in the original configuration). M71-V5 has the most extreme mass ratio of the binaries in the sample (see Table 4), so the luminosity excursions of the other stars would be even smaller. The maximum change in luminosity occurs when $q_{initial} = 1.0$; for smaller initial mass ratios the primary's gain in mass – and therefore luminosity – is smaller. We conclude that the brightening expected as a result of binary evolution can only partially account for the crowding effect.

Another obvious possibility is that the M71 binaries came into contact (or in the case of V4, underwent mass transfer) as a direct result of the evolutionary expansion of the primary. Four of the binaries are located near the cluster turnoff where the radii of the primaries are 90% larger than they were when the stars were on the main sequence (VandenBerg and Bell 1985). If this is the correct explanation of the crowding effect, then some or all of the short-period binaries in M71 may have evolved into contact systems more rapidly than predicted by the magnetic braking model (Vilhu 1982, 1992; Guinan and Bradstreet 1988; Eggen and Iben 1989). We shall discuss this further in section 3.5.5.

Another striking feature of Figure 6 is the large separation of M71-V3 from the principal sequences in the CM diagram. Similar binaries have been identified in other clusters. The open clusters NGC 188 and Be 39 (Kaluzny and Shara 1987; Kaluzny *et al.* 1993) and the globular cluster NGC 4372 (Kaluzny and Krzeminski 1993)

each contain contact systems that lie in similar locations relative to the cluster main sequences, so M71-V3 is not unique in this respect. As noted in section 3.3, M71-V3 exhibits a strong O'Connell effect, probably due to starspots. The anomalous photometric properties of this star (assuming it is a cluster member) may be related to its unusually strong surface activity. Of course, M71-V3 may simply be a field star. This is not inconsistent with our earlier arguments because the distribution of contact systems has a broad peak centered nearly at the distance of the cluster. Even though the expected number of contact systems in the field is small (0.11), one can of course never rule out the possibility that one field binary would show up in our survey.

3.5.2. The Spatial Distribution of the Binaries

The M71 eclipsing binaries do not show any significant central concentration. This is partly an illusion since these stars are actually located between 0.1 to 0.3 tidal radii of the cluster center. In addition, the increased crowding near the center reduces the recovery efficiency in that region of the CCD images; this is confirmed by our false-star experiments described in section 3.2. We conclude that we cannot meaningfully comment on the degree of concentration or mass segregation exhibited by the binaries in M71.

3.5.3. Are the Short-Period Binaries in M71 Primordial?

One mechanism of forming contact binaries involves braking torques from magnetized stellar winds in tidally synchronized systems. This idea has been explored by many people (Huang 1967, Vilhu 1982, 1992; Guinan and Bradstreet 1988; Eggen and Iben 1989); the most detailed models suggest that binaries with initial orbital periods in the range 2.5-5 days may evolve into a contact configuration on a timescale of 5-15 Gyr. Is it plausible that the short-period binaries we find in M71 formed in this manner from primordial binary systems?

To answer this we adopt a central density of the globular cluster M71 of 631 $M_\odot$ pc^{-3} and a central velocity dispersion of 2.3 km s^{-1} (Peterson and Latham 1986). The timescale for destroying binaries with periods less than 2.5-5 days and component masses of 0.7 $M_\odot$ exceeds 10^{11} yrs (Hills 1984), considerably longer than the age of the cluster. This calculation considers only binary-single star encounters; the cross-section for dynamical interactions with primordial wide binaries is considerably larger (Leonard and Fahlman 1991; hereafter LF).

There are two possible ways in which interactions with wide binaries could significantly affect the evolution of short-period systems. First, short-period binaries may be *destroyed* during encounters with wider systems. However, Hills (1984) showed that when a binary interacts with another star at a relative velocity that is less than the binary orbital velocity, the binary becomes tighter. Interactions with wide binaries (which will have considerably smaller orbital velocities) would actually tend to harden short-period systems, hastening the formation of contact binaries (Hills 1990).

The second option is that the short-period binaries in M71 were *formed* during wide-binary interactions. The typical time between binary encounters in the core of M71 for systems with maximum orbital semi-major axes of 100 AU is $\tau_{bb} \sim 6\times10^7$ yrs (we derived this by scaling the relation for τ_{bb} from LF for a binary frequency of 0.25; see section 3.5.4). At least 70 encounters must occur before a single short-period binary is formed during the interaction of passing wide binaries (LF), taking into account that the maximum stable binary orbital period in M71 is $\sim$ 800 yrs (Hills 1984). Thus, a total of 3-4 short-period binaries would have been expected to form in M71 during wide-binary encounters. The actual rate is lower since we adopted the parameters for the *core* of M71. Since τ_{bb} scales as $n^{-2}\sigma^{-1}$ (n is the number density of binaries and σ is the velocity dispersion), the average rate is considerably lower outside the core of M71. M71 is probably a pre-core-collapse cluster (Chernoff and Djorgovski 1989; Drukier *et al.* 1992), so the rate was probably even lower in the

past. If contact systems survive for $\sim 10^9$ yrs (see section 3.5.4), the entire quota of collisionally manufactured short-period binaries in M71 would have had to form during the past 7% of the age of the cluster to account for the observed systems. This seems unlikely and we conclude that most – possibly all – of the short-period binaries in M71 evolved from primordial binaries with 2.5-5 day initial periods (though see section 3.5.5).

3.5.4. The Primordial Binary Frequency of M71

As discussed in section 3.2, we have monitored approximately 7000 stars for variability in our M71 field. Of these, we estimate 1700 are foreground or background stars based on our photometry of a control field located about one degree from the cluster at the same Galactic latitude. Thus, a lower limit to the primordial binary frequency in M71 is $5/5300 = 0.09\%$. This limit is 0.08% if only the contact systems are considered and 0.06% if we assume one of the contact systems (most likely M71-V3) is a field star (see section 3.5.1). For this discussion we will adopt 0.07% which is equivalent to giving M71-V3 half weight in our calculation of the observed short-period binary frequency.

Vilhu (1982; 1992), Guinan and Bradstreet (1988), and Eggen and Iben (1989) argue that magnetic braking will cause a detached binary with an initial orbital period of 5 days to evolve into a contact system with a period of 0.34 days in about 14 Gyr, the age of M71 (Richer and Fahlman 1988 using the VandenBerg and Bell 1985 models). If we assume the shortest orbital periods of primordial binaries in M71 was 2.5 days (this is the shortest period observed in zero-age binary populations studied by Giuricin *et al.* 1984, Matheiu *et al.* 1989, and Bodenheimer *et al.* 1993), magnetic braking would have caused such binaries to evolve into contact in 3-6 Gyr.

The lifetimes of contact binaries are extremely uncertain; estimates range from 10^8 to 10^{10} yrs, depending on assumptions regarding the relevant angular momentum loss mechanisms (van't Veer 1979; Rahunen 1981; Eggen and Iben 1989). Most

studies seem to favor $\tau_{\rm contact} \sim 1 \times 10^9$ yrs which we adopt. Thus, for every 5300 main sequence stars in M71 one new contact binary must be formed each 3×10^8 yrs to account for the 3.5 observed contact systems. Over the 10 Gyr period during which contact systems could have formed in M71, about 33 stars out of the 5300 main sequence stars in our sample would have evolved into observable systems like the ones we identified. This number should be doubled to account for systems that remain undetected because of unfavorable inclinations (Hut *et al.* 1992). These assumptions and our observations imply a primordial binary frequency of 1.3% for systems with initial periods of 2.5-5 days.

To estimate the total binary frequency, we assume that the distribution of binaries is given by

$$\frac{df}{d\log P} = k \log P + \beta_0, \tag{3.3}$$

where f is the binary frequency, and k and β_0 are constants. We will assume throughout this discussion that only binaries with orbital periods less than 800 yrs can survive star-star interactions in the cluster (Hills 1984). For $k = 0$ (a flat binary frequency distribution) our observations imply an overall binary frequency of 22% in M71.

This result is consistent with the observed frequency of spectroscopic binaries among globular cluster red giants. Pryor (see Hut *et al.* 1992) reports that of 393 red giants monitored in six clusters (including M71), nine are radial velocity variables and are almost surely binaries. This survey is capable of unambiguously identifying binaries with periods ranging from about 0.5-20 yrs with an efficiency of $\sim$ 33%; thus, 27 of 393 (7%) of the red giants in these clusters are probable binaries with periods in this range. For $k = 0$ (equation 3.3), the 1.3% frequency of short-period eclipsing systems that we derived above implies that 7% of the red giants should be binaries with periods between 0.5-20 yrs, in excellent agreement with the red giant observations.

Duquennoy and Mayor (1991) recently derived a log-normal frequency distribution for G-dwarf binaries in the solar neighborhood. For periods $\lesssim$ 800 yrs their results can be adequately described by equation 3.3 if $k = 0.032$ (we have assumed their one star with $\log P < 0.0$ evolved from a system with a period longer than 1 day). For this case the primordial binary frequency in M71 for 2.5 days $\leq P \leq$ 800 years is 57%. For the period range 0.5-20 yrs, the binary frequency is 19%, in rather poor agreement with the red giant results.

For $k = 0$ in equation 3.3, an overall binary frequency of 10% (again, for 2.5 days $\leq P \leq$ 800 yrs) corresponds to our having observed 1σ too many contact systems, while the upper limit (1σ too few systems were observed) is 48%. The corresponding range in the predicted red-giant binary frequency for $k = 0$ is 3-15%. For $k = 0.032$ the lower and upper limits on the overall binary frequency are 49% and 72%, respectively, while the 1σ range in the predicted frequency of red-giant binaries is 16-24%, significantly larger than presently observed. We tentatively conclude that the existing data on short-period and red giant binaries favor a flat frequency-period distribution ($k = 0$ in equation 3.3) over the distribution given by Duquennoy and Mayor (1991).

A significant primordial binary population in M71 may help explain the apparent contradictions discussed by Drukier *et al.* (1992). Specifically, Fokker-Planck models of a post-core-collapse cluster without binaries (Drukier *et al.* 1992) produces a central surface density that is steeper than observed, while a pre-core-collapse model reproduces the observed surface density profile, but does not account for the mass segregation reported by Richer and Fahlman (1989). Moreover, for this model the present dynamical configuration of M71 is uncomfortably short-lived. Drukier *et al.* (1992) emphasize that a large population of primordial binaries may provide the heat source needed to maintain the observed low-density core.

3.5.5. Latent Blue Stragglers: Implications for the Primordial Binary Frequency

The short-period binaries described in this paper (see also Mateo & Krzeminski 1990; Kaluzny & Krzeminski 1992; Hut *et al.* 1992) are reminiscent of the eclipsing blue stragglers found in NGC 5466 by Mateo *et al.* (1990; see Mateo 1993 for a census of other eclipsing blue stragglers in globular clusters). Regardless of how they arrived in a contact or near-contact configuration, the components of contact binaries are doomed to merge eventually into a single star (Webbink 1976). If the final merged remnant has a mass that exceeds the cluster turnoff, the star will immediately be seen as a blue straggler in the cluster. If the combined mass of the merged star is below the cluster turnoff mass, the star will remain 'hidden' on the main sequence as a 'latent' blue straggler (LBS). M71-V3 and M71-V5 will probably become LBS when their components merge.

One new clue that M71 may be providing for the study of blue stragglers is related to the crowding effect described in section 3.5.1. There we concluded that contact systems may form only when the more massive component of a short-period binary starts to evolve off the main sequence (this is closer to the scenario originally envisioned by Webbink 1976). This may help explain the apparent contradiction posed by the existence of hot blue stragglers in clusters such as NGC 5466. Such stars are not believed to have sufficiently strong winds to drive the magnetic braking mechanism that Eggen and Iben (1989) and Mateo *et al.* (1990) argued might be crucial to form blue stragglers. Perhaps it is only due to the evolutionary expansion of the primary that such stars form contact systems and ultimately merge and form blue stragglers or LBS. This may also help explain why blue stragglers are not fast rotators compared to other stars of similar spectral types (Peterson *et al.* 1984).

Secular and global gravitational instabilities may also significantly alter the late stages of evolution of close binaries (Rasio 1994; Lai *et al.* 1994), and in particular hasten the final stages of merging in contact and even pre-contact binaries. Such

instabilities are *more* effective for lower-mass main sequence stars. Thus, an additional part of the explanation of the crowding effect may involve the depletion of contact binaries among lower-luminosity stars.

If evolutionary and gravitational instability effects accelerate the formation of contact systems, the present-day binaries in M71 may have arisen from primordial systems with initial periods longer than the 5-day upper limit we derived from magnetic braking alone (see section 3.5.3); the observed binary frequency corresponds to a wider primordial-binary period range than we assumed in section 3.5.4. This would be offset by the fact that the contact-binary lifetimes would also be shorter and so the observed number of contact systems represent a larger number of primordial systems. The models describing these effects are too uncertain to be able to determine which effect dominates, and our estimate of the primordial binary frequency based on contact systems is an over- or underestimate of the true global frequency.

3.6. Summary and Conclusions

We have obtained time-series CCD photometry of a $6.3' \times 6.3'$ field centered on the globular cluster M71 and have identified five faint variables in the field of the cluster. Four of these stars are contact binary systems of the W UMa type; one is a short-period Algol binary; one appears to be a periodic variable of unknown type. Two of these stars were suspected to be binaries by Hodder *et al.* (1992) based on their smaller-scale photometric survey of the cluster. We have used a variety of arguments to conclude that all five binaries in our sample are likely to be members of M71 although we cannot rule out that one of the stars is a field star superimposed on the cluster.

If the M71 binaries represent the final stages of evolution of initially detached binaries whose components have come into contact via magnetic braking (Vilhu 1982), they correspond to primordial binaries with initial orbital periods in the range 2.5-5

days. This implies a global binary frequency of $f = 22\%$ for binaries with periods ranging from 2.5 days to 800 years. if $k = 0$ in equation (3.3). For a binary period distribution consistent with G-dwarf binaries in the solar neighborhood (Duquennoy and Mayor 1991), we derive an overall binary frequency for M71 of $f = 57\%$. For $k = 0$, our results are consistent with the frequency of spectroscopic binaries observed among red giants in globular clusters, including M71 itself. However, for the Duquennoy-Mayor case, we significantly overestimate the number of red-giant binaries. We tentatively conclude that a flat ($k = 0$ in equation 3.3) frequency-period relation is most consistent with existing constraints on the period distribution of binaries in M 71.

All of the M71 binaries are located in a fairly narrow luminosity range just below the luminosity of the main sequence turnoff. One possible implication of this 'crowding effect' is that some effect – normal stellar evolution and/or gravitational instabilities – accelerate the evolution of initially detached systems into contact binaries or merged stars. If so, the contact binaries in M71 may have evolved from systems with initial periods longer than 5 days. If gravitational instabilities are important, the lifetime of the contact stage would be shorter than expected from a simple model of angular momentum loss. Reliable calculations of these effects are needed to determine how the crowding effect alters our estimate of the overall binary frequency in M71.

A number of additional observations of M71 and other globular clusters would be useful to extend the results of this study. First, a careful effort to monitor the M71 blue stragglers may help elucidate the nature of the relationship between blue stragglers and short-period binaries. The M71 blue stragglers were generally saturated in our data set so we have obtained no useful information regarding their variability. Second, further surveys of fainter stars in M71 will test the reality of the crowding effect. Additional searches for main sequence short-period binaries in other clusters are needed to extend the results presented here and obtain meaningful

statistics on the phenomenon. It is important to emphasize that future studies must provide detailed information on both the numbers of binaries found and the number of cluster stars that were monitored. It is important to stress that statistically significant null results are equally important as positive detections in understanding of the binary frequencies of globulars.

On the theoretical side, two major areas must be studied in greater detail. First, do interactions of wide binaries really lead to the formation of bound, short-period systems such as the contact systems found in M71? The results of hydrodynamic models of stellar collisions (Benz and Hills 1987; Goodman and Hernquist 1991) suggest that collisions lead promptly to stellar mergers; it is not at all clear that contact systems can really be formed via stellar collisions. Second, the 'theory' of how detached systems evolve into a contact configuration through magnetic braking is, at best, crude. Advances in this area are needed to a) improve the interpretation of the ages of contact systems into initial orbital period, and b) provide better estimates of the lifetimes of contact systems. The effects of metallicity on these timescales is also obviously relevant for globular clusters.

Photometric binaries are likely to become the most common type of binary star known in globular clusters. Future work should strive to optimize how we can use these objects to reliably constrain the primordial binary frequencies in globular clusters, an advance that will greatly improve our understanding of the dynamical evolution of these majestic stellar systems.

We thank the Palomar staff for their help during this project. MM was partially supported by a Hubble Fellowship through grant HF-1007.01-90A awarded to STScI which is operated by AURA for NASA under contract NAS5-26555, and by NSF grant AST-9223968. DoPHOT was developed by Paul Schechter with the support of NSF grant AST83-18504. LY acknowledges the financial support from the Palomar Observatory and NSF grant AST-9123646. We thank the referee for the constructive suggestions, which has helped us to improve the paper.

REFERENCES

Benz, W. & Hills, J. G. 1987, ApJ, 323, 614

Bodenheimer, P., Ruzmaikina, T. & Mathieu, R. D. 1993, in *Protostars and Planets III*, eds. E. H. Levy, J. I. Lunine (Tucson: University of Arizona Press), p. 367

Böhm-Vitense, E. 1981, ARA&A, 19, 295

Cardelli, J. A., Clayton, G. C. & Mathis, J. S. 1989, ApJ, 345, 245

Chernoff, D. F. & Djorgovski, S. 1989, ApJ, 339, 904

Cudworth, K. 1985, AJ, 90, 65

Davidge, T. J. & Milone, E. F. 1984, ApJS, 55, 571

Djorgovski, S. G. 1993, in *Structure and Dynamics of Globular Clusters*, eds. S.G. Djorgovski & G. Meylan (San Francisco: A. S. P.), 373

Drukier, G. A., Fahlman, G. G. & Richer, H. B. 1992, ApJ, 386, 106

Duquennoy, A. & Mayor, M. 1991, A&A, 248, 485

Eggen, O. J. & Iben, I. 1989, AJ, 97, 431

Giuricin, G., Mardirossian, F. & Mezzetti, M. 1984, ApJS, 54, 421

Goodman, J. & Hernquist, L. 1991, ApJ, 378, 637

Guinan, E. F. & Bradstreet, D. H. 1988, in *Formation and Evolution of Low Mass Stars*, eds. A. K. Dupree and M. T. V. T. Lago (Dordrecht: Kluwer), 345

Heggie, D. C. & Aarseth, S. J. 1992, MNRAS, 257, 513

Hills, J. G. 1984, AJ, 89, 1811

Hills, J. G. 1990, AJ, 99, 979

Hodder, P. J. C., Nemec, J. M., Richer, H. B. & Fahlman, G. G. 1992, AJ, 103, 460

Huang, S. S. 1967, ApJ, 150, 229

Hut, P., McMillan, S., Goodman, J., Mateo, M., Phinney, E. S., Pryor, C., Richer, H. B., Verbunt, F. & Weinberg, M. 1992, PASP, 104, 981

Kaluzny, J. & Krzeminski, W. 1993, MNRAS, 264, 785

Kaluzny, J., Mazur, B. & Krzeminski, W. 1993, MNRAS, 262, 49

Kaluzny, J. & Shara, M. M. 1987, ApJ, 314, 585

Lafler, J., Kinman, T. D. 1965, ApJS, 11, 216

Lai, D., Rasio, F. A. & Shapiro, S. L. 1994, ApJ, 423, 344

Landolt, A. 1992, AJ, 104, 430

Leonard, P. J. T. & Fahlman, G. G. 1991, AJ, 102, 994

Livio, M. 1993, in *Blue Stragglers*, ed. R. Saffer (San Francisco: A. S. P.), 3

Mateo, M. 1993, in *Blue Stragglers*, ed. R. Saffer (San Francisco: A. S. P.), 74

Mateo, M., Harris, H. C., Nemec, J. & Olszewski, E. W. 1990, AJ, 100, 469

Mateo, M. & Krzeminski, W. 1990, BAAS, 22, 1284

Matheiu, R. D., Walter, F. M. & Myers, P. C. 1989, AJ, 98, 987

Peterson, R. C., Carney, B. W. & Latham, D. W. 1984, ApJ, 279, 237

Peterson, R. C. & Latham, D. W. 1986, ApJ, 305, 645

Rahunen, T. 1981, A&A, 102, 81

Rasio, F. A. 1994, Mem Soc Astron It, in press

Richer, H. B. & Fahlman, G. G. 1988, ApJ, 325, 218

Richer, H. B. & Fahlman, G. G. 1989, ApJ, 339, 178

Rucinski, S. M. 1985, in *Interacting Binary Stars*, eds. J. E. Pringle, and R. A. Wade (Cambridge: Cambridge University Press), 113

Rucinski, S. M. 1993, PASP, 105, 1433

Rucinski, S. M. 1994, AJ, 107, 738

Schechter, P. L., Mateo, M. & Saha, A. 1993, PASP, 105, 1342

Stryker, L. L. 1993, PASP, 105, 1081

VandenBerg, D. A. 1985, ApJS, 58, 711

VandenBerg, D. A. & Bell, R. A. 1985, ApJS, 58, 561

van't Veer, F. 1979, A&A, 109, 17

Vilhu, O. 1982, A&A, 109, 17

Vilhu, O. 1992, in Evolutionary Processes in Interacting Binary Stars, eds. Y. Konda, R. F. Sisteró, and R. S. Polidan (Dordrecht: Kluwer), 61

Webbink, R. F. 1976, ApJ, 209, 829

Table 1 - Summary of Observations

Date	UT Range hh:mm	N_v	N_i	Exp. Time sec
1991 June 7/8	07:19-11:37	11	10	600
1991 June 8/9	07:30-11:35	11	10	600
1991 Aug. 18/19	03:30-07:38	11	11	600
1991 Aug. 19/20	04:57-07:41	7	8	600
1993 June 23/24	07:42-11:44	16	15	300
1993 June 24/25	07:59-11:34	17	16	300
1993 July 5/6	07:29-11:33	18	18	300
1993 July 6/7	06:25-11:22	14	12	600
1993 July 7/8	08:59-11:34	11	10	300
1993 July 8/9	08:46-11:28	8	7	600
1993 July 9/10	09:13-11:37	11	10	300
1993 July 10/11	09:12-11:34	6	5	600
1993 July 11/12	08:44-11:30	7	6	600
1993 July 21/22	04:08-11:42	31	16	600
1993 July 22/23	07:04-11:53	20	9	600
Total		199	163	

Note: N_V and N_i are the number of V and i images obtained in each sequence. Some of the frames were not used in the analysis described in this paper; see section 3.2.

Table 2(a) – Johnson V band Photometry Data for the Six Short Period Variables in M71

No	HJD days	ET sec	V1	V2	V3	V4	V5
1	2448415.811379	600.0	99.999	18.170	19.361	18.092	99.999
2	2448415.830824	600.0	18.294	17.920	19.179	18.476	99.999
3	2448415.882216	600.0	18.686	17.801	19.075	17.981	99.999
4	2448415.899578	600.0	18.845	17.853	19.111	17.900	99.999
5	2448415.923885	600.0	18.755	17.893	19.117	17.896	99.999
6	2448415.940553	600.0	18.499	18.084	19.168	17.890	99.999
7	2448415.957220	600.0	18.382	18.357	19.215	17.881	99.999
8	2448415.973888	600.0	18.319	18.461	19.316	17.868	99.999
9	2448415.990556	600.0	18.264	18.353	19.375	17.862	99.999
10	2448416.819075	600.0	18.405	17.843	19.196	17.857	99.999
11	2448416.838520	600.0	18.327	17.863	19.112	17.874	99.999
12	2448416.847549	600.0	18.274	18.348	19.189	17.896	99.999
13	2448416.855188	600.0	99.999	17.934	19.134	17.859	99.999
14	2448416.872550	600.0	18.274	18.137	19.125	17.878	99.999
15	2448416.905885	600.0	18.366	18.248	19.296	17.923	99.999
16	2448416.921858	600.0	18.483	18.046	19.374	18.087	99.999
17	2448416.938526	600.0	18.696	17.939	19.304	18.411	99.999
18	2448416.955888	600.0	18.796	17.860	19.157	18.647	99.999
19	2448416.972556	600.0	18.719	17.825	19.129	18.498	99.999
20	2448416.989223	600.0	18.468	17.813	19.137	18.157	99.999
21	2448487.653574	600.0	99.999	99.999	19.116	17.923	17.890
22	2448487.711362	600.0	99.999	99.999	19.149	17.873	18.047
23	2448487.719509	600.0	99.999	17.930	19.132	17.903	18.152
24	2448487.727704	600.0	99.999	99.999	19.224	17.882	18.281
25	2448487.752090	600.0	99.999	99.999	19.288	17.867	18.316
26	2448487.768443	600.0	99.999	99.999	19.374	17.868	18.202
27	2448487.784762	600.0	99.999	99.999	19.362	17.872	18.142

28	2448487.818083	600.0	99.999	99.999	19.161	17.894	17.942
29	2448488.722294	600.0	18.310	99.999	19.278	18.345	18.094
30	2448488.738265	600.0	18.275	17.826	19.137	18.074	18.208
31	2448488.754885	600.0	18.266	17.783	19.124	17.933	18.289
32	2448488.771170	600.0	99.999	17.776	19.105	17.906	18.265
33	2448488.787419	600.0	99.999	17.779	19.117	17.898	18.139
34	2448488.803761	600.0	99.999	17.819	19.110	17.871	18.033
35	2448488.819999	600.0	99.999	17.905	19.138	17.871	17.974
36	2449163.838277	600.0	99.999	17.836	19.069	18.080	18.127
37	2449163.848000	600.0	99.999	17.799	19.097	18.236	18.186
38	2449163.857028	600.0	99.999	17.832	19.087	18.435	18.261
39	2449163.866056	600.0	99.999	17.839	19.130	18.611	18.314
40	2449163.875084	600.0	99.999	17.884	19.188	18.648	18.301
41	2449163.884113	600.0	99.999	17.921	19.301	18.617	18.270
42	2449163.893141	600.0	99.999	17.944	19.367	18.397	18.213
43	2449163.902863	600.0	99.999	18.020	19.428	18.214	18.148
44	2449163.913280	600.0	99.999	18.191	19.370	18.058	18.080
45	2449163.922309	600.0	99.999	18.323	19.338	17.952	18.042
46	2449163.931337	600.0	99.999	18.409	19.231	17.921	17.998
47	2449163.940365	600.0	99.999	18.381	19.208	17.929	17.969
48	2449163.950087	600.0	99.999	18.308	19.190	17.907	17.943
49	2449163.959116	600.0	99.999	18.247	19.169	17.904	17.924
50	2449163.968838	600.0	99.999	18.060	19.152	17.909	17.920
51	2449163.978561	600.0	99.999	18.005	19.128	17.909	17.913
52	2449163.987589	600.0	99.999	17.941	19.128	17.905	17.919
53	2449174.861785	600.0	99.999	17.766	19.123	17.874	17.946
54	2449174.870790	300.0	18.259	17.761	19.174	17.873	17.955
55	2449174.879702	300.0	18.274	17.782	19.173	17.881	17.931
56	2449174.888765	300.0	18.347	17.853	19.179	17.868	17.936
57	2449174.897920	300.0	18.337	17.909	19.226	17.875	17.936
58	2449174.906995	300.0	18.445	17.975	19.277	17.880	17.993
59	2449174.916162	300.0	18.522	18.039	19.276	17.878	17.976

60	2449174.925653	300.0	18.631	18.168	19.306	17.938	18.005
61	2449174.934600	300.0	18.762	18.279	19.304	17.900	18.006
62	2449174.943836	300.0	99.999	18.343	19.373	17.923	18.069
63	2449174.955815	300.0	18.761	18.336	19.266	18.013	18.129
64	2449174.964843	300.0	99.999	18.330	19.228	18.168	18.242
65	2449174.974022	300.0	18.517	18.233	19.113	18.300	18.270
66	2449174.983258	300.0	99.999	18.072	19.125	18.527	18.355
67	2449175.775710	600.0	18.401	17.795	19.034	17.878	18.207
68	2449175.791567	600.0	18.590	17.783	19.053	17.918	18.300
69	2449175.807447	600.0	18.829	17.801	19.118	17.960	18.312
70	2449175.823547	600.0	18.438	18.409	99.999	17.861	17.995
71	2449175.839554	600.0	18.659	18.016	19.211	17.985	18.113
72	2449175.851973	600.0	18.779	18.454	19.027	99.999	17.960
73	2449175.867934	600.0	18.381	99.999	19.418	17.920	17.952
74	2449175.883965	600.0	18.290	18.294	19.309	17.878	17.926
75	2449175.902056	600.0	18.629	17.958	19.065	17.873	17.910
76	2449175.918005	600.0	18.259	17.941	19.160	17.882	18.015
77	2449175.933908	600.0	18.286	99.999	19.137	17.887	18.005
78	2449175.949881	600.0	18.335	17.761	19.319	17.962	18.075
79	2449175.965796	600.0	18.501	17.836	19.114	17.878	18.103
80	2449175.981907	600.0	18.779	17.848	19.161	17.880	18.235
81	2449176.880888	300.0	18.721	17.778	19.089	17.895	18.016
82	2449176.889928	300.0	18.566	17.739	19.067	17.890	17.964
83	2449176.899083	300.0	18.495	17.787	19.096	17.929	17.928
84	2449176.908088	300.0	18.404	17.812	19.084	17.937	17.942
85	2449176.917070	300.0	18.343	17.853	19.044	17.940	17.931
86	2449176.926237	300.0	18.297	17.887	19.064	17.965	17.938
87	2449176.938344	300.0	18.272	17.994	19.149	17.989	17.962
88	2449176.947510	300.0	99.999	18.096	19.078	17.997	17.992
89	2449176.956504	300.0	18.269	18.202	19.152	17.991	18.020
90	2449176.979699	300.0	99.999	18.329	19.320	17.925	18.147
91	2449177.873574	600.0	18.456	18.318	19.162	17.903	18.044

92	2449177.889651	600.0	18.662	18.422	19.144	17.885	17.974
93	2449177.905531	600.0	18.846	18.326	19.270	17.892	17.926
94	2449177.921620	600.0	18.832	18.103	19.345	99.999	17.903
95	2449177.937673	600.0	18.578	17.936	19.290	17.874	17.900
96	2449177.953600	600.0	18.405	17.880	19.169	17.882	18.027
97	2449177.969595	600.0	18.313	17.794	19.094	17.876	18.166
98	2449177.985660	600.0	18.264	17.785	19.087	17.896	18.132
99	2449178.890484	300.0	18.310	17.777	19.198	18.657	18.009
100	2449178.899536	300.0	18.335	17.759	19.161	18.611	17.976
101	2449178.908610	300.0	18.358	17.816	19.137	18.432	17.946
102	2449178.927187	300.0	18.517	17.863	19.130	18.077	17.939
103	2449178.937916	300.0	18.684	17.907	19.155	17.966	17.908
104	2449178.946724	300.0	18.820	17.971	19.093	17.919	17.871
105	2449178.960301	300.0	18.828	18.086	19.159	17.896	17.983
106	2449178.972998	300.0	18.735	18.285	19.136	17.905	18.057
107	2449178.981887	300.0	18.592	18.389	19.131	17.900	18.044
108	2449178.990776	300.0	18.483	18.399	19.182	17.907	18.062
109	2449179.891305	600.0	18.319	18.178	19.063	17.880	18.051
110	2449179.907381	600.0	18.291	18.347	19.074	17.895	17.984
111	2449179.933701	600.0	18.269	18.263	19.099	17.889	17.934
112	2449179.941734	600.0	18.313	18.022	19.122	17.911	17.910
113	2449179.957637	600.0	18.386	17.882	19.226	99.999	17.938
114	2449179.974073	600.0	18.531	17.814	19.383	18.194	17.980
115	2449180.880330	600.0	18.765	17.902	19.159	17.897	18.178
116	2449180.900793	600.0	18.577	17.784	19.306	17.887	18.062
117	2449180.917275	600.0	18.411	17.769	19.343	17.914	17.988
118	2449180.935585	600.0	18.306	17.758	19.268	17.868	17.939
119	2449180.952380	600.0	18.279	17.817	19.153	99.999	17.909
120	2449180.978098	600.0	18.293	18.043	19.074	99.999	17.938
121	2449180.987288	600.0	18.297	18.163	19.079	99.999	17.965
122	2449190.709410	600.0	18.295	18.059	19.071	17.874	18.036
123	2449190.715313	600.0	18.247	18.143	19.074	17.855	18.073

124	2449190.750383	600.0	18.261	18.389	19.079	17.873	18.298
125	2449190.756286	600.0	99.999	18.277	19.092	17.879	18.310
126	2449190.771216	600.0	18.365	18.110	19.106	17.880	18.302
127	2449190.777119	300.0	18.412	18.041	19.088	17.882	18.249
128	2449190.791355	600.0	18.564	99.999	19.143	17.905	18.158
129	2449190.797953	300.0	18.651	17.894	19.193	17.877	18.126
130	2449190.812189	600.0	18.847	99.999	19.332	99.999	18.069
131	2449190.818786	300.0	18.840	17.876	19.394	17.936	17.982
132	2449190.833022	600.0	18.805	99.999	19.374	18.020	17.936
133	2449190.838925	300.0	18.687	17.828	19.324	17.992	17.945
134	2449190.853161	600.0	18.478	99.999	19.186	17.996	17.924
135	2449190.859064	300.0	18.426	17.846	19.177	17.992	18.017
136	2449190.873995	600.0	18.326	99.999	19.148	17.962	18.102
137	2449190.879898	300.0	18.316	17.944	19.142	17.934	19.270
138	2449190.894134	600.0	18.261	99.999	19.123	99.999	17.956
139	2449190.900037	300.0	18.213	18.157	19.126	17.886	17.897
140	2449190.914273	600.0	18.229	99.999	19.125	17.852	18.014
141	2449190.920176	300.0	18.254	18.384	19.137	17.879	18.038
142	2449190.935106	600.0	18.288	99.999	19.123	17.894	18.405
143	2449190.941009	300.0	18.310	18.277	19.107	17.868	18.175
144	2449190.955246	600.0	18.379	18.068	19.126	17.853	18.249
145	2449190.961148	300.0	18.405	18.007	19.149	17.878	18.302
146	2449190.975385	600.0	18.613	17.909	19.152	17.879	18.262
147	2449190.983023	600.0	18.698	17.873	19.179	17.869	18.237
148	2449190.989621	300.0	18.757	17.839	19.210	17.884	18.195
149	2449191.810807	600.0	18.374	99.999	19.091	17.872	18.171
150	2449191.824348	300.0	18.387	18.343	19.059	17.873	18.035
151	2449191.830946	600.0	18.455	18.409	99.999	17.872	18.006
152	2449191.836848	300.0	18.534	18.422	19.040	17.876	17.987
153	2449191.851779	600.0	18.769	18.454	19.041	99.999	17.966
154	2449191.857682	300.0	18.840	18.385	19.034	17.871	17.936
155	2449191.872613	600.0	18.840	18.093	19.041	17.915	17.908

156	2449191.878515	300.0	18.795	18.076	19.074	17.879	17.889
157	2449191.892752	600.0	18.609	17.958	19.071	17.873	17.905
158	2449191.898654	300.0	18.518	17.936	19.088	17.890	17.953
159	2449191.912891	600.0	18.390	99.999	19.148	99.999	17.965
160	2449191.918793	300.0	18.358	17.867	19.191	17.911	17.954
161	2449191.933030	600.0	18.339	17.761	19.309	17.957	18.068
162	2449191.939627	300.0	18.260	17.824	19.350	17.978	18.095
163	2449191.954557	600.0	18.315	17.779	19.361	18.015	18.191
164	2449191.960460	300.0	18.245	17.856	19.350	18.001	18.209
165	2449191.974697	600.0	99.999	17.855	19.184	18.005	99.999
166	2449191.980599	300.0	18.270	17.951	19.141	17.985	18.339
167	2449191.994836	600.0	18.367	18.028	19.152	17.934	18.241
168	2449192.001433	300.0	18.367	18.104	19.143	17.921	18.257

Notes: The second column HJD is the heliocentric date. An entry of 99.999 means there are no photomteric data for the corresponding heliocentric date.

Table 2(b) – Johnson I band Photometry Data for the Six Short Period Variables in M71

No	HJD days	ET sec	V1	V2	V3	V4	V5
169	2448415.821762	600.0	17.207	17.093	17.427	17.866	99.999
170	2448415.841728	600.0	17.259	16.907	17.718	17.753	99.999
171	2448415.880874	600.0	17.425	16.867	17.241	17.684	99.999
172	2448415.897646	600.0	17.639	16.879	17.120	17.685	99.999
173	2448415.932416	600.0	17.515	17.053	17.052	17.736	99.999
174	2448415.949339	600.0	17.340	17.236	17.035	17.785	99.999
175	2448415.965809	600.0	17.262	17.485	17.035	17.856	99.999
176	2448415.982477	600.0	17.198	17.477	17.024	17.952	99.999
177	2448416.829238	600.0	17.272	16.869	17.022	17.733	99.999
178	2448416.864518	600.0	17.197	17.069	17.028	17.743	99.999
179	2448416.880989	600.0	99.999	99.999	17.045	17.765	99.999
180	2448416.897598	600.0	17.220	17.430	17.096	17.822	99.999
181	2448416.914104	600.0	17.314	17.247	17.141	17.920	99.999
182	2448416.930401	600.0	17.463	17.041	17.374	17.968	99.999
183	2448416.947543	600.0	17.664	16.959	17.696	17.799	99.999
184	2448416.964558	600.0	17.682	16.868	17.716	17.733	99.999
185	2448416.981041	600.0	17.478	16.869	17.434	17.709	99.999
186	2448487.662069	600.0	99.999	99.999	17.061	17.712	16.943
187	2448487.694927	600.0	99.999	99.999	17.039	17.748	17.039
188	2448487.711362	600.0	99.999	99.999	17.023	17.732	17.120
189	2448487.727704	600.0	99.999	99.999	17.031	17.780	17.235
190	2448487.743977	600.0	99.999	99.999	17.026	17.853	17.311
191	2448487.760192	600.0	99.999	17.538	17.003	17.946	17.287
192	2448487.776569	600.0	99.999	99.999	17.027	17.959	17.195
193	2448487.793663	600.0	99.999	99.999	17.020	17.853	17.062
194	2448487.809959	600.0	99.999	99.999	17.038	17.808	17.001
195	2448487.826220	600.0	99.999	99.999	17.070	17.730	16.957
196	2448488.713961	600.0	99.999	17.013	17.662	17.928	17.089
197	2448488.729933	600.0	17.207	16.927	17.345	17.817	17.172

198	2448488.746599	600.0	17.191	16.842	17.140	17.744	17.281
199	2448488.762999	600.0	17.191	16.862	17.081	17.712	17.292
200	2448488.779318	600.0	99.999	99.999	17.052	17.717	17.225
201	2448488.811875	600.0	99.999	16.952	17.026	17.714	17.043
202	2448488.828101	600.0	99.999	17.057	17.035	17.737	16.962
203	2449162.831293	300.0	99.999	17.456	99.999	17.758	17.188
204	2449162.840321	300.0	99.999	17.465	17.035	17.746	17.241
205	2449162.856294	300.0	17.269	17.308	17.047	17.729	17.321
206	2449162.865322	300.0	17.306	17.192	17.045	17.723	17.287
207	2449162.874350	300.0	17.368	99.999	99.999	17.713	17.273
208	2449162.883378	300.0	17.503	99.999	99.999	17.713	17.211
209	2449162.892406	300.0	17.619	16.946	17.045	17.716	17.158
210	2449162.901434	300.0	17.710	16.936	17.034	17.736	17.089
211	2449162.910463	300.0	17.711	99.999	17.033	17.735	17.067
212	2449162.920185	300.0	17.658	16.873	17.030	17.782	17.033
213	2449162.929213	300.0	17.561	99.999	17.011	17.797	16.995
214	2449162.937547	300.0	99.999	99.999	17.018	17.786	16.972
215	2449162.947270	300.0	17.355	99.999	17.038	17.875	16.952
216	2449162.956298	300.0	17.285	99.999	17.029	17.896	16.961
217	2449162.972271	300.0	17.206	99.999	17.033	17.940	16.955
218	2449162.981299	300.0	17.214	17.035	17.033	17.898	16.946
219	2449162.990327	300.0	99.999	99.999	17.049	17.855	16.974
220	2449163.843139	300.0	99.999	99.999	17.299	17.690	17.182
221	2449163.852167	300.0	99.999	99.999	17.481	17.718	17.259
222	2449163.861196	300.0	99.999	99.999	17.659	17.739	17.311
223	2449163.870918	300.0	99.999	99.999	17.731	17.759	17.326
224	2449163.879946	300.0	99.999	99.999	17.739	17.832	17.350
225	2449163.888974	300.0	99.999	99.999	99.999	17.911	17.262
226	2449163.898003	300.0	99.999	17.095	17.461	17.978	17.205
227	2449163.908420	300.0	99.999	99.999	17.270	18.007	17.144
228	2449163.917448	300.0	99.999	17.349	17.154	17.935	17.074
229	2449163.927170	300.0	99.999	99.999	17.100	17.855	17.036
230	2449163.936198	300.0	99.999	99.999	17.103	17.795	17.018
231	2449163.945227	300.0	99.999	99.999	17.068	17.776	17.055
232	2449163.954949	300.0	99.999	17.368	17.060	17.779	16.958

233	2449163.963977	300.0	99.999	17.192	17.046	17.733	16.952
234	2449163.973700	300.0	99.999	99.999	17.039	17.720	16.966
235	2449163.982728	300.0	99.999	16.996	17.046	17.720	16.912
236	2449174.838128	300.0	17.216	99.999	17.001	17.755	17.081
237	2449174.847179	300.0	17.217	99.999	17.024	17.766	17.045
238	2449174.857329	300.0	17.187	16.865	17.024	17.719	17.008
239	2449174.866288	300.0	17.185	16.900	17.022	17.725	16.980
240	2449174.884309	300.0	17.232	16.912	17.034	17.759	16.939
241	2449174.893314	300.0	17.257	99.999	17.031	17.763	16.937
242	2449174.901868	300.0	17.282	16.995	99.999	17.804	16.970
243	2449174.911590	300.0	17.370	17.068	99.999	17.853	16.966
244	2449174.916891	300.0	17.205	16.881	17.022	17.751	16.952
245	2449174.920792	300.0	17.449	17.145	17.057	17.907	16.990
246	2449174.930155	300.0	17.553	17.268	17.067	17.950	17.028
247	2449174.938929	300.0	17.663	17.404	17.081	17.938	17.073
248	2449174.950932	300.0	17.681	99.999	17.136	17.874	17.131
249	2449174.960341	300.0	17.594	17.431	17.228	17.785	17.181
250	2449174.969451	300.0	17.503	17.310	17.351	17.754	17.235
251	2449174.978560	300.0	17.379	17.287	99.999	17.694	17.307
252	2449174.987669	300.0	99.999	17.081	17.683	17.693	17.326
253	2449175.783627	600.0	17.376	99.999	99.999	17.692	17.291
254	2449175.799484	600.0	17.594	99.999	17.142	17.693	17.337
255	2449175.815457	600.0	17.695	99.999	17.220	17.725	17.277
256	2449175.831441	600.0	17.632	99.999	99.999	17.791	17.185
257	2449175.859983	600.0	17.320	99.999	17.135	17.943	17.050
258	2449175.875944	600.0	17.250	99.999	17.106	17.962	16.971
259	2449175.892542	600.0	17.189	99.999	99.999	17.844	16.937
260	2449175.910019	600.0	17.171	99.999	99.999	17.755	16.939
261	2449175.926038	600.0	17.193	99.999	99.999	17.736	16.969
262	2449175.941930	600.0	17.251	99.999	16.964	17.735	17.019
263	2449175.957960	600.0	17.356	99.999	16.954	17.718	17.096
264	2449175.973991	600.0	17.536	99.999	99.999	17.719	17.203
265	2449176.885368	300.0	17.530	16.874	17.055	17.680	17.008
266	2449176.894547	300.0	17.415	16.865	17.071	17.672	16.978
267	2449176.903598	300.0	17.337	16.903	17.082	17.693	16.957

268	2449176.912580	300.0	17.288	16.909	17.125	17.676	16.959
269	2449176.921503	300.0	17.273	16.893	17.157	17.683	16.957
270	2449176.930555	300.0	17.237	16.984	17.185	17.681	16.975
271	2449176.943009	300.0	17.195	99.999	17.219	17.713	17.002
272	2449176.951956	300.0	17.201	17.213	17.202	17.756	17.039
273	2449176.966632	300.0	17.218	17.374	17.154	17.862	17.095
274	2449176.984086	300.0	17.246	99.999	17.073	17.971	17.216
275	2449177.881538	600.0	17.443	99.999	99.999	17.758	17.030
276	2449177.897511	600.0	17.665	99.999	99.999	17.819	16.981
277	2449177.913460	600.0	17.694	99.999	99.999	17.897	16.932
278	2449177.929757	600.0	17.568	99.999	99.999	17.906	16.914
279	2449177.945799	600.0	17.346	99.999	17.036	17.837	16.953
280	2449177.961644	600.0	17.266	99.999	99.999	17.739	16.988
281	2449177.977594	600.0	17.223	99.999	17.011	17.714	17.048
282	2449178.895022	300.0	17.237	99.999	17.720	17.774	17.032
283	2449178.904096	300.0	17.281	99.999	17.652	17.761	16.997
284	2449178.912395	300.0	17.310	99.999	17.478	17.772	16.970
285	2449178.922638	300.0	17.372	99.999	17.317	17.759	16.946
286	2449178.933507	300.0	17.510	99.999	99.999	17.750	16.961
287	2449178.942257	300.0	17.623	99.999	17.114	17.727	16.942
288	2449178.955822	300.0	17.692	17.078	17.075	17.716	16.967
289	2449178.964804	300.0	17.718	17.190	17.062	17.722	16.988
290	2449178.977454	300.0	17.556	17.396	17.059	17.709	17.029
291	2449178.986355	300.0	17.444	17.457	17.064	17.746	17.071
292	2449179.899419	600.0	17.235	99.999	99.999	17.681	17.060
293	2449179.915299	600.0	17.213	99.999	99.999	17.673	17.004
294	2449179.933702	600.0	17.230	99.999	99.999	17.725	16.965
295	2449179.949744	600.0	17.274	99.999	17.139	17.772	16.977
296	2449179.966179	600.0	17.356	99.999	99.999	17.906	16.984
297	2449180.871834	600.0	17.641	99.999	99.999	17.751	17.293
298	2449180.892205	600.0	17.560	99.999	17.026	17.832	17.124
299	2449180.909046	600.0	17.393	99.999	99.999	17.930	17.060
300	2449180.925366	600.0	17.296	99.999	99.999	17.905	17.005
301	2449180.943769	600.0	17.191	99.999	17.033	17.752	17.068
302	2449180.969938	600.0	17.207	99.999	17.009	17.712	16.965

303	2449190.680244	600.0	17.341	99.999	17.057	17.715	16.975
304	2449190.701078	600.0	17.224	99.999	17.064	17.692	17.027
305	2449190.721911	600.0	17.207	99.999	99.999	17.641	17.125
306	2449190.742745	600.0	17.202	99.999	17.046	17.667	17.251
307	2449190.763578	600.0	17.243	99.999	17.035	17.690	17.352
308	2449190.783717	600.0	17.366	99.999	99.999	17.720	17.254
309	2449190.803856	600.0	17.618	99.999	99.999	17.857	17.105
310	2449190.824690	600.0	17.690	99.999	17.201	17.975	99.999
311	2449190.845523	600.0	17.480	99.999	17.190	17.851	17.002
312	2449190.865662	600.0	17.286	99.999	17.152	17.772	16.952
313	2449190.885801	600.0	17.208	99.999	99.999	17.727	16.956
314	2449190.905940	600.0	17.185	99.999	99.999	17.734	17.029
315	2449190.927468	600.0	17.200	99.999	99.999	17.714	99.999
316	2449190.947607	600.0	17.252	99.999	17.015	17.712	17.238
317	2449190.967746	600.0	17.413	99.999	99.999	17.752	17.321
318	2449190.995524	600.0	17.658	99.999	17.032	17.871	17.221
319	2449191.802474	600.0	17.210	99.999	99.999	17.730	17.244
320	2449191.818446	600.0	17.261	99.999	99.999	17.691	17.087
321	2449191.843446	600.0	17.496	99.999	99.999	17.673	16.984
322	2449191.864280	600.0	17.685	99.999	17.006	17.651	16.997
323	2449191.884419	600.0	17.618	99.999	17.045	17.682	17.047
324	2449191.904558	600.0	17.379	99.999	99.999	17.733	17.001
325	2449191.925391	600.0	17.250	99.999	99.999	17.863	17.179
326	2449191.946225	600.0	17.221	99.999	99.999	17.964	17.203
327	2449191.967058	600.0	17.289	99.999	99.999	17.856	17.336
328	2449191.987197	600.0	17.264	99.999	99.999	17.752	17.338

Notes: The second column HJD is the heliocentric date. An entry of 99.999 means there are no photomteric data for the corresponding heliocentric date.

Table 3 - Basic Properties of the Five Eclipsing Binaries in M 71

Name	α_{1950}	δ_{1950}	Type	Period days	HJD_0 -2440000.0	$I_{\Lambda mp}$ mag	$\langle I \rangle$ mag	$\langle V-I \rangle$ mag	$\langle I \rangle_0$ mag	$\langle V-I \rangle_0$ mag	R arcsec
V1	19:51:43.55	18:35:39.1	W UMa	0.34890	8415.482	0.5	17.20	1.09	16.83	0.754	247.3
V2	19:51:43.23	18:37:52.3	W UMa	0.36719	8415.730	0.65	16.87	0.94	16.52	0.604	166.5
V3	19:51:37.03	18:39:57.4	W UMa	0.37386	8415.669	0.35	17.67	1.40	17.24	1.064	99.2
V4	19:51:35.17	18:39:55.8	Algol	0.55615	8415.713	0.75	17.02	0.85	16.58	0.541	81.6
V5	19:51:20.39	18:36:12.2	W UMa	0.40450	8487.441	0.45	16.96	0.98	16.56	0.644	225.8

Notes: $I_{\Lambda mp}$ is the maximum eclipse depth in the I band light curve, $\langle I \rangle$ and $\langle V-I \rangle$ are maximum-light I magnitude and intesity mean (V−I) color, respectively, while $\langle I \rangle_0$ and $\langle (V-I) \rangle_0$ are the reddening-corrected values. The last column lists the radial distance (in arcsecond) of each star relative to the center of the cluster M 71. Here we used E(B-V)=0.28 (Hodder *et al.* 1992), A_V=0.87, A_I=0.53 and E(V-I)=0.34 (Cardelli *et al.* 1989). Variables V3 and V4 correspond to stars H3 and H4, respectively, from Hodder *et al.* (1992).

Table 4 - Distance Estimates for the M71 Contact Binaries

Star	$\langle V_0 \rangle$ mag	$\langle V-I \rangle_0$ mag	T_{eff} K	BC mag	q	M_{tot} mag	$(m-M)_0$ mag
V1	17.58	0.75	5660	−0.09	0.5	0.7-1.1	12.7-13.0
V2	17.12	0.60	6180	−0.05	0.8	0.9-1.5	12.7-13.1
V3	18.30	1.06	4820	−0.25	0.2	0.9-1.1	13.2-13.4
V5	17.20	0.64	6020	−0.05	0.3	0.8-1.0	12.9-13.0

Notes: The ranges in M_{tot} are explained in the text. The ranges in the distance moduli correspond to the adopted ranges in M_{tot}. The uncertainty in the mass ratios is ± 0.1.

Table 5 - Distance Estimates for the Semi-Contact Binary M71-V4

	Transit Eclipse		Occultation Eclipse	
	Primary	Secondary	Primary	Secondary
$\langle V-I\rangle_0$	0.44	1.03	0.45	0.58
V_0	17.11	19.50	17.73	17.77
I_0	16.67	18.47	17.27	17.18
T_{eff} (K)	6460	4540	6330	5850
R/a	0.34	0.24	0.28	0.32
R ($R_\odot$)	1.0	0.7	0.8	0.9
L ($L_\odot$)	1.66	0.18	0.92	0.88
$M_{V,tot}$	4.1		4.2	
$V_{0,tot}$	17.1		17.1	
$(m-M)_0$	13.0		12.9	

Notes: a = the orbital semi-major axis. The ratio R/a was constrained by the duration of the eclipses and assuming the inclination is 90 degrees. A lower (yet plausible) inclination would result in larger radii, larger luminosities, and a smaller distance moduli. The maximum effect is about 0.3 mag in the modulus.

Table 6 - Distance Estimates for the M71 Contact Binaries

Star	$\langle V \rangle_0$ mag	$\langle V-I \rangle_0$ mag	$\log P$(days)	M_V mag	$(m-M)_0$ mag	$(m-M)_0$ $\log(Z/Z_\odot) = -0.7$
V1	17.6	0.75	−0.4573	4.4	13.2	12.9
V2	17.1	0.60	−0.4351	3.7	13.4	13.1
V3	18.3	1.06	−0.4273	5.4	12.9	12.6
V5	17.2	0.64	−0.3931	3.7	13.5	13.2

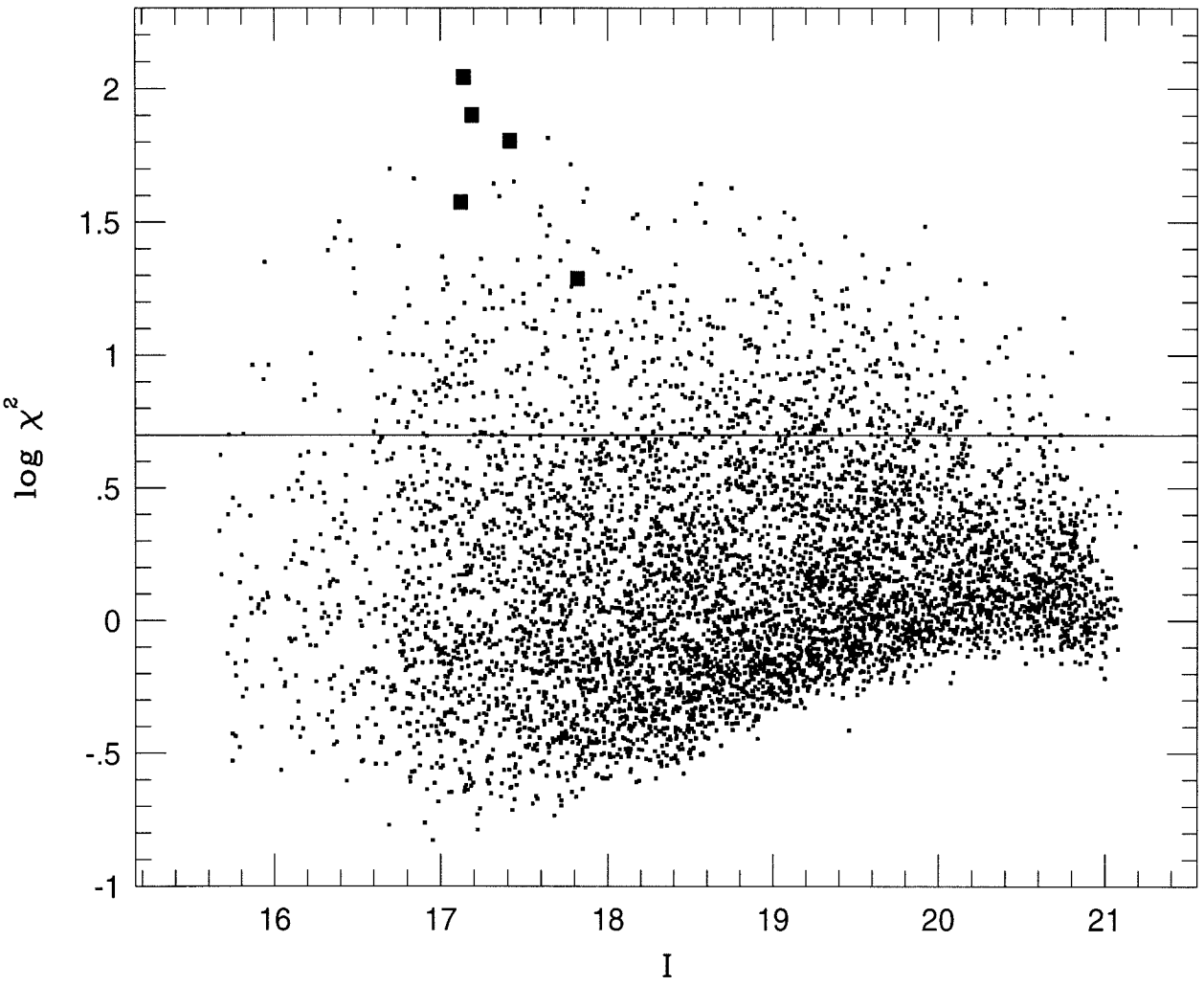

Figure 3.1: The reduced χ^2 statistic

A plot of the reduced chi-squared statistic, χ^2_ν as a function of I magnitude for 6172 stars with photometric measurements on at least 40% of all I-band images. The solid line shows the adopted cutoff at $\chi^2_\nu = 5.0$. For all stars located above this line we explicitly searched for periodic variability in the period range 0.1-5 days. The five variables are denoted as large filled squares.

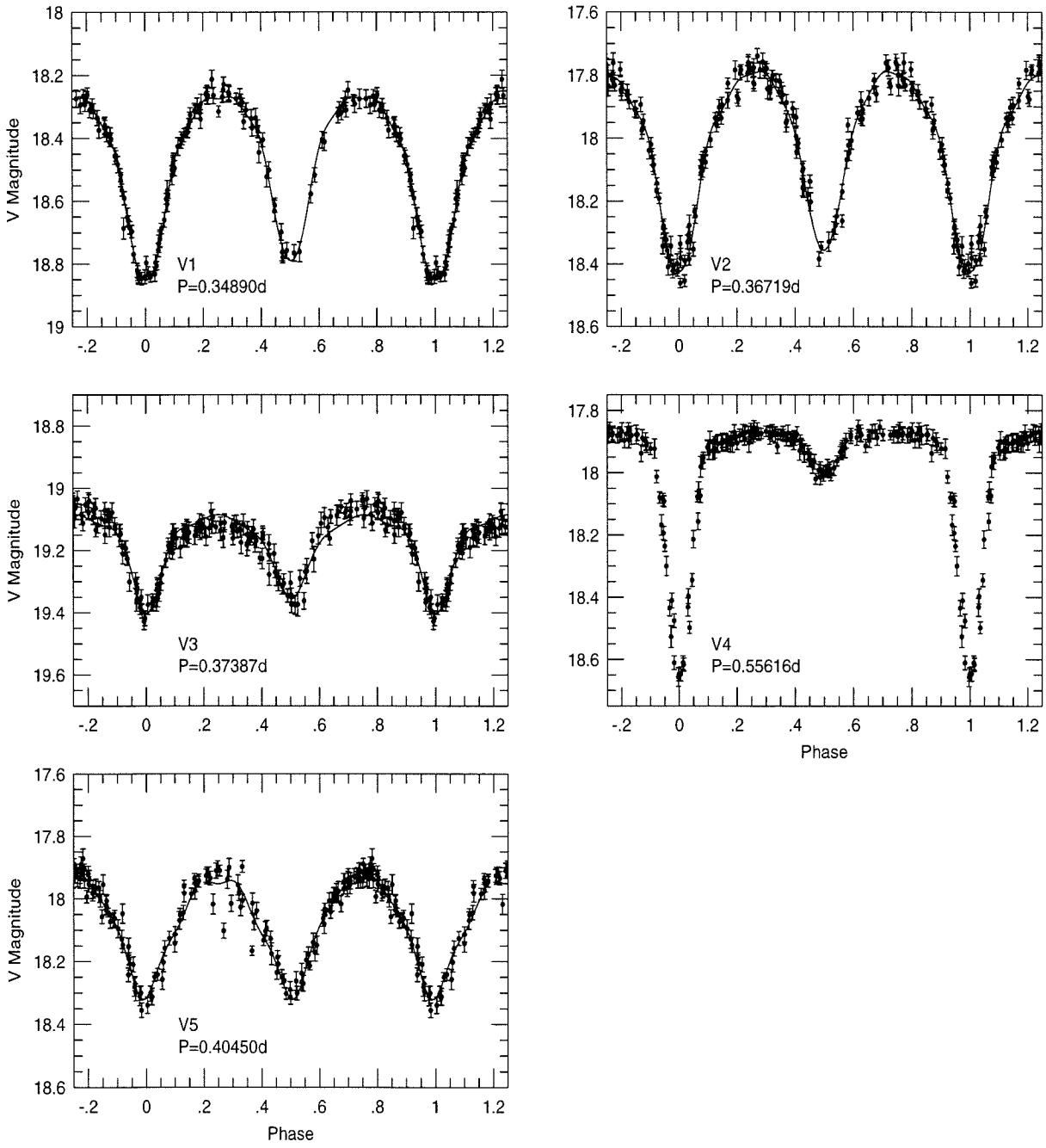

Figure 3.2: The V-band light curves

The V-band light curves of the five newly-discovered short-period binaries in M71. The solid lines show the best-fitting Fourier series using the functional form described by Rucinski (1993).

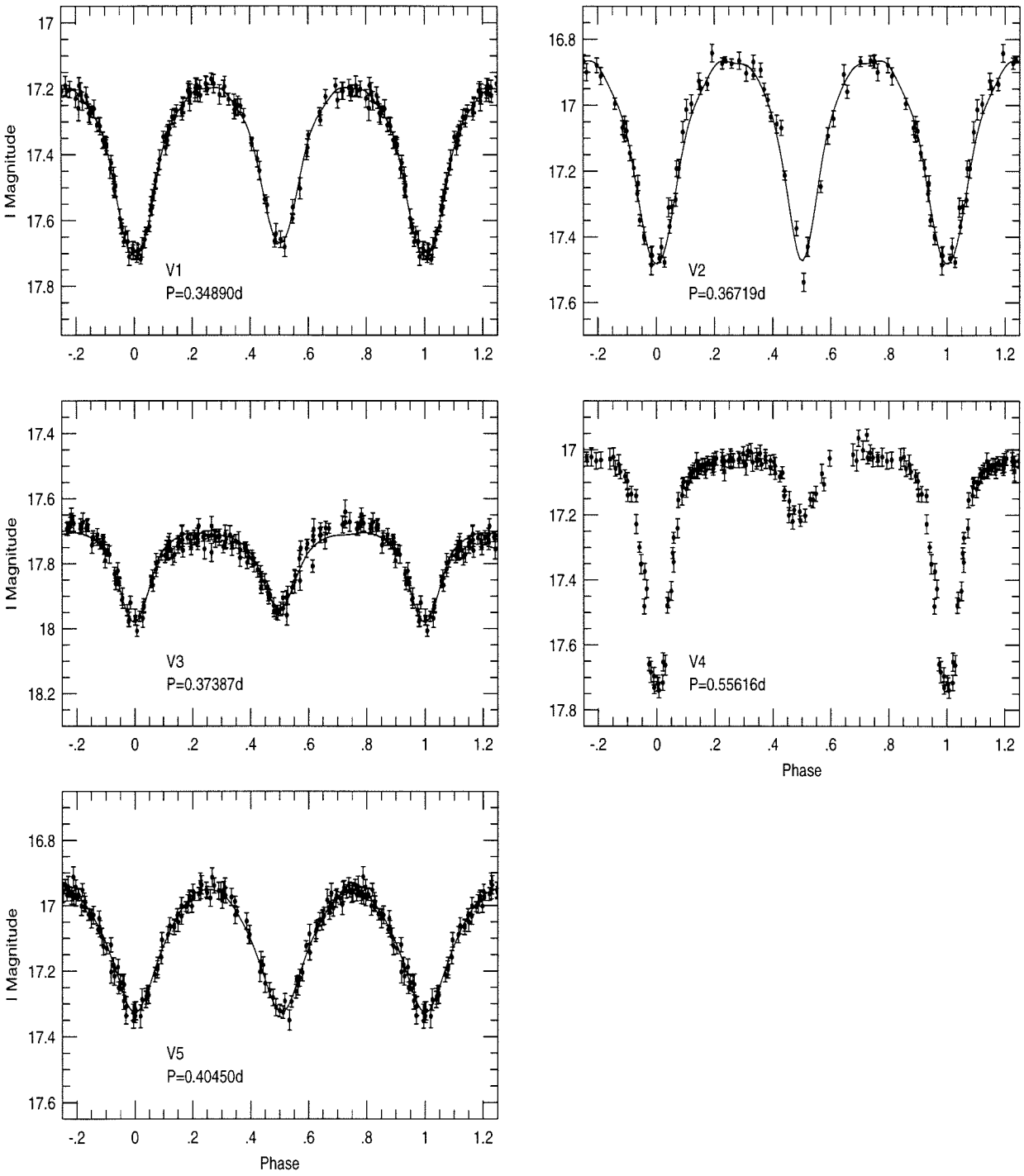

Figure 3.3: The I-band light curves

The I-band light curves of the five newly-discovered short-period binaries in M71. The solid lines show the best-fitting Fourier series using the functional form described by Rucinski (1993).

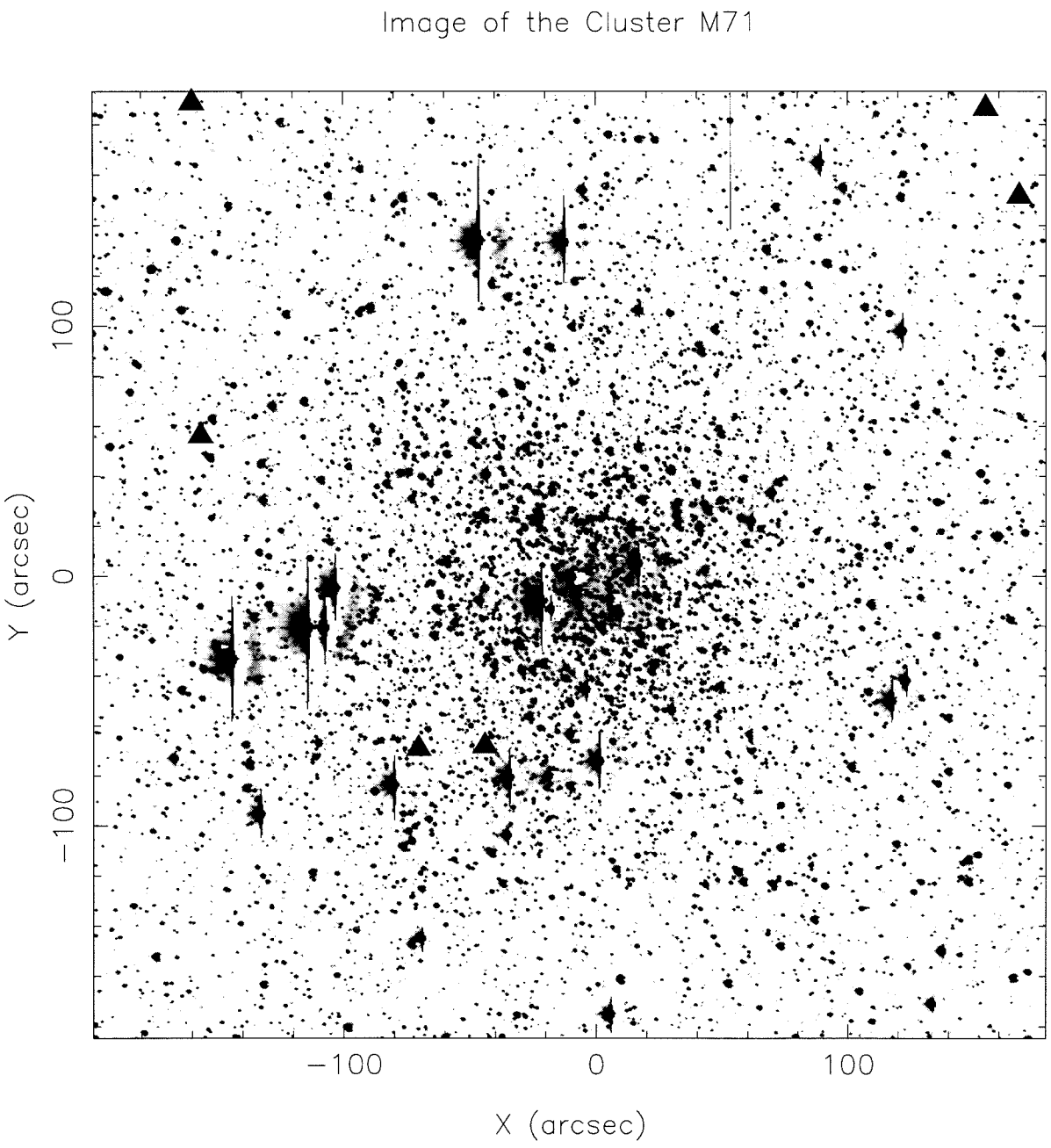

Figure 3.4: A wide-field identification chart

A wide-field identification chart for the five short-period binary stars in M71. The locations of these variables are denoted with filled triangles.

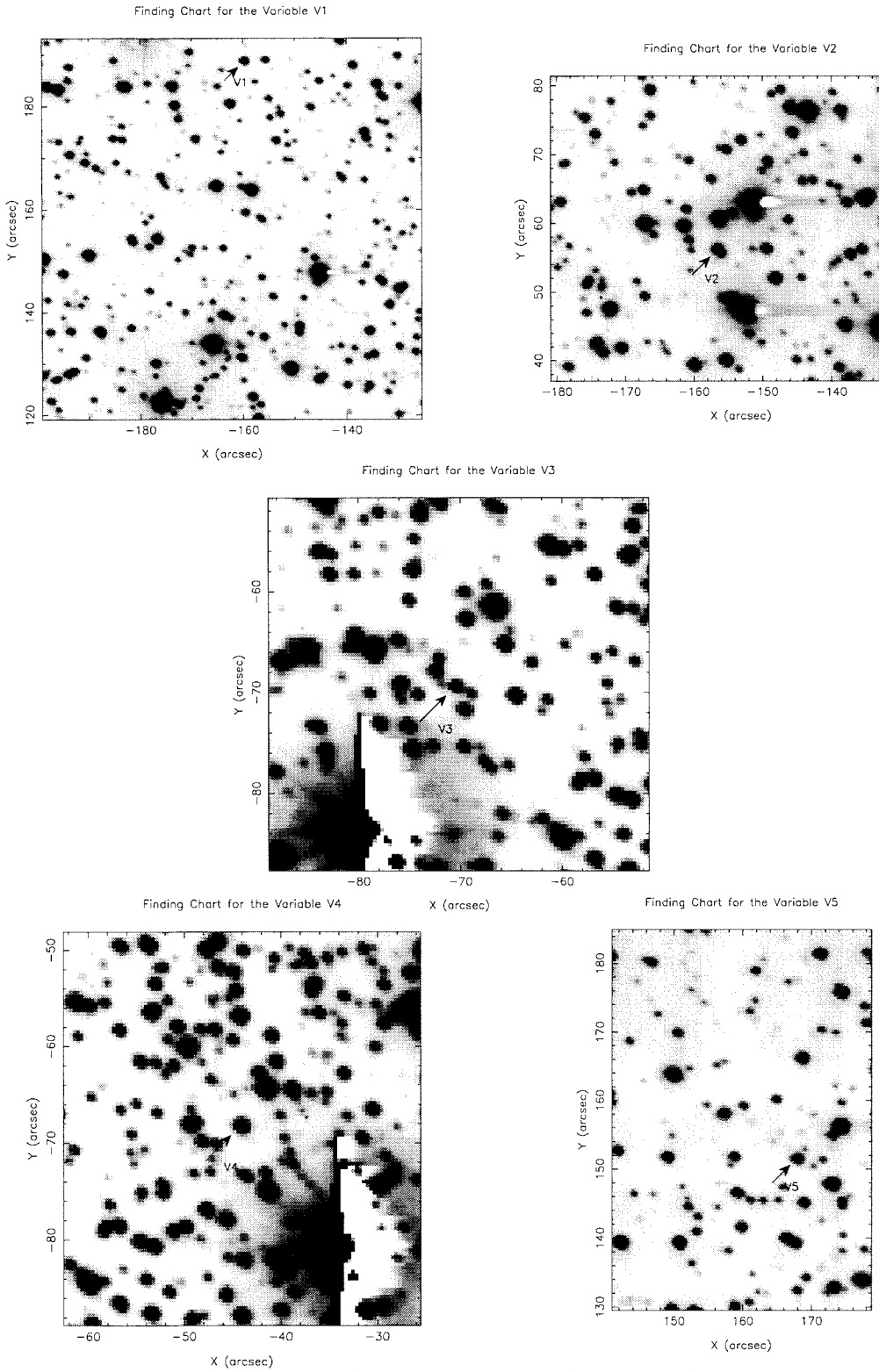

Figure 3.5: Detailed finding charts

Detailed finding charts for the five short-period binaries in M71.

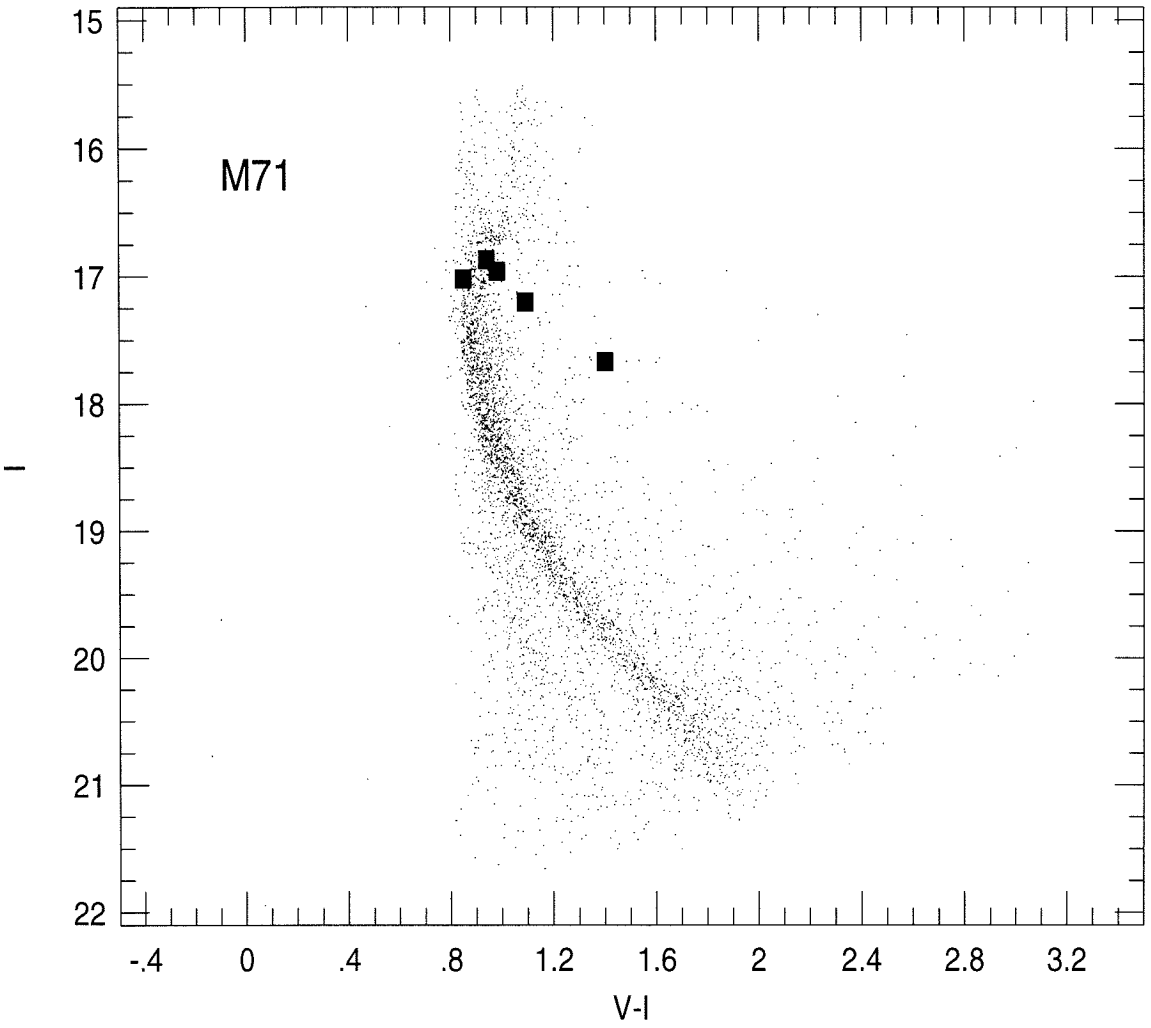

Figure 3.6: The cluster colour-magnitude diagram

The I-(V−I) color-magnitude diagram of M71. For stars fainter than I $\sim$ 17, the points show the average magnitudes and colors of 4257 stars measured on the 20 best-seeing V and I CCD frame pairs. The photometric data for 371 stars brighter than I $\sim$ 17 were derived from a single pair of poor-seeing frames. The main sequence turnoff is visible at I $\sim$ 16.8; the apparent splitting into two sequences above this point corresponds to field stars and blue stragglers on the left, and M71 subgiant stars on the right. The sharp blue edge of the field stars is also noticeable for I $\gtrsim$ 18.8. The filled squares show the maximum-light magnitudes and colors of the newly-discovered binaries.

Chapter 4

THE IMAGING SURVEY FOR SHORT -PERIOD ECLIPSING BINARIES IN THE GLOBULAR CLUSTER M 5*

ABSTRACT

We report the identification of six short-period variables in the dense globular cluster M 5. Our observations consist of multiple-epoch VI CCD images centered on the cluster and covering a $6.3' \times 6.3'$ field. Of the six short-period variables, one is a possible blue straggler, four lie on the cluster main-sequence turnoff and one is about one magnitude fainter than the main-sequence turnoff. The light curves of these six variables show that five of them are probably W UMa type contact eclipsing binaries and one of them is a semi-contact Algol system. Due to incomplete phase coverage, the type identification is fairly uncertain. The periods of these six interacting binaries are between 0.4 and 0.7 days. All six variables lie in the region beyond the $4r_c$ radius; here r_c is the cluster core radius of $24''$. Using detailed artificial eclipsing binary star simulations, we have applied incompleteness corrections and estimate a total number of 11 short-period binaries in the region beyond $4r_c$. Adopting a flat period distribution and a contact binary lifetime of 3 Gyrs, we estimate an overall primordial binary frequency of $28^{+11}_{-6}\%$ for the period range of 2.5 days to 550 yrs. To make comparative studies of short-period main-sequence eclipsing binaries (SPMSEB) in different globular clusters, we estimate that the specific frequency of SPMSEB is

* Adapted from a paper entitled "Discovery of six short-period eclipsing binaries in globular cluster M 5," by L. Yan & I.N. Reid, accepted for publication by the Monthly Notice of Royal Astronomical Society.

0.5% in M 5 excluding the possible blue straggler, similar to the fraction of 0.6% derived in M 71 with the data published in Yan & Mateo (1994).

4.1. Introduction

In recent years it has been widely recognized that the binary star population is related intimately to both the cluster dynamical evolution and the formation of various exotic objects in globular clusters. A primordial binary frequency as small as 3% can change fundamentally the dynamical evolution of an entire globular cluster (Heggie & Aarseth 1992) since binary stars can serve as a very efficient energy source, releasing their gravitational binding energy through close stellar encounters. The existence of binaries, and in particular primordial binaries in globular clusters, has been demonstrated by a number of observational techniques (see the detailed review by Hut *et al.* 1992). However, overall binary frequencies, and especially period distributions, are still very uncertain.

The technique of photometric time series analysis is an efficient and sensitive method of detecting binary stars with periods between 0.25 days and a few days. Binaries with such short periods generally do not contribute a significant amount of energy to the cluster dynamical evolution with the cluster density less than $10^{5.5}/\mathrm{pc}^3$ because of their small cross sections. However, these short-period eclipsing binaries, discovered mostly in the outer parts of clusters from ground based observations, provide important information on the primordial binary frequency since they are either primordial, as in M 71 (Yan & Mateo 1994), or are formed by processes involving primordial binaries, such as star-binary and/or binary-binary encounters. Tidal captures between two single stars are not important in the outer parts of a cluster, but may be significant in the high density cluster cores. Recent HST observations have revealed 2 short-period variables candidates among blue stragglers in the center of M 3 (Guhathakurta *et al.* 1994) and several in 47 Tuc (Edmonds *et al.* 1994).

More importantly, these short-period interacting binaries are directly linked to the formation of blue stragglers in globular clusters. A variety of mechanisms have been proposed to explain how blue stragglers are formed in star clusters (see recent

reviews by Stryker 1993; Livio 1993). One mechanism – mass transfer between the components of short-period main-sequence binary stars – is supported directly by observations (Yan & Mateo, 1994; Mateo *et al.* 1990). The first discovery of short-period eclipsing binaries among blue stragglers in the ultra-low density globular cluster NGC 5466 (Mateo *et al.* 1990) provides clear evidence that the progenitors of at least some globular cluster blue stragglers are short-period interacting binary stars. In the mass-transfer scenario a blue straggler is formed if the total initial mass of an interacting binary exceeds the current mass of stars located at the main-sequence turnoff. The three binary blue stragglers discovered in NGC 5466 represent very late stages in this mass transfer. Binaries in an earlier stage of mass transfer or with total masses less than the cluster turnoff mass should lie amongst the present-day main-sequence stars in the colour-magnitude (CM) diagram. These stars are destined to become blue stragglers when either a) the primary gains enough mass to push it over the turnoff mass, or b) the cluster turnoff mass evolves below the mass of the primary or the merged binary remnant.

To understand fully how a short-period binary star evolves along the main-sequence of the cluster HR diagram to the blue straggler region, we need to identify short-period eclipsing binaries among both main-sequence stars and blue stragglers in globular clusters. Observationally, the study of such systems in globular clusters is in its infancy – one main-sequence eclipsing binary was found in NGC 4372 (Kaluzny & Krzeminski 1993), 5 in M 71 (Yan & Mateo 1994) and 1 in NGC 6397 (Rubenstein & Bailyn 1995).

In this paper we present results of a search for short-period variables stars in the field of M 5. A total of 340 images of the cluster were originally obtained for studying the abundant RR Lyrae population in M 5 (Reid 1995). Since the whole dataset has a large temporal coverage, we choose a subset of the data with seeing better than $1.2''$ for this project. The rest of the paper is organized as follows. The section 4.2 is the description of the observations, data reduction and analysis. We

present the result in the section 4.3. In the section 4.4 we describe in detail the artificial eclipsing binary simulations for estimating the incompleteness corrections. In the last section 4.5 we discuss the implication of our result and relevant problems.

4.2. Observations and Data Reductions

The globular cluster M 5 has RA of 15^h16^m and DEC of $2°15'51''$ (B1950) with the corresponding galactic coordinate of (4°, 47°). It lies at a distance of $\sim$ 7 kpc from the Sun, $\sim$ 5.5 kpc from the Galactic center and 4.9 kpc above the plane of the disk. It is a high density cluster with the central density of $10^4 M_\odot/pc^3$. Its central concentration parameter $c = \log(r_t/r_c)$ is $\sim$ 2 with a core radius of 24 arcseconds. All of our observations of this cluster were taken with a 1024x1024 Tektronix CCD on the 60-inch telescope at the Palomar Observatory during the nights of 23 – 29 May, 1991 and 16 – 18 July, 1991. A total of 340 images, centered on the cluster, were obtained with the two filters, Johnson V and Gunn i. Each image has a scale of $0.37''$ per pixel and a total field of view of $\sim$ 6.3× 6.3 square arcminutes. Generally, images in both V and i colours have the same exposure time of 150 seconds. The observational data used for the current project are tabulated in Table 1.

All frames were trimmed and bias-subtracted using standard procedures. The stellar photometry was performed using the two-dimensional photometry reduction program DoPHOT (Schechter *et al.* 1993). This program uses an analytic, position-independent point spread function (PSF) to determine relative photometry of stars on a CCD image; this is appropriate for our purpose since there is no significant PSF variation across any of our cluster frames. For each CCD image, DoPHOT determines the positions, magnitudes and uncertainties of all the stars it finds. Some of these 'stars' do not correspond to actual objects in the sky, but rather regions of excess flux, diffraction spikes or scattered light in the wings of bright stars, cosmic rays, unflattened CCD defects, *etc.* This algorithm identified 'false' detections as

objects with significantly larger errors than the mean error of other stars of similar brightness.

The following steps were used to search for variable stars in our data set. First, we transformed the positions of the stars measured on every CCD image to a common CCD coordinate system. One good-seeing frame was chosen to define this master coordinate system and transformations were determined using the positions of numerous bright stars common to most of the frames. These transformations typically consisted of small shifts in both axes for CCD frames obtained during the same run as the master frame. For frames acquired during other runs, a small rotation was also needed. The typical rms of the transformations was less than 0.01 pixel in both coordinates.

Second, we transformed all of the photometry to a common photometric system. We chose the best-seeing frames in each band to define a master photometric reference system (hereafter the master frame). For every star we then identified a set of "local comparison stars" consisting of nearby isolated stars with good-quality photometry. The photometric offset for any star was the median magnitude difference calculated for its local comparison stars relative to the photometry of the same stars on the master frame.

Third, we compiled lists of the instrumental V and I magnitudes for each star in the field where each entry corresponds to the observed instrumental magnitude (on a common system) at each epoch. We used only the positions of stars to match objects from different frames. A matching tolerance of about 0.25 arcsec effectively avoided all false matches.

Fourth, candidate variables were identified using the reduced chi-squared, which is defined as $\chi^2_\nu = (1/\nu)\sum_i (m_i - \overline{m})/\sigma_i^2$, where ν is the number of degrees of freedom, m_i is the measured magnitude at epoch i, $\overline{m}$ is the mean magnitude of the star, and σ_i is the DoPHOT-supplied formal error of the ith observation. Figure 1 shows a plot of χ^2_ν as a function of V magnitude; every star with $\chi^2_\nu \geq 5.0$ was checked for

variability. We also demanded that every candidate was measured on at least 40% of frames in each color. Most of the stars with $\chi^2_\nu > 5.0$ turned out to be non-variable; their large values of χ^2_ν generally resulted from just one or two spurious measurements.

We further restricted our candidate variables to those with strong evidence for *periodic* variability. To do this, we used the period-finding algorithm described by Lafler and Kinman (1965) and determined possible periods for every candidate variable in the range 0.02−5 days. We then visually examined the phased light curves to confirm periodicity and the adopted period. All *bona fide* variables were required to show evidence for variability at the same period in both colors. We identified six short period variables in our M 5 field that satisfied these criteria. The phased V and I light curves for these stars are shown in Figure 2 and 3 respectively. The vertical bars in the plots indicate the $\pm 1\sigma$ error in the photometry, which characterizes the photon statistical fluctuation. However, these error bars do not represent the photometric errors caused by crowding and seeing variations, which are difficult to quantify. To provide an informative comparison, we also plot the V-band light curves for three non-variables in Figure 4. These three stars were selected from the same part of the cluster HR diagram which is occupied by the six eclipsing variables. Spatially, the non-variable star 3 is located within the $4r_c$ region, and stars 1 & 2 are in the region beyond the $4r_c$ radius.

We calibrated the photometry by observing Landolt standards (Landolt 1992). The following equations were derived from these observations to transform the instrumental magnitudes to the Kron-Cousins VI system:

$$I = I_{inst} - 2.24 \tag{4.1}$$

$$(V - I) = 1.1(V - I)_{inst} + 0.906 \tag{4.2}$$

Here the instrumental magnitude in the equation is normalized to the magnitude of 1 second exposure. These colour terms were determined separately during each

observing run, with good internal agreement. The V and I light curves in Figures 2 and 3 were all calibrated with the above equations. A complete listing of the photometry for each variable can be found in Table 2. A wide-field identification chart showing the locations of the variables is shown in Figure 5, while detailed charts of each variable star are presented in Figure 6. Table 3 provides the ephemerides for the six eclipsing systems.

4.3. Results

We have found six short-period interacting binary stars in the globular cluster M 5. Their periods are in the range of 0.4 days to 0.7 days. Of the six variables, one is a possible blue straggler, four lie near the main-sequence turnoff in the colour-magnitude diagram of the cluster, and one is $\sim$ 1 magnitude below the turn-off (Figure 7). We classified the star V1 only as a possible blue straggler candidate because its (V - I) colour lies less than $2\sigma_{V-I}$ bluer than the turnoff, where σ_{V-I} is the uncertainty in the colour. We have limited our search to the I magnitude brighter than 19, or $\sim$ 2 magnitude below the main-sequence turnoff. Among the six short-period variables, five of them are probably W UMa type contact eclipsing binaries, and one variable V3 may be a semi-contact Algol system, as shown by their light curves in Figure 2 and 3. W UMa type contact eclipsing binaries are composed of components which both fill their critical Roche surfaces, forming a common envelope of approximately constant temperature. The shape and depths of the two eclipses of a W UMa type binary are typically similar despite the mass ratio being far from unity. The light curve of V3 shows that in this case the two eclipses may have different depths, indicating that the two components have unequal effective temperatures, which is more characteristic of a semi-contact Algol type eclipsing binary system. As demonstrated by the light curves, the classification of the variable type is fairly uncertain because of incomplete phase coverage and photometric errors caused by

crowding in the light curves. Deeper observations of this cluster should clarify the uncertainty.

Table 3 lists the fundamental properties of the six newly discovered interacting binaries in M 5. In Column 4 of the table, EW represents a W UMa type contact eclipsing binary and EA, an Algol type detached or semi-detached eclipsing binary. In addition, TO indicates that the variable lie on the main-sequence turnoff, BSS is an abbreviation for blue straggler star and MS is for a main-sequence star. In this table V_{Amp} is the maximum V band amplitude of a light curve, $\langle V \rangle$ is the mean V magnitude, $\langle V - I \rangle$ is the mean colour, $\langle V_0 \rangle$ is the reddening-corrected value of $\langle V \rangle$, and $\langle (V - I)_0 \rangle$ is the extinction-corrected mean color. We have adopted E(V−I)= 0.03 (Harris & Racine 1979) and $A_V = 2.58E(V - I)$ (Cardelli, Clayton & Mathis 1989) in order to make extinction corrections.

The next pertinent question is whether these six short-period variables are cluster members. Unfortunately, without proper motion or radial velocity data, it is difficult to definitively determine the variable memberships. Due to limited telescope time, we did not have similar observations of a background control field to statistically subtract the foreground/background variables from our sample. However, since M 5 has galactic latitude of 47°, the number of foreground/background stars is small. Based on the galaxy model derived by Reid and Majewski (1993), we estimate that there are $\sim$ 40 field stars within our 40 square arcminutes field. Approximately 70% of these stars are predicted to have colours consistent with stars in M 5. In contrast, we have measurements of $\sim$ 5000 stars in M 5 in the same magnitude range. Given that the eclipsing binary frequency among field stars is only $\sim$0.1% (Rucinski 1993), the formal probability of any of our six short-period variables being a field star is insignificant, particularly given the location of these variables on the M 5 colour-magnitude diagram (Figure 7).

In addition to these six variables, Reid (1995) has identified four possible eclipsing variables, two on the horizontal branch and two on the giant branch. The black

square symbols in Figure 7 indicate the variables found by Reid (1995). Again, these four variables lie in the region beyond the $4r_c$ radius. The periods of these variables are uncertain because only one eclipse is clearly detected. The horizontal branch variable 651 and the giant variable star 652 have periods less than 25 days and $\sim$ 400 days respectively. The shape of the detected eclipse in the light curve is narrow, and the missing secondary eclipse could be very shallow. These characteristics of the light curves suggest that all four variables are Algol type eclipsing binaries. The two variables on the giant branch are definitely long period eclipsing binaries, and the two on the horizontal branch could have short periods. The period upper limit of 25 days for the variable 651 suggests that this binary is formed either by star-binary or binary-binary encounters, or by a main-sequence star spiraling into an expanding giant star in a long period primordial binary system. Since the four eclipsing binaries found by Reid (1995) have a relatively complicated and uncertain evolution history, we exclude them in our estimate of the overall binary frequency in M 5.

4.4. Artificial Eclipsing Binary Star Simulations

To interpret our result, we have to quantify what fraction of these types of variables we might have missed during our search. This is achieved by carrying out artificial eclipsing binary star simulations. Generally, the efficiency of detecting a short-period eclipsing variable is a function of 1) the variable's position in a cluster (crowding effect), 2) the brightness of the variable (photometric errors), 3) the amplitude of the light curve, 4) the variable's period, and finally 5) the light curve phase coverage of the available data.

In this paper, to reduce the amount of computing time to a reasonable level, we fixed the light curve amplitudes of our artificial eclipsing binaries as 0.25 magnitude, which is the smallest amplitude among the five eclipsing binaries we found in M 71 (Yan & Mateo 1994). The simulations were done at three different I magnitudes:

15.0, 17.6 and 18.6. The positions of the artificial binaries were drawn from a uniform random distribution relative to the cluster center that was generated as follows:

$$x = xc + \sqrt{r_0^2 \times ran1} \times \cos(2\pi ran1) \tag{4.3}$$

$$y = yc + \sqrt{r_0^2 \times ran1} \times \sin(2\pi ran1) \tag{4.4}$$

where ran1 is a random number generator (Press 1988) with a uniform distribution between 0 and 1, r_0 is the radius from the cluster center, and xc, yc are the coordinates of the cluster center in pixels on a CCD image. To simulate a contact eclipsing binary, we define all of our artificial binary stars to have light curves of the form shown in Figure 8. For each artificial binary star, the period P and initial phase ϕ_0 are randomly chosen within the limits of 0.25 days to 1.2 days and 0.0 to 2π respectively. Finally, an artificial binary star is added into a CCD image with the same PSF as that determined from real stars in the same image and with the allowance of poisson noise.

These simulations allow us to determine how the detection efficiency varies both with the distance from the cluster center and with the mean magnitude. Here the detection efficiency is defined as the ratio of the number of recovered binaries and the total number of initially input binary stars. Figures 9(a), 9(b) and 9(c) show the detection efficiency versus the distance from the cluster center in units of the cluster core radius r_c at the three different mean I magnitudes 15.0, 17.6 and 18.6 respectively. The vertical bar at each point indicates the $\pm 1\sigma$ error due to poisson statistics of the simulations, and the horizontal bar indicates the width of each bin, which is $1r_c$. It is clearly shown in Figure 9 that within the central $4r_c$ region the binary detection efficiency drops off rapidly, and the possibility of detecting any short period variables, especially main-sequence ones, is reduced severely by crowding effect. All of the eclipsing binaries, including four discovered by Reid (1995), are located beyond the $4r_c$ radius. Thus we limit our calculations and the incompleteness corrections to stars in the outer parts of the cluster with $R > 4r_c$.

Figure 9(a) shows that the detection efficiency for short period variables at the I mean magnitude of 15.0 varies from 90% to 100% for R > $4r_c$. This implies that the search for short period eclipsing binaries is ~100% complete among horizontal branch stars. There is one possible short-period eclipsing binary discovered among a total of 207 horizontal branch stars in M 5 (Reid 1995).

Of the six eclipsing variables we found in M 5, one is located between the radii of $4r_c$ and $5r_c$ with I magnitude of 18.0, four between $5r_c$ and $6r_c$ with I magnitudes from 17.1 to 17.46, and one between $7r_c$ and $8r_c$ with I of 17.45 mag. We label these three annuli as A1, A2 and A3. From Figures 9(b) and 9(c), the incompleteness corrected number of binaries in A1, A2 and A3 are 2.1, 7.7 and 1.3 respectively. Thus after incompleteness correction, the expected total number of short period eclipsing binaries is $11^{+4.4}_{-2.3}$.

4.5. Discussion

4.5.1. The Binary Frequency in M 5

In the region beyond $4r_c$ from the cluster center, we have monitored approximately a total of 3600 stars from I magnitude 13.2 down to 19.0 for variability in M 5. We have discovered six short-period eclipsing binaries with the dataset tabulated in Table 1. If these six binaries represent the final stages of evolution of initially detached binaries whose components have come into contact via magnetic braking (Vilhu 1982), we can thus infer the cluster overall binary frequency from our observations.

There are two mechanisms which could produce the six short-period interacting binary stars in M 5. One mechanism of forming contact binaries involves braking torques from magnetized stellar winds in tidally synchronized systems. This idea has

been explored by many people (Huang 1967, Vilhu 1982, 1992; Guinan and Bradstreet 1988; Eggen and Iben 1989); the most detailed models suggest that binaries with initial orbital periods in the range 2.5−5 days may evolve into a contact configuration on a timescale of 5−15 Gyr. With the cluster central density of $10^4 M_\odot/pc^3$ and radial velocity dispersion of 5.7 km/s (Pryor & Meylan 1993), the timescale for destroying binaries (only star-binary encounters) with periods less than 2.5−5 days and component masses of $0.7 M_\odot$ exceeds 10^{11}yrs (Hills 1984). If we assume the shortest orbital periods of primordial binaries in M 5 was 2.5 days (this is the shortest period observed in zero-age binary populations studied by Giuricin *et al.* 1984, Matheiu *et al.* 1989, and Bodenheimer *et al.* 1993), magnetic braking would have caused such binaries to evolve into contact in less than 17 Gyr, the lifetime of M 5 (Richer & Falhman 1987).

The second option is that the interacting binaries in M 5 were formed during binary-binary encounters. They could be produced by two wide binary-binary or one wide binary and one short-period binary encounters. However, accounting for all six short-period binaries in M 5, which lie in the low density regions of the cluster, would require a very large fraction of primordial binary stars. It is not clear at all if the binary-binary collision rate is high enough to produce all six variables if we adopt the usual estimate of $10 - 30\%$ for the overall binary frequency. Further detailed theoretical calculations are certainly needed. For the present calculation, we simply assume that the six short-period interacting binaries have evolved from primordial binary systems.

If a contact binary has a lifetime shorter than the age of M 5, it will have merged to form a single star. The lifetimes of contact binaries are extremely uncertain; estimates range from 10^8 to 10^{10} yrs, depending on assumptions regarding the relevant angular momentum loss mechanisms (Rahunen 1981; Eggen and Iben 1989). Most studies seem to favor $\tau_{\rm contact} \sim 3 \times 10^9$ yrs which we adopt. Thus, with the discovery of six eclipsing binaries in the period range of 2.5−5 days among a total

of 3600 stars (28 estimated background/foreground stars), we calculated a primordial binary frequency f_b for systems with initial periods of 2.5−5 days as follows: $11/(3600-28) \times \frac{\tau_{\rm gc}}{\tau_{contact}} = 1.7\%$, here $\tau_{\rm contact}$ and τ_{gc} are the lifetimes of a contact binary and M 5 respectively. It is clear that the lifetime of a contact binary is the major uncertainty in calculating f_b since the ratio $\frac{\tau_{\rm gc}}{\tau_{contact}}$ can vary over two orders of magnitude.

Soft binaries in a globular cluster are binaries with periods so long that their orbital kinetic energy is less than the kinetic energy of cluster single stars. These soft binaries are quickly disrupted during stellar encounters and do not affect the cluster dynamical evolution (Hills 1984). On other hand, hard binaries have relatively shorter periods and their orbital kinetic energy is higher than the cluster single star kinetic energy. Hard binaries are the heat source for the evolution of a cluster. Thus we will only estimate the binary frequency for binaries with periods up to the longest period a hard binary could have. In M 5, we estimated that the upper limit on the periods of hard binaries is $\sim$ 550 years. For a flat binary period distribution $\frac{df}{d\log P} = constant$, our observations imply an overall binary frequency of $28^{+11}_{-6}\%$ in M 5, which is consistent with the binary frequency measured in other clusters (Yan & Mateo 1994; Hut *et al.* 1992).

4.5.2. Comparison With Other Globular Clusters

To compare blue straggler stars (BSS) population in different globular clusters, a popular and useful tool people generally use is to calculate blue straggler specific frequency, which is generally defined as the ratio of the number of BSS and the total number of subgiant stars that fall in the same magnitude range as the BSS (Nemec & Harris 1987; Bolte, Hesser & Stetson 1993). Here to understand the relationship between short-period main-sequence eclipsing binaries (SPMSEB) and BSS and their dependence on the cluster environment, we derive the specific frequency of SPMSEB, *i.e.*, the ratio of the number of SPMSEB and the number of main-sequence

stars within the same magnitude range as the SPMSEB. In M 5, excluding the possible blue straggler, we derived $\sim$ 0.5% for the SPMSEB specific frequency. Using the published M 71 data (Yan & Mateo 1994), we obtained $\sim$ 0.6% for the SPMSEB specific frequency in M 71. Recent deep photometric study of M 5 (Sandquist 1995, personal communication) revealed a large population of blue stragglers in M 5, comparable to that in M 71 (Hodder *et al.* 1992). It is still premature to make any conclusive comparison of the number of eclipsing binaries and blue stragglers in different clusters. Clearly we need to increase short-period eclipsing binary database before we understand how SPMSEB are related to BSS. Monitoring variabilities for both main-sequence stars and blue stragglers in the same cluster will be useful for defining quantitatively the evolution rate from SPMSEB to BSS.

The eclipsing binary search procedure we used in this paper was developed in collaboration with M. Mateo (Yan & Mateo 1994). We would like to thank M. Mateo for his unreserved help and for useful discussions. We thank the Palomar staff for their help during all of the observations. DoPHOT was developed by Paul Schechter with the support of NSF Grant No. AST83-18504.

REFERENCES

Bodenheimer, P., Ruzmaikina, T. & Mathieu, R. D., 1993, in *Protostars and Planets III*, eds. E. H. Levy, J. I. Lunine (Tucson: University of Arizona Press), 367

Bolte, M., Hesser, J. E. & Stetson, P. B., 1993, ApJ, 408, L89

Cardelli, J. A., Clayton, G. C. & Mathis, J. S., 1989, ApJ, 345, 245

Edmonds, P.D., Gilliland, R.L., Petro, L.D., Saha, A. & Shara, M.M. 1994, BAAS, 26, 1487

Eggen, O. J. & Iben, I. 1989, AJ, 97, 431

Giuricin, G., Mardirossian, F. & Mezzetti, M. 1984, ApJS, 54, 421

Guhathakurta, P., Yanny, B., Bahcall, J.N. & Schneider, D.P. 1994, AJ, 108, 1786

Guinan, E. F. & Bradstreet, D. H. 1988, in *Formation and Evolution of Low Mass Stars*, eds. A. K. Dupree and M. T. V. T. Lago (Dordrecht: Kluwer), 345

Harris, W.E. & Racine, R. 1979, ARAA, 17, 241

Heggie, D.C. & Aarseth, S.J. 1992, MNRAS, 257, 513

Hills, J. G. 1984, AJ, 89, 1811

Hodder, P. J. C., Nemec, J. M., Richer, H. B. & Fahlman, G. G. 1992, AJ, 103, 460

Huang, S. S. 1967, ApJ, 150, 229

Hut, P., McMillan, S., Goodman, J., Mateo, M., Phinney, E.S., Richer, H.B., Verbunt, F. & Weinberg, M. 1992, PASP, 104, 981

Kaluzny, J. & Krzeminski, W. 1993, MNRAS, 264, 785

Lafler, J. & Kinman, T. D. 1965, ApJS, 11, 216

Landolt, A. 1992, AJ, 104, 430

Livio, M. 1993, in *Blue Stragglers*, ed. R. Saffer (San Francisco: ASP), 3

Mateo, M., Harris, H.C., Nemec, J. & Olszewski, E.W. 1990, AJ, 100, 469

Matheiu, R. D., Walter, F. M. & Myers, P. C. 1989, AJ, 98, 987

Nemec, J. M. & Harris, H. C. 1987, ApJ, 316, 172

Press, W.L., Flannery, B.P., Teukolsky, S.A. & Vetterling, W.T. 1988, in *Numerical Recipes*, Cambridge University Press, 196

Pryor, C. & Meylan, G., 1993, in *Structure and Dynamics of Globular Clusters*, ed. S. G. Djorgovski and G. Meylan (San Francisco: ASP), 325

Rahunen, T. 1981, A&A, 102, 81

Reid, I. N. 1995, MNRAS, in press

Reid, I. N. & Majewski, S. R. 1993, ApJ, 409, 635

Richer, H. B. & Falhman, G. G. 1987, ApJ, 316, 189

Rubenstein, E.P. & Bailyn, C.D. 1995, preprint.

Rucinski, S. M., 1993, in *The Realm of Interacting Binary Stars*, ed. J. Sahade *et al.* (Dordrecht: Kluwer), 111

Schechter, P. L., Mateo, M. & Saha, A. 1993, PASP, 105, 1342

Stryker, L. L. 1993, PASP, 105, 1081

Yan, L. & Mateo, M. 1994, AJ, 108, 1810

van't Veer, F. 1979, A&A, 109, 17

Vilhu, O. 1982, A&A, 109, 17

Vilhu, O. 1992, in *Evolutionary Processes in Interacting Binary Stars*, eds. Y. Konda, R. F. Sisteró, and R. S. Polidan (Dordrecht: Kluwer), 61

Table 1 - Summary of Observations

Date	UT Range hh:mm	N_v	N_i	Exp. Time sec
1991 May 22/23	05:32–08:15	21	5	150
1991 May 23/24	04:45–08:23	5	6	150
1991 June 15/16	07:19–09:28	12	11	150
1991 June 16/17	05:47–08:40	26	10	150
Total		64	32	

Note: N_V and N_i are the number of V and i images obtained in each sequence. All images have seeing better than 1.2". Here exposure time in the last column is for a single image.

Table 2(a) – Johnson V Band Photometry Data for the Six Short Period Variables in M 5

No.	HJD days	V1	V2	V3	V4	V5	V6
13	2448399.73712	99.999	18.201	18.899	17.917	18.246	18.006
15	2448399.74408	17.730	18.011	18.566	17.855	18.045	17.953
16	2448399.74669	17.694	17.941	18.733	99.999	99.999	17.966
17	2448399.74952	17.680	17.95	18.676	17.761	99.999	17.957
18	2448399.75240	17.591	99.999	18.646	17.789	18.044	17.924
20	2448399.75837	17.646	17.938	18.647	17.826	18.043	17.972
21	2448399.76124	17.763	18.11	18.635	17.871	18.275	17.918
22	2448399.76402	99.999	17.93	18.657	17.897	18.065	17.935
23	2448399.76695	17.674	17.971	18.617	17.864	18.065	17.935
25	2448399.77292	17.702	17.973	18.684	17.755	18.059	17.940
26	2448399.77575	17.650	17.951	18.588	17.75	18.023	17.910
27	2448399.77857	99.999	17.977	18.63	17.812	18.056	17.937
28	2448399.78134	99.999	99.999	18.667	17.805	18.059	17.992
30	2448399.79016	17.604	17.944	18.601	17.784	18.052	17.901
32	2448399.79625	17.623	17.948	18.601	17.747	18.122	17.923
33	2448399.79936	17.647	17.957	18.611	17.811	99.999	17.916
40	2448399.82104	17.655	17.947	18.633	17.857	18.100	17.950
41	2448399.82407	17.676	17.957	18.626	17.827	18.064	17.947
45	2448399.83561	17.701	18.005	18.611	17.844	18.095	17.973
48	2448399.84403	17.697	17.925	18.608	17.834	18.113	17.926
50	2448399.85012	99.999	18.054	18.641	17.794	18.026	17.952
105	2448400.70451	17.715	18.004	99.999	17.796	99.999	17.986
107	2448400.71050	99.999	17.953	18.69	17.806	18.049	17.963
136	2448400.79623	17.667	17.946	18.646	17.916	99.999	17.978

149	2448400.83527	17.697	17.975	18.652	17.941	18.051	17.960
156	2448400.85589	17.705	17.972	18.67	17.839	18.081	17.948
221	2448423.81022	17.958	18.162	99.999	18.016	18.241	18.046
223	2448423.83093	17.974	18.131	99.999	18.116	18.204	18.127
226	2448423.84512	99.999	18.054	18.708	17.976	18.226	99.999
228	2448423.85222	17.802	18.043	99.999	17.905	18.178	17.995
230	2448423.85817	17.897	18.098	99.999	17.929	18.219	18.088
232	2448423.86412	99.999	18.102	18.716	17.978	18.048	18.015
234	2448423.87023	17.703	18.09	18.697	17.827	18.062	17.923
236	2448423.87628	17.695	18.071	99.999	17.828	18.064	17.933
238	2448423.88251	17.725	18.025	18.668	17.787	18.119	99.999
240	2448423.88847	17.694	18.051	18.733	17.809	18.183	17.948
242	2448423.89431	17.694	17.95	99.999	99.999	18.036	17.933
244	2448423.90027	99.999	99.999	99.999	99.999	99.999	99.999
281	2448424.74669	17.777	18.096	18.705	18.041	18.158	17.956
282	2448424.74951	17.793	18.041	18.671	17.960	18.235	18.002
284	2448424.75560	17.891	18.091	18.888	17.999	18.235	18.034
285	2448424.75850	17.883	18.112	18.742	18.003	18.252	18.168
287	2448424.76446	17.849	18.158	18.808	17.997	18.314	18.031
290	2448424.77333	17.861	18.192	19.017	18.017	18.259	18.157
291	2448424.77623	18.053	18.136	18.991	18.048	18.260	18.191
294	2448424.78510	17.870	18.177	18.793	17.980	18.290	18.116
295	2448424.78801	18.080	18.169	99.999	18.035	18.206	18.086
296	2448424.79092	17.945	18.17	18.914	17.998	18.333	18.143
298	2448424.79964	18.006	18.177	19.005	18.065	18.279	18.133
299	2448424.80255	17.977	18.139	18.924	17.992	18.310	18.088
300	2448424.80545	18.001	18.189	18.963	18.032	18.287	18.177
302	2448424.81141	17.972	18.143	99.999	99.999	99.999	18.108
303	2448424.81432	17.907	18.153	18.842	17.929	18.185	18.114

304	2448424.81722	17.943	18.17	18.925	18.007	18.348	18.141
306	2448424.82318	17.997	18.153	18.824	17.968	18.220	18.188
307	2448424.82610	17.902	18.119	18.92	17.994	18.149	18.203
308	2448424.82899	99.999	18.146	18.805	17.952	18.126	18.017
310	2448424.83495	99.999	18.135	18.678	17.860	99.999	17.932
311	2448424.83786	17.869	18.105	18.727	17.852	18.070	17.961
312	2448424.84076	17.756	18.117	18.697	99.999	18.046	17.988
314	2448424.85190	17.792	18.094	18.686	17.760	18.036	17.935
316	2448424.85772	99.999	18.12	18.776	17.765	18.010	17.966
318	2448424.86367	17.845	18.159	18.838	99.999	18.019	17.987
319	2448424.86657	99.999	18.102	18.692	99.999	18.037	17.963

Notes: The second column HJD is the heliocentric date. An entry of 99.999 means there are no photomteric data for the corresponding heliocentric date.

Table 2(b) – Kron-Cousin I Band Photometry Data for the Six Short Period Variables in M 5

No.	HJD days	V1	V2	V3	V4	V5	V6
14	2448399.74059	17.152	17.483	18.018	17.183	17.413	17.527
19	2448399.75537	17.085	17.397	17.986	17.085	17.368	17.299
24	2448399.76996	99.999	17.28	17.958	17.086	17.410	17.297
29	2448399.78425	16.96	17.293	17.955	17.163	17.394	17.280
44	2448399.83269	17.076	17.745	18.052	17.169	17.434	17.273
127	2448400.7689	16.920	17.262	17.945	17.148	17.417	17.304
133	2448400.78699	17.013	99.999	17.966	17.059	17.412	17.281
142	2448400.81413	17.027	17.273	17.899	17.212	17.388	17.325
144	2448400.82002	16.987	17.278	17.973	17.206	17.377	17.308
148	2448400.83231	17.024	17.360	17.955	17.325	17.347	17.304
157	2448400.85879	17.121	17.365	17.923	17.308	17.375	17.318
222	2448423.81482	17.38	17.513	18.25	17.241	17.442	17.446
224	2448423.83442	17.464	17.526	18.293	17.219	17.45	17.470
225	2448423.83875	17.344	17.531	18.266	17.251	17.452	17.540
227	2448423.84925	17.261	17.485	18.068	17.343	17.473	17.565
229	2448423.85520	17.314	17.518	18.221	17.342	17.475	17.439
231	2448423.86114	17.343	17.491	18.092	17.148	17.423	17.570
233	2448423.86709	17.335	17.512	18.124	17.283	17.463	17.532
235	2448423.873310	99.999	17.681	18.118	17.163	17.524	17.282
237	2448423.87953	99.999	99.999	99.999	17.238	17.344	17.286
239	2448423.88548	17.114	99.999	18.008	17.117	17.343	17.290
241	2448423.89135	99.999	17.405	17.972	17.048	17.349	17.281
283	2448424.75261	17.258	17.446	17.997	17.313	17.58	17.364

286	2448424.76147	17.147	17.46	18.114	17.379	17.584	17.502
289	2448424.77035	99.999	17.473	18.126	17.349	17.593	17.561
293	2448424.78212	99.999	17.517	18.292	17.347	17.564	17.433
297	2448424.79675	17.367	17.459	18.147	17.349	17.6	17.358
301	2448424.80843	17.379	17.514	99.999	17.344	17.652	17.533
305	2448424.82021	17.310	17.456	99.999	17.305	17.62	17.646
309	2448424.83197	17.315	17.468	18.030	17.290	17.451	17.557
313	2448424.84892	17.039	17.408	18.032	17.303	17.530	17.288
317	2448424.86069	99.999	17.456	18.102	17.307	17.507	17.511

Notes: The second column HJD is the heliocentric date. An entry of 99.999 means there are no photomteric data for the corresponding heliocentric date.

Table 3 - Basic Properties of the Six Eclipsing Binaries in M 5

Name	X arcsec	Y arcsec	Type	Period days	HJD_0 +2440000.0	V_{Amp} mag	$\langle V \rangle$ mag	$\langle V-I \rangle$ mag	$\langle V \rangle_0$ mag	$\langle V-I \rangle_0$ mag	R r_c
V1	-132.83	18.50	EW, BSS	0.4971	8423.830926	0.45	17.78	0.59	17.71	0.56	5.6
V2	-46.99	-133.94	EW, TO	0.6442	8424.790917	0.30	18.06	0.61	17.99	0.58	5.9
V3	103.97	4.44	EA, MS	0.6260	8424.790917	0.40	18.73	0.67	18.66	0.64	4.3
V4	-16.65	-134.31	EW, TO	0.6973	8424.823184	0.30	17.89	0.65	17.82	0.62	5.6
V5	124.69	20.25	EW, TO	0.6186	8424.799644	0.35	18.14	0.68	18.07	0.65	7.2
V6	131.35	-41.81	EW, TO	0.4116	8424.805454	0.25	18.01	0.60	17.94	0.57	5.7

Notes: In column 4, EW represents the W UMa type contact eclipsing binaries, EA, the Algol type detached or semi-detached binaries. BSS indicates a blue straggler star, TO, a star on the main sequence turnoff and MS, a main sequence star. Due to incomplete phase coverage of the light curves, the variable type listed in column 4 is fairly uncertain and star V1 is a possible blue straggler. V_{Amp} is the maximum eclipse depth in the V-band light curve, $\langle V \rangle$ and $\langle V-I \rangle$ are maximum-light V magnitude and intensity mean V−I color, respectively, while $\langle V \rangle_0$ and $\langle (V-I) \rangle_0$ are the reddening-corrected values. The last column lists the radial distance (in units of the core radius r_c, where $r_c = 24''$) of each star relative to the cluster center. Here we used E(V-I)=0.03 (Harris & Racine 1979), A_V=0.075, A_I=0.045 derived from $A_I = 0.6A_V$ (Cardelli *et al.* 1989).

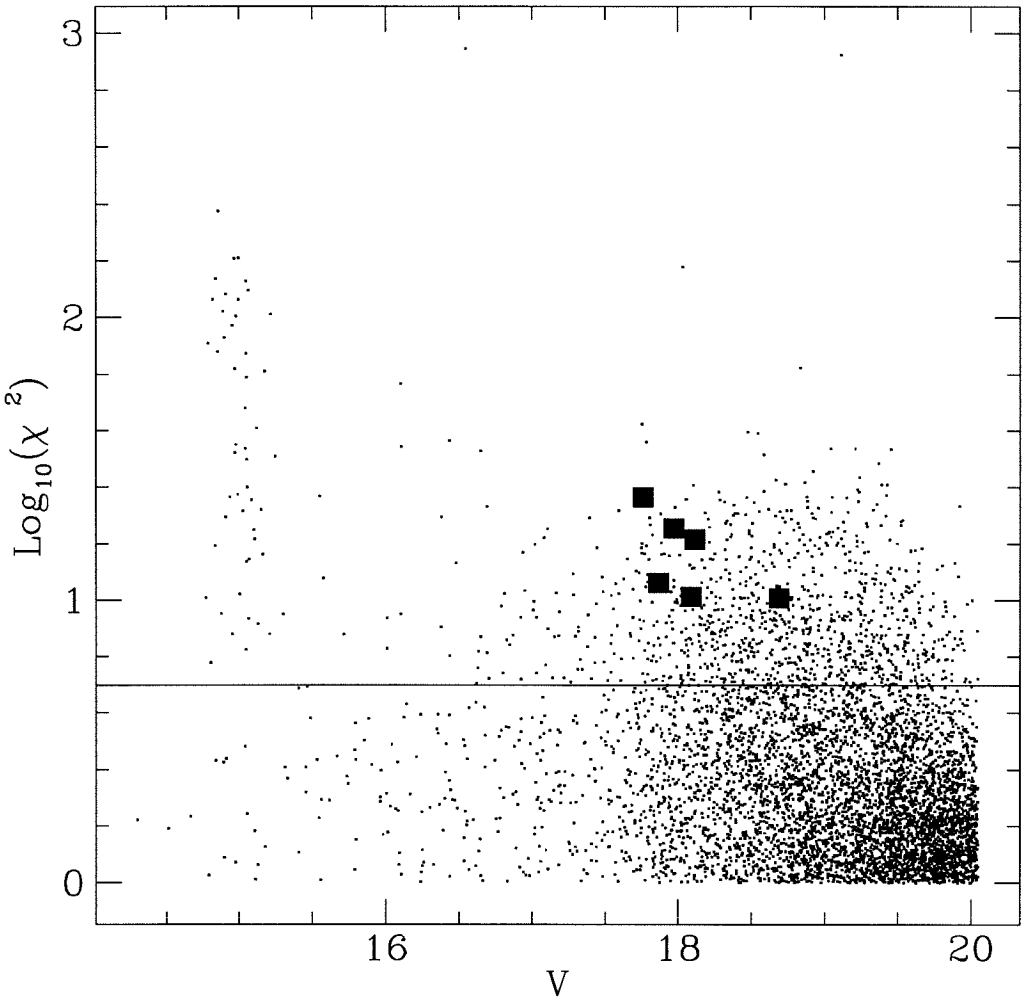

Figure 4.1: The reduced χ^2 statistic

A plot of the reduced chi-squared statistic, χ^2_ν as a function of I magnitude for 6172 stars with photometric measurements on at least 40% of all I-band images. The solid line shows the adopted cutoff at $\chi^2_\nu = 5.0$. For all stars located above this line we explicitly searched for periodic variability in the period range 0.1-5 days. The six variables are denoted as large filled squares. In the plot, most of the points with large chi^2 values at the bright magnitude have been identified as RR Lyrae stars in Reid (1995).

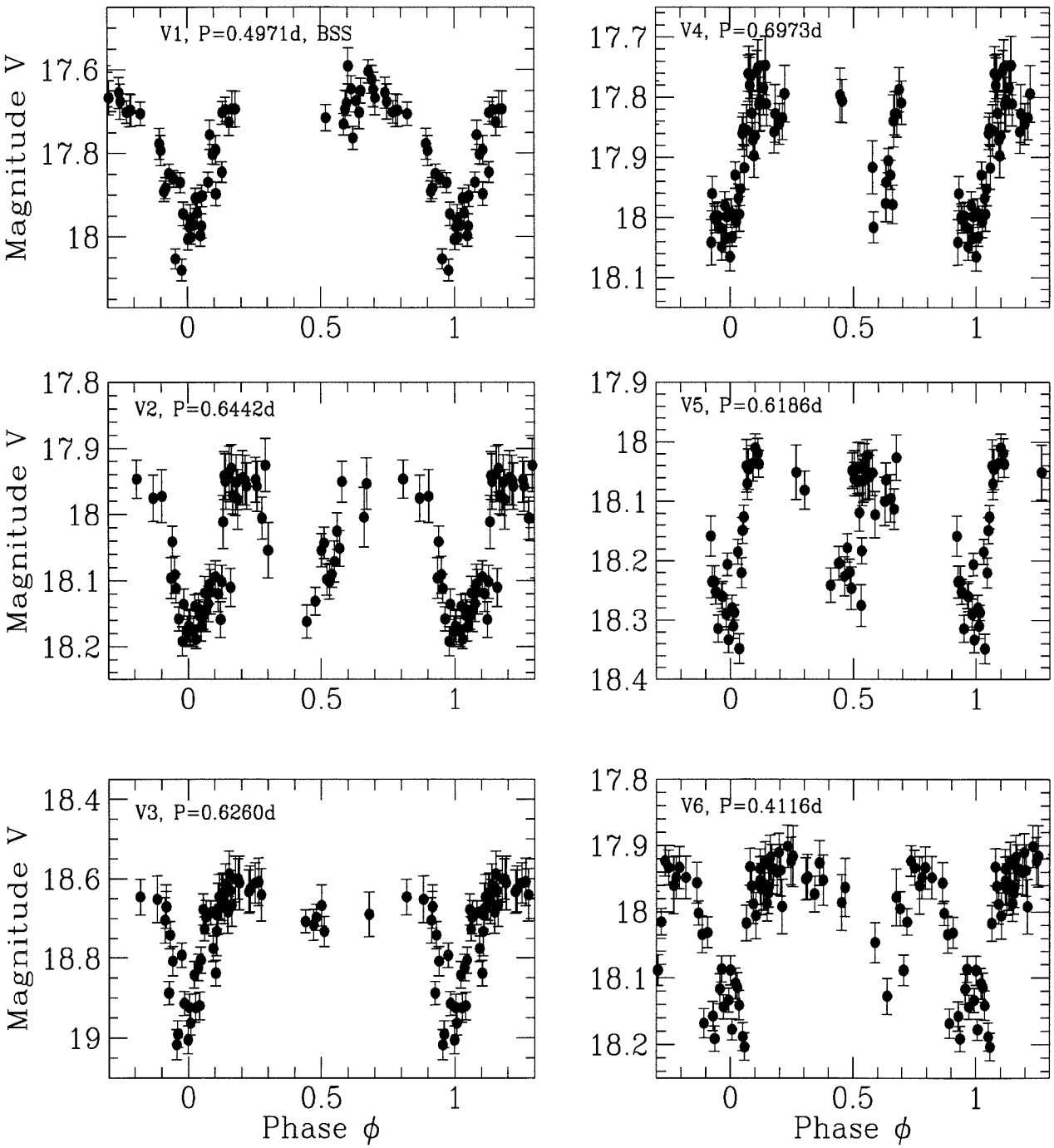

Figure 4.2: The V-band light curves

The V-band light curves of the six newly-discovered short-period binaries in M 5.

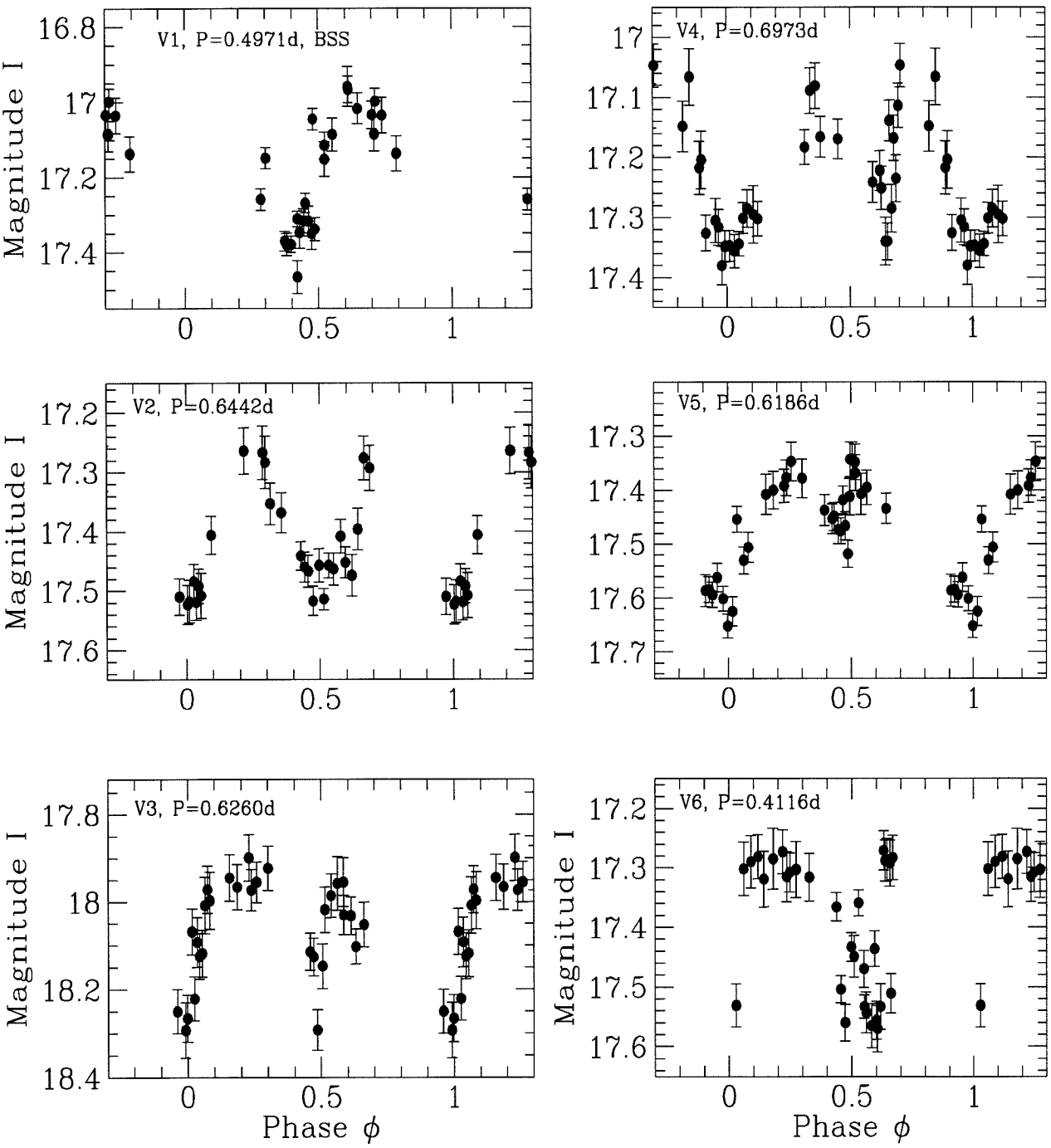

Figure 4.3: The I-band light curves

The I-band light curves of the six newly-discovered short period binaries in M 5.

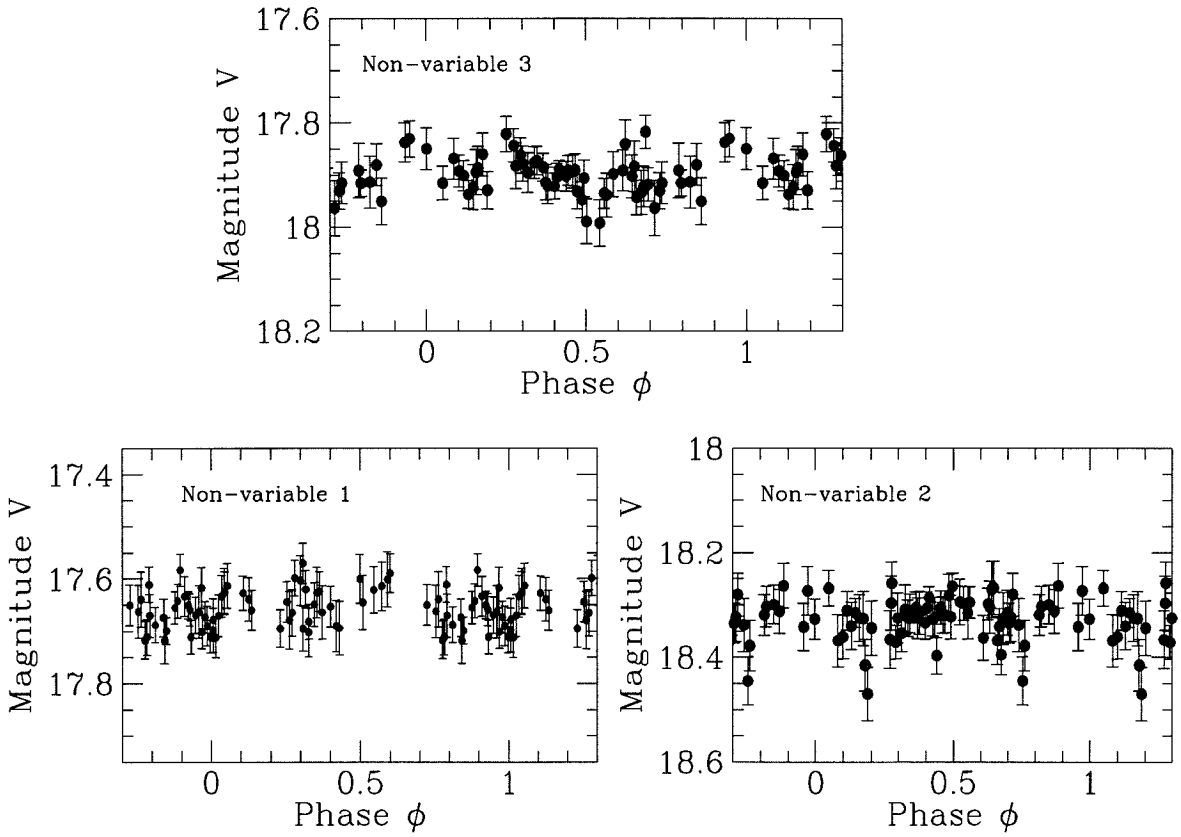

Figure 4.4: The V-band light curves of non-variables

The V-band light curves of three non-variables. These three non-variables occupy the same part of the cluster HR diagram as the six variables. Spatially, the non-variable star 3 is located within the $4r_c$ region from the cluster center and stars 1 & 2 are in the region beyond the $4r_c$ radius.

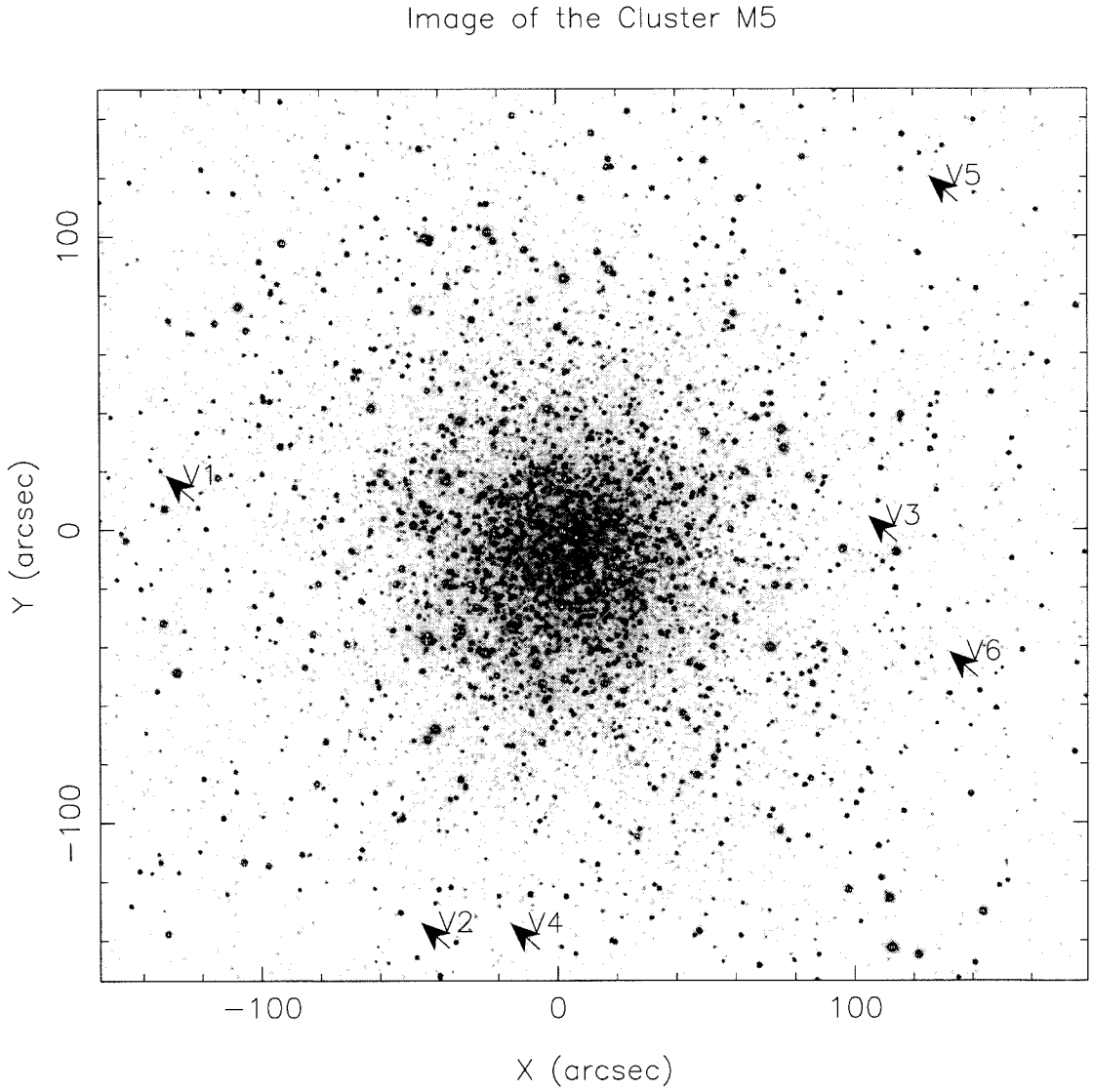

Figure 4.5: A wide-field finding chart

A wide-field identification chart for the six short period binary stars in M 5. The locations of these variables are marked by the arrows and variable names.

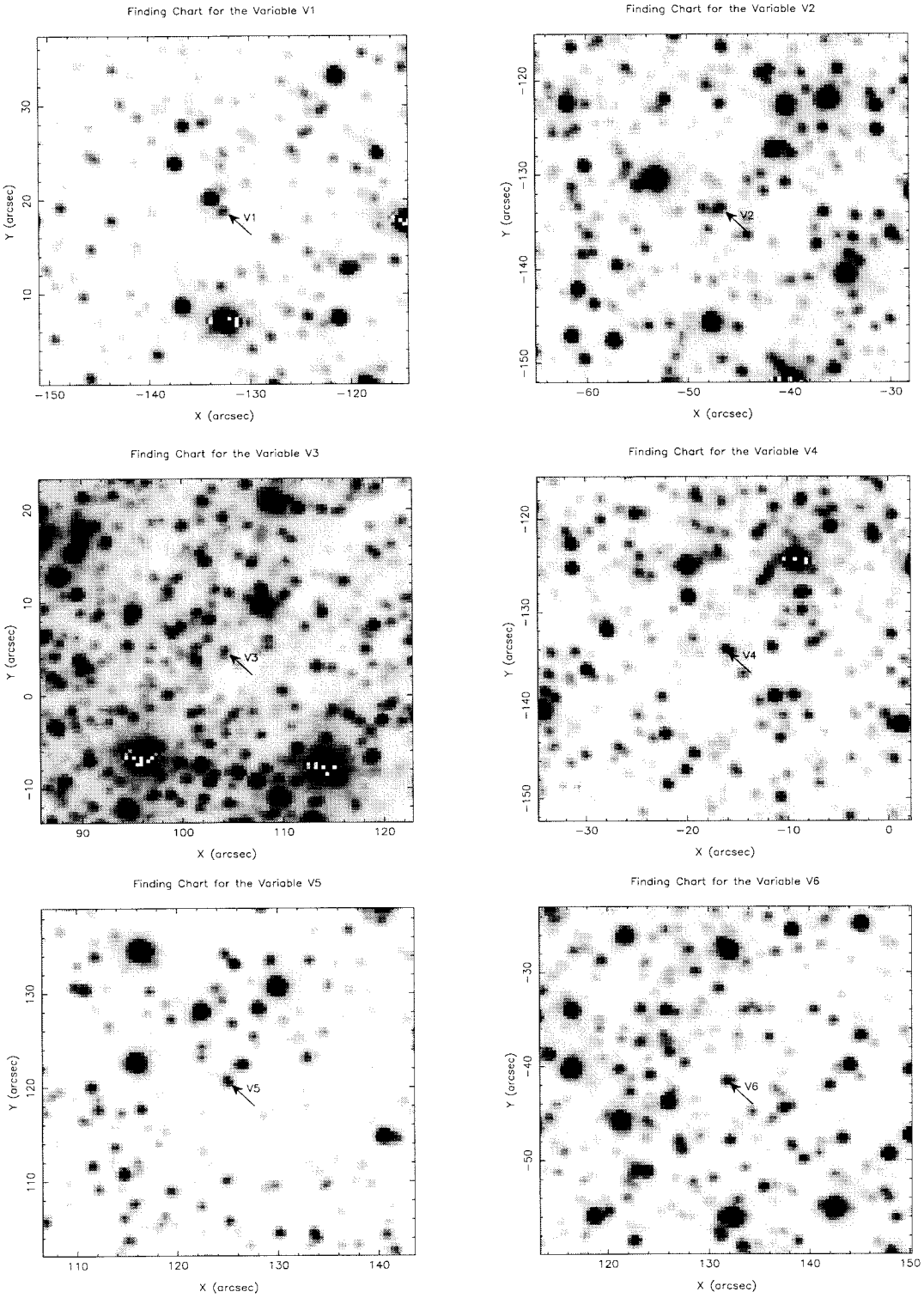

Figure 4.6: Detailed finding charts

Detailed finding charts for the six short period interacting binaries in M 5. The coordinates are relative to the cluster center in arcseconds.

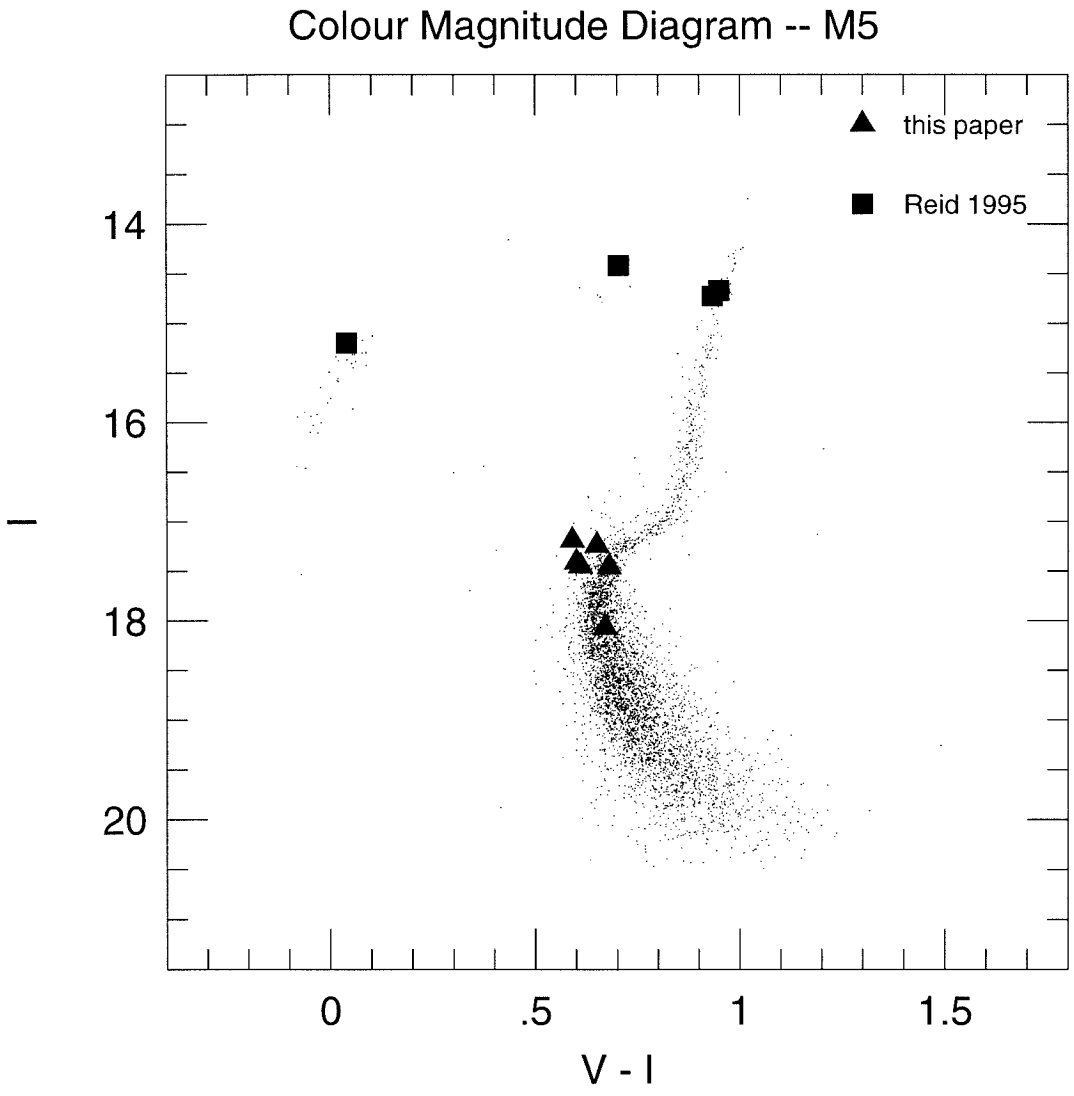

Figure 4.7: The cluster colour-magnitude diagram

The I-(V−I) colour-magnitude diagram of M 5. The six black triangles right at the main-sequence turn-off are the six short period eclipsing binaries. Here we used the mean magnitude and mean colour for each variable.

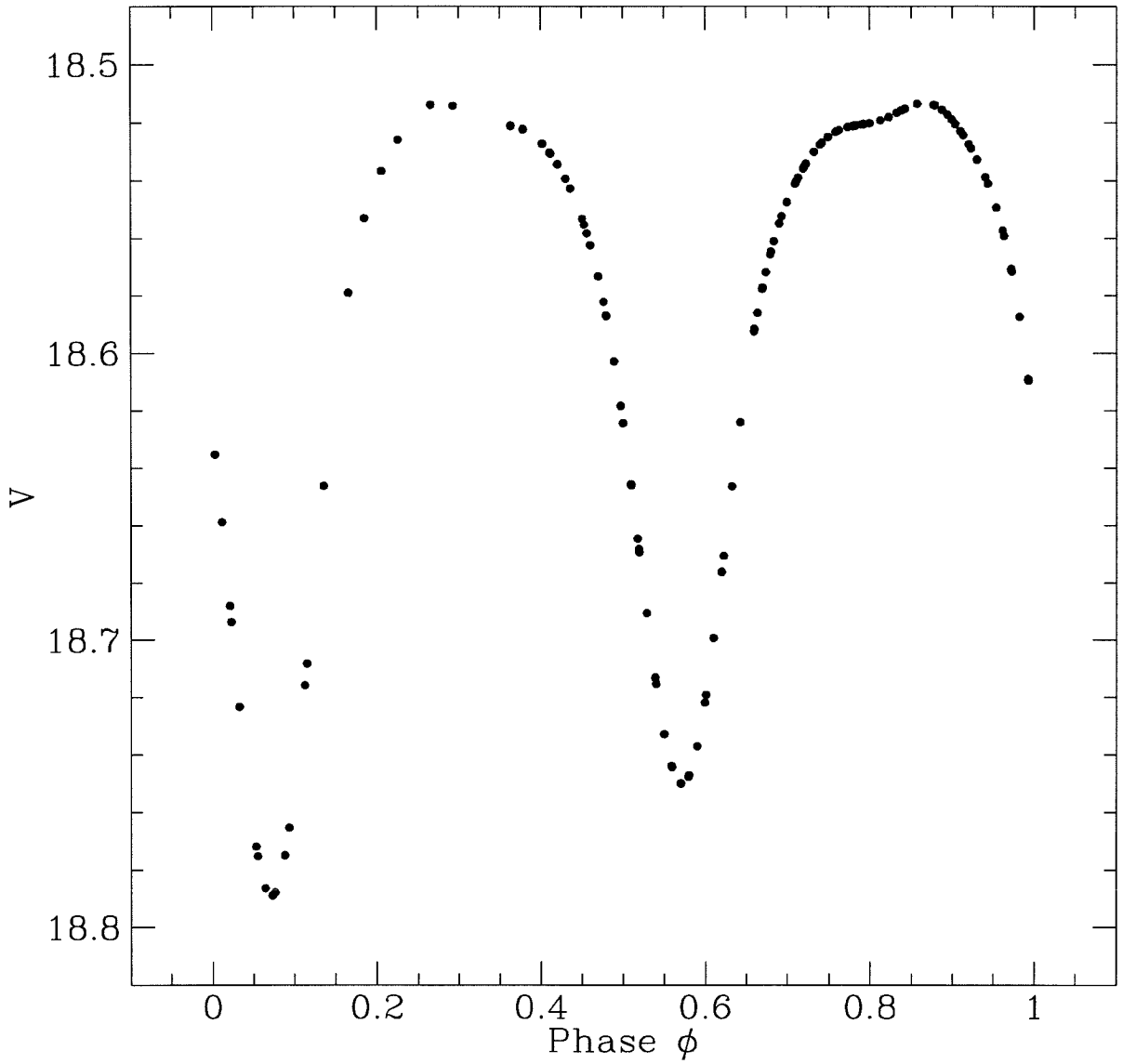

Figure 4.8: The input light curve for the simulations

The input light curve of an artificial short period eclipsing variable for the simulation. In the simulation, we used the same procedure for real stars to recover the artificial light curves in order to quantify the detection efficiency.

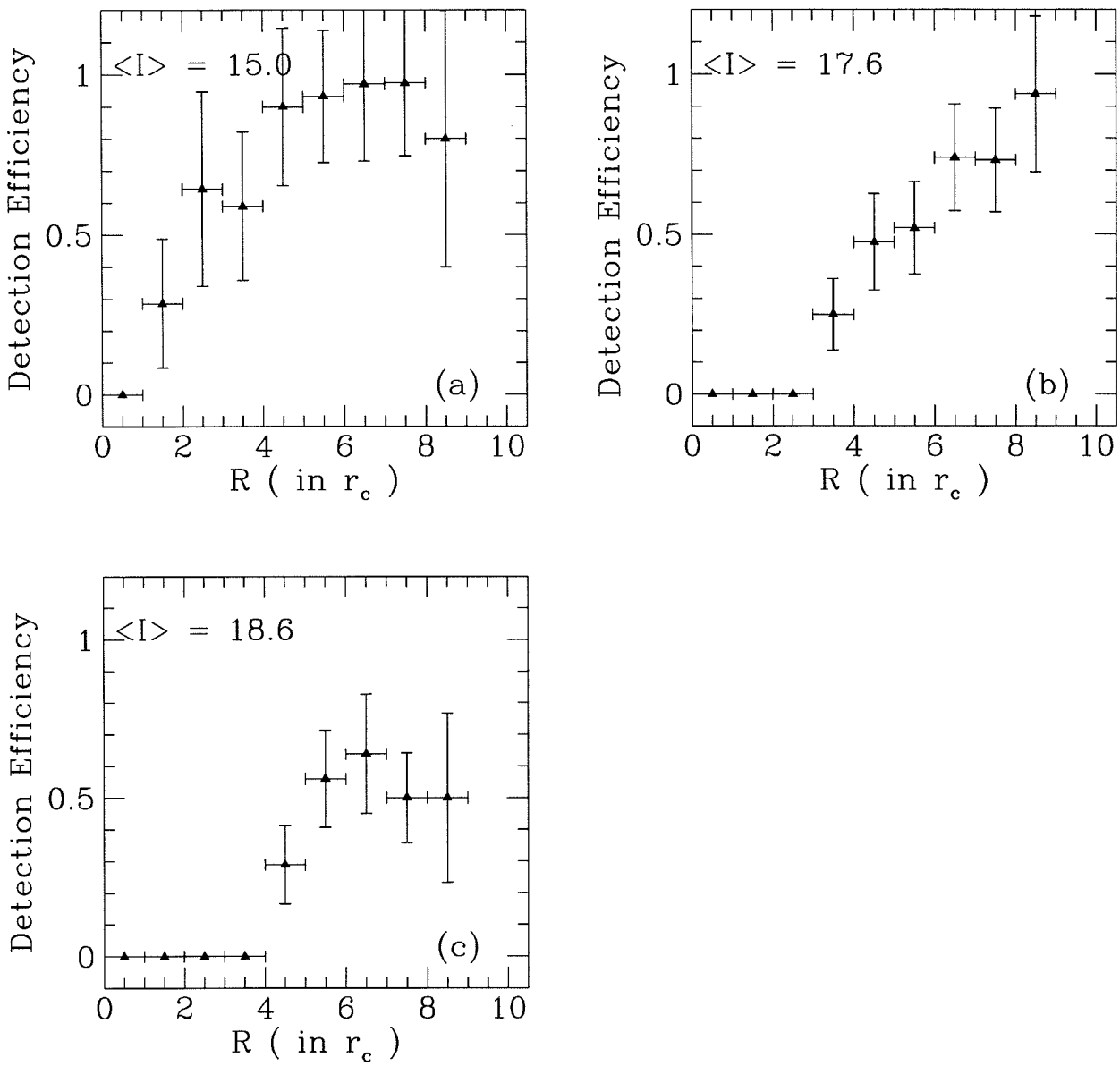

Figure 4.9: The eclipsing binary detection efficiency

The binary detection efficiency calculated from artificial eclipsing binary star simulation. For details about the simulation, see the text. Here the binary detection efficiency is defined as the ratio of the number of recovered eclipsing binaries and the total number of initially input binary stars. The detection efficiency is plotted as a function of radial distance from the cluster center. Figure 9(a), 9(b) and 9(c) are for the average variable I magnitude of 15.0, 17.6 and 18.6. The vertical bar at each point indicates the $\pm 1\sigma$ error due to poisson statistics of the simulations, and the horizontal bar indicates the width of each bin, which is $1r_c$; here r_c is the cluster core radius of $24''$.

Chapter 5

SUMMARY AND FUTURE WORK

Two types of surveys have been carried out in this thesis for searching for binary stars in globular clusters. The purposes of these searches are to estimate the frequencies of binary populations and to understand several apparently different phenomena, which are closely associated with binary populations. The results of this thesis work and of potential future work are summarized as follows:

5.1. Summary of the Thesis

1) The Radial Velocity Survey: This survey was carried out to search for spectroscopic binary stars in the globular cluster NGC 5053 using the Norris Multi-fiber Spectrograph on the Palomar 200 inch telescope. This cluster was chosen because its half-mass relaxation timescale is comparable to a Hubble time and the cluster is dynamically young. Thus the primordial binary population in NGC 5053 has not been significantly altered by stellar encounters. The survey observed a total of 65 cluster member stars with visual magnitudes of 14.5−18.6 over a timespan of 3 years. We obtained a total of 223 velocities with a typical velocity error per measurement of $\sim$3 kms^{-1}. We surveyed three times as many stars as in the previous study of the same cluster by Pryor et al. (1989), and our sample objects are also 3 magnitudes fainter. Thus, our survey is sensitive to binaries with much shorter periods of 4 d $\leq$ P $\leq$ 10 yr. Among these 65 stars, we discovered 5 spectroscopic binary candidates, one of which star S5 was discovered previously by Pryor et al. (1989).

Using Monte-Carlo simulation methods, we estimated the fraction of binary systems which may have been missed from detection due to unfavourable orbital configurations. With our survey, the estimated binary discovery efficiency is 30% for

systems with 4 d $\leq$ P $\leq$ 10 yr, 0.125 $\leq$ q $\leq$ 1.75 and eccentric orbits. This yields a binary frequency of 26%. In the case of circular orbits, the estimated binary frequency is $\sim$24%. The binary discovery efficiency is higher for binaries with higher mass ratios. This results in a smaller binary frequency of 22% for systems with 4 d $\leq$ P $\leq$ 10 yr, 0.3 $\leq$ q $\leq$ 1.75 and eccentric orbits.

We also applied Kolmogorov-Smirnov (K-S) tests to the cumulative distributions of maximum velocity variations from the actual measurements and the synthetic velocity data. The results from these tests are consistent with 20$-$30% binary population with 4 d $\leq$ P $\leq$ 10 yr, 0.125 $\leq$ q $\leq$ 1.75 in NGC 5053. The hypothesis of a binary frequency in NGC 5053 higher than 50% is rejected with a confidence level higher than 90%. The binary frequency in NGC 5053 derived from our survey is somewhat higher than estimates for other clusters by various surveys. This is perhaps related to the fact that NGC 5053 is fairly dynamically young compared to these clusters. We also argue that the binary population in globular clusters is not significantly deficient compared to binaries in other stellar environments such as open clusters, or to field and low metallicity halo stars.

2) The Imaging Surveys: The second part of this thesis utilizes a different technique — the analysis of time series photometry. This method is very efficient in searching for eclipsing binaries with periods of a few days, as demonstrated in our surveys in the two globular clusters M 71 and M 5. In both clusters, we monitored the photometry of more than 6000 stars in two colours continuously for 3$-$6 hours per night over 4$-$15 nights. Each image covers a 6.3′ $\times$ 6.3′ field. We discovered a total of 11 eclipsing binaries, 5 in M 71, and 6 in M 5. These binaries have periods 0.3$-$0.7 days and are main-sequence stars except one in M 5, which is a possible blue straggler. Their light curves indicate that one variable in M 71 and one in M 5 are detached or semi-detached eclipsing binaries; the rest of the 11 systems are W UMa type contact binaries. The binary type classification is somewhat uncertain for the systems in M 5 due to poor phase coverage in their light curves.

We have used a variety of arguments to conclude that all five binary stars are probable members of M 71, a result that is consistent with the low number (0.15) of short-period field binaries expected along this line of sight. (As discussed below, the radial velocity data for these five binaries recently obtained by Yan & Mateo should determine definitely their memberships. These data are not included in this thesis.) Based on a simple model of how contact binaries evolve from initially detached

binaries, we have determined a lower limit of 1.3% on the frequency of primordial binaries in M 71 with initial orbital periods in the range 2.5-5 days. This implies that the overall primordial binary frequency, f, is 22% assuming $df/d\log P = const$ (the "flat distribution"), or $f = 57\%$ for $df/d\log P = 0.032\log P + const$ as observed for G-dwarf binaries in the solar neighborhood (the "sloped distribution"). Both estimates of f correspond to binaries with initial periods shorter than 800 yrs; longer-period binaries would have been disrupted over the lifetime of the cluster. Our short-period binary frequency is in excellent agreement with the observed frequency of red-giant binaries observed in globulars if we adopt the flat distribution. For the sloped distribution, our results significantly overestimate the number of red-giant binaries. All of the M71 binaries lie within 1 mag of the luminosity of the cluster turnoff in the color-magnitude diagram despite the fact we should have easily detected similar eclipsing binaries 2−2.5 magnitudes fainter than this.

The number of foreground/background stars in the field of M 5 is small because of its high galactic latitude. In addition, the location of these variables on the cluster colour-magnitude diagram also suggests that all six eclipsing binaries are cluster members. Adopting a flat period distribution and a contact binary lifetime of 3 Gyrs, we estimated an overall primordial binary frequency of $28^{+11}_{-6}\%$ for the period range of 2.5 days to 550 yrs. We should point out that the major uncertainty in this calculation is our poor understanding of the lifetime of contact eclipsing binaries. To make comparative studies of short-period main-sequence eclipsing binaries in different globular clusters, we estimate that the specific frequency of such binaries is 0.5% in M 5 excluding the possible blue straggler, similar to the fraction of 0.6% derived in M 71.

The discovery of ten short-period main-sequence eclipsing binaries in M 71 and M 5 for the first time provides strong physical evidence which supports the scenario that some blue stragglers are formed by mass transfer and mergers in short-period main-sequence binary systems. Some of these systems are destined to become blue stragglers when either a) the primary gains enough mass to push it over the turnoff mass, or b) the cluster turnoff mass evolves below the mass of the primary or the merged binary remnant.

5.2. Future Work

Continuing efforts in searching for binary stars in globular clusters will shed light on the following issues:

1) Does the binary frequency depend on the cluster dynamical property? Theoretically, we understood that binary populations can be significantly altered by stellar encounters; the present binary populations in a cluster should reflect the dynamical evolution history of the cluster. The result from our survey in NGC 5053 hints that the binary frequency is higher in this dynamically young cluster. However, observationally, this effect is still very uncertain and further studies in this area are needed.

2) Mass segregation of binary stars in globular clusters. Binary stars are heavier and should have a centrally concentrated spatial distribution in dynamically relaxed clusters. With increasing numbers of binaries discovered in globular clusters, this effect should be seen observationally in the near future. Moreover, some short-period binaries are produced in stellar encounters and those in the outer parts of a cluster are perhaps ejected from recoils of star-binary and binary-binary encounters. Thus, the spatial distribution of short-period eclipsing binaries may be useful for tracing the initial binary population as well as its spatial distribution.

3) Determine binary period distribution in globular clusters. The binary period distribution in globular clusters contains information about the initial binary star formation processes, and the cluster dynamical evolution processes as well. It is not yet feasible to obtain an unbiased sample of binaries in globular clusters with orbital solutions. However, it remains our ultimate goal to determine the distribution functions of orbital parameters for binary stars in globular clusters.

4) Finally and most importantly, short-period main-sequence eclipsing binaries can be used to determine masses of main-sequence stars in globular clusters. An outstanding problem in modern cosmology is the persistent discrepancy between the ages of globular clusters and the expansion age of the Universe. Most measurements — both ground-based and space-based — appear to favor an age of the Universe of $\sim$10 Gyr. However, studies of the ages of the oldest globular clusters consistently yield 12$-$16 Gyr.

The cause of this apparent discrepancy continues to be the subject of much debate. One approach to this problem is to check stellar evolution models using an independent method. These models, used in calculating the ages of globular

clusters, are complex and rely on extensive tabulations of a wide variety of atomic and nuclear data (opacities, nuclear cross sections, ionization potentials, etc). Even the most ambitious models remain incomplete — rotation and magnetic fields, for example, are rarely included.

The discovery of short-period main-sequence eclipsing binaries in globular clusters, for the first time, provides a unique opportunity to check stellar evolutionary models and test the reliability of the derived ages for globular clusters. The classic method of measuring stellar masses is to observe double-lined eclipsing binaries. For many years this method has been used to determine the masses of nearby field stars to high precision (Anderson *et al.* 1987; Schiller & Milone 1988; Anderson 1991). For a double-lined eclipsing binary system, with spectroscopic observations we can obtain $M_1 \sin^3 i$ and $M_2 \sin^3 i$ for the both components of the binary system. Here i is the orbital inclination angle of the binary system relative to the line of sight. For an eclipsing binary, i can be determined from the photometric light curve. Therefore, with double-lined main-sequence eclipsing binaries in a globular cluster, we can obtain accurate mass measurement of the cluster main-sequence stars and thus derive independently the cluster age.

Specifically, of the five eclipsing binaries discovered in M 71 (Yan & Mateo 1994), only one binary V4 is a detached system located near the main-sequence turnoff in the cluster colour-magitude diagram. The detailed photometric analyses of V4 (McVean & Milone 1995) suggest that the components of this star are evolved and have probably exchanged mass. However, these stars can still be used to measure a lower limit to the cluster turnoff mass and thus an upper limit to the cluster age. This test requries no knowledge of the cluster distance. Mario Mateo and I have obtained spectroscopic observations of these five eclipsing binaries using the multi-slit spectrograph on the 4-meter telescope at the Kitt Peak Observatory. To have a good phase coverage, we monitored these stars continuously for four nights and obtained a total of 40 velocities per star. Preliminary data reduction indicates that our velocity measurements are accurate to 5 km s^{-1}. This is sufficient for deriving the radial velocity curves because of much larger radial velocity variations in these short period systems.

Our ultimate goal is to find truely detached double-lined main-sequence eclipsing systems in globular clusters. With increasing numbers of surveys being carried out by various groups, we should be able to estimate the masses of main-sequence stars

and thus ages of globular clusters in the not too distant future. In fact, Kaluzny et al. (personal communication) have discovered two possible detached systems in ω Cen. Figure 1 shows the light curves of the systems with periods of 1.497 days and 2.467 days respectively. Both stars are located at the bottom of the subgiant branch in the cluster HR diagram.

REFERENCES

Anderson, Garcia, Giménez & Nordström, 1987, AA, 174, 107

Anderson, 1991, AAR, 3, 91

McVean, J.R. & Milone, E.F., 1995, in *Binary Stars*, ed. E.F. Milone, in press

Schiller, S.J. & Milone, E.F., 1988, AJ, 95, 1466

Yan, L. & Mateo, M., 1994, AJ, 108, 1810

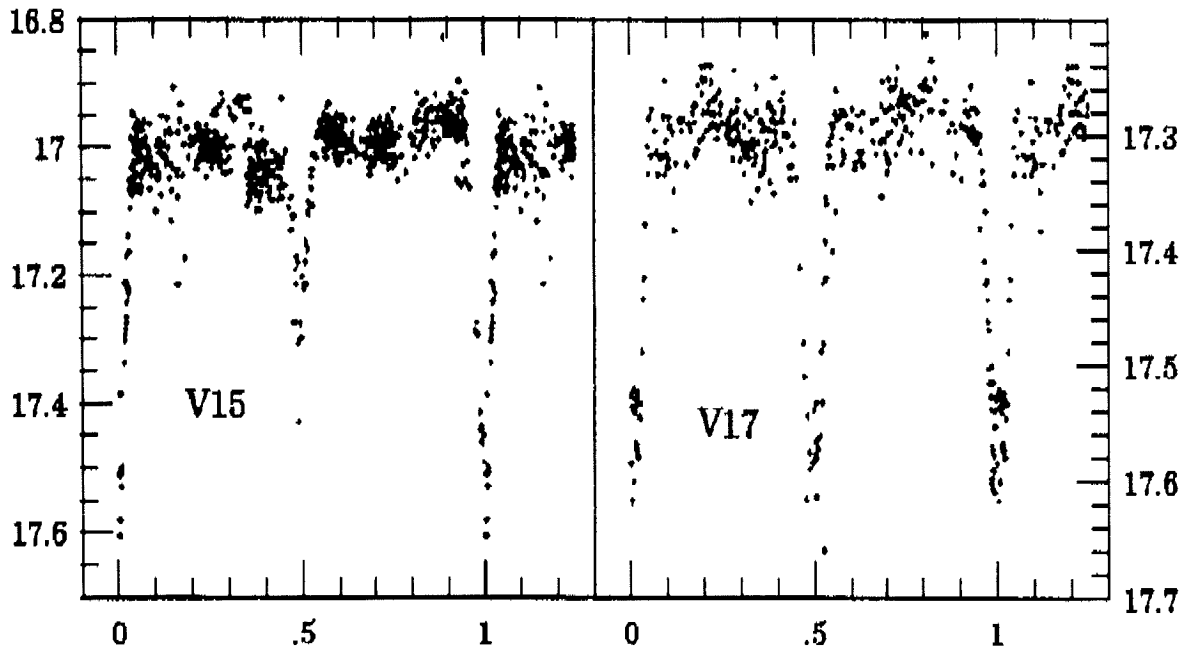

Figure 5.1. V-band light curves of ω Cen. variables

The V-band light curves of two possible detached eclipsing binaries in ω Cen. The two variables have periods of 1.497 days and 2.467 days respectively.

Appendix A

The Efficiency of The Norris Multi-fiber Spectrograph

In this appendix, I will briefly discuss several issues related to the throughput efficiency of the Norris Multi-fiber Spectrograph.

The spectral signal-to-noise ratios depend on the following factors: 1) the accuracy of the object astrometry, 2) the accuracy of the measured transformation coefficients from the surface of a sphere to the plane of the 2-dimensional XY-fiber stage, 3) the seeing conditions, an especially important factor for stellar observations because the diameter of the fiber aperture is only 1.6″, 4) the throughput efficiency of the spectrograph, including the telescope efficiency and the CCD detector quantum efficiency.

The issues related to the obtaining accurate astrometry for the program objects are discussed in section 2.2.2.1 of Chapter 2 of the thesis. The measurement of transformation coefficients from the surface of a sphere to the XY-stage is usually obtained by using bright stars in open clusters. Obviously, the accuracy of this measurement and the time required to complete it depend on the precision of the astrometry of these bright stars, as well as the experience of those using the spectrograph. Before going to the detailed discussions about the spectrograph throughput efficiency, we briefly touch on the subject of the spectrograph flexure.

The Spectrograph Flexure: The data we obtained indicate that the Norris spectrograph does not have a severe flexure problem. Figure 1 shows the pixel position of 4965.09Å on the CCD versus the hour angle for fiber 132. The plot was made from Thorium-Argon comparison spectra taken during the same run — the spectrograph setup was not changed during the run. While the spectrograph moves around, the pixel positions of spectrum lines along the dispersion direction on the

CCD may change. This is called spectrograph flexure. Obviously, the size of the flexure depends on where the telescope is pointed. As shown in Figure 1, at the declination 17.9°, the pixel position of 4965.09Å changed less than 0.5 pixels while the telescope was tracked from the hour angle −2 to +3 hours within the same night. However, the flexure between different nights can be as large as 3.0 pixels. For doing accurate radial velocity measurements, it is good to know that the spectrograph flexure during the consecutive exposures of a same object in one night is small; it can be easily calibrated out.

The Spectrograph Throughput Efficiency: We used the data obtained for NGC 5053 and for the bright stars in M 13 to check the Norris spectrograph efficiency. The calculation was done for a total of 12 stars in M 13 using the data from seven different exposures in two different observing runs in 1994. The formula for calculating the throughput efficiency is as follows:

$$T = \frac{N_{obs}}{N_{exp}} \tag{1}$$

Here N_{obs} and N_{exp} are the observed and theoretically calculated number of photons per second per Angstrom from a star. All calculations are done at 5500Å.

$$N_{obs} = \frac{DN \times pscale \times Gain}{t_{exp}} (photon\, s^{-1} Å^{-1}) \tag{2}$$

Here DN is the observed data number counts per pixel at 5500Å in a spectrum, pscale is the pixel scale — 0.54Å/pixel, the gain of the detection electronics is 1.7 electrons per data number counts and t_{exp} is the total exposure time in seconds.

$$N_{exp} = 1000 \times 10^{-0.4 m_v} \times \pi R_{eff}^2 \times 10^{-0.4 A(\lambda) airmass} (photon\, s^{-1} Å^{-1}) \tag{3}$$

Here m_v is the apparent visual magnitude, R_{eff} is $\sqrt{(100^2 - 36^2)} = 93.8$ inches, the effective radius of the 200 inch telescope. $A(\lambda)$ is the atmospheric extinction at the Palomar observatory, which is 0.15 mag airmass^{-1} at 5500Å.

Table 1 lists the throughput efficiency T calculated for 12 bright stars in M 13 using equations (1), (2) and (3). Table 2 lists the fiber identification numbers for the stars in M 13. The fibers have different transmission efficiencies. Using the dome flat exposures at the zenith, we calculated the fiber transmission efficiency relative to fiber 124 (which has the highest apparent transmission efficiency), as listed in

the fourth column in Table 2. T_c represents the throughput after corrected for the relative fiber transmission efficiency. In Table 2, the relative fiber transmission efficiencies were calculated using the dome flat exposures taken in different nights and runs, and don't have much variations.

Table 3 lists the spectrograph throughput efficiency calculated using the two brightest stars in NGC 5053. Again, the calculations were done at 5500Å, and the throughput values listed were not corrected for the different relative fiber transmission.

The small values of throughput T in these tables reflect the integrated effects of the errors in the object astrometry, transformation coefficients, bad seeing conditions, the relatively low fiber transmission efficiency, the photon losses due to the telescope, the spectrograph and the CCD detector. The highest value of T ($\sim$ 5%), although it is rare in the table, perhaps closely presents the true throughput efficiency of the Norris spectrograph. The visual band photometry in Table 1 is from Lupton, Gunn and Griffin (1987). Any photometric errors (which should be less than 0.1 mag) will also contribute to the scattering of values of T in Table 1.

If we remove the telescope, the spectrograph camera plus the grating, and the CCD detector (the telescope has two mirrors with an assumed reflectivity of 90% each; the camera plus the grating have an assumed total throughput efficiency of 70%; the measured CCD quantum efficiency of 85% — this totals 48%), then the highest throughput efficiency T in Table 1 from the remaining contributors, including the fibers, the seeing losses and all other factors, is about 11%.

To compare the throughput of the Norris spectrograph with those of other multi-fiber spectrographs, we obtained some estimates from Sam Barden at NOAO and from Steve Schectman at the Observatory of Carnegie Institute of Washington (OCIW). The mulit-fiber spectrograph Hydra at the 4-meter telescope at NOAO has the measured throughput efficiency of 3.1% at 5000Å. This number was calculated in the same way as the throughput efficiencies listed in the tables. Since their camera has a low throughput of 50% (which is in the process of being replaced by one of higher throughput), we have to multiply the Hydra throughput by a factor of $\sim$1.8 in order to compare it with that of the Norris spectrograph. An approximate estimate from Steve Shectman indicated that the multi-fiber spectrograph at OCIW also has a similar throughput efficiency around 5%. From these data we conclude

that the throughput efficiency of the Norris spectrograph is comparable to those of other multi-fiber spectrographs in use at other large telescopes.

REFERENCES

Lupton, R.H., Gunn, J.E. & Griffin, R.F., 1987, AJ, 93, 1114

Table 1 — The Norris Spectrograph Throughput Calculated with the Bright Stars in M 13

Star	m_v	T	T	T	T	T	T	T
	mag	11/04/94	11/04/94	13/04/94	13/04/94	10/05/94	10/05/94	10/05/94
I-13	12.54	2.0%	2.5%	1.2%	2.9%	3.2%	4.0%	4.3%
II-67	12.12	1.6%	2.0%	0.9%	1.8%	1.8%	3.6%	3.8%
III-76	12.84	2.0%	2.4%	0.9%	2.2%	2.4%	3.0%	3.2%
III-56	12.44	1.1%	1.5%	0.6%	1.4%	1.4%	2.1%	2.1%
III-52	12.67	2.7%	3.1%	1.5%	3.7%	4.0%	5.4%	5.8%
III-63	12.20	0.2%	0.2%	0.1%	0.2%	0.1%	0.2%	0.1%
III-41	13.32	1.7%	2.2%	1.0%	2.2%	2.2%	3.2%	3.2%
IV-17	14.16	2.2%	2.9%	1.4%	3.0%	3.1%	4.6%	4.6%
III-73	12.32	1.0%	1.1%	0.5%	1.3%	1.2%	2.6%	2.5%
IV-25	12.09	0.4%	0.5%	0.3%	0.5%	0.4%	0.5%	0.4%
B-273	13.65	1.5%	1.8%	1.0%	2.1%	2.1%	3.5%	3.1%
B-286	13.58	0.7%	1.0%	0.4%	0.8%	0.7%	0.8%	0.7%

Notes: All calculations were done at 5500Å. For the definition of T, see the text for the details. The first two columns in the table are the star's name and its apparent visual magnitude from (Lupton, Gunn & Griffin 1987). The remaining columns are throughput calculated from data taken in different dates. The weather conditions during these seven exposures were clear.

Table 2 — The Norris Spectrograph Throughput Corrected For Relative Fiber Transmission

Fiber ID	Star	m_v mag	Eff	T_c 11/04/94	T_c 11/04/94	T_c 13/04/94	T_c 13/04/94	T_c 10/05/94	T_c 10/05/94	T_c 10/05/94
36	I-13	12.54	0.90	2.3%	2.8%	1.3%	3.2%	3.5%	4.5%	4.8%
53	II-67	12.12	0.84	1.9%	2.4%	1.0%	2.2%	2.1%	4.3%	4.5%
50	III-76	12.84	0.84	2.3%	2.9%	1.1%	2.6%	2.9%	3.5%	3.8%
47	III-56	12.44	0.87	1.3%	1.7%	0.7%	1.6%	1.6%	2.4%	2.4%
133	III-52	12.67	0.95	2.9%	3.3%	1.6%	3.9%	4.2%	5.7%	6.1%
135	III-63	12.20	0.56	0.3%	0.4%	0.2%	0.3%	0.2%	0.4%	0.2%
138	III-41	13.32	0.84	2.0%	2.6%	1.2%	2.6%	2.6%	3.8%	3.8%
124	IV-17	14.16	1.00	2.2%	2.9%	1.4%	3.1%	3.1%	4.6%	4.6%
141	III-73	12.32	0.66	1.5%	1.6%	0.8%	1.9%	1.9%	3.9%	3.9%
121	IV-25	12.09	0.64	0.7%	0.8%	0.5%	0.8%	0.6%	0.8%	0.6%
145	B-273	13.65	0.88	1.7%	2.1%	1.1%	2.4%	2.4%	4.0%	3.5%
147	B-286	13.58	0.62	1.1%	1.6%	0.7%	1.4%	1.2%	1.3%	1.1%

Notes: As in Table 1, all calculations were done at 5500Å. The first column is the fiber identification number. The second and third columns are the star's name and its apparent visual magnitude from (Lupton, Gunn & Griffin 1987). The fourth column is the fiber transmission efficiency relative to fiber 124 which has the apparent highest transmission. The rest columns are throughput with the correction for the relative fiber transmission efficiency. For details, see the text.

Table 3 — The Spectrograph Throughput Calculated Using Two Bright Object Stars in NGC 5053

Date UT	T (GSC-37)	T (GSC-72)
11/04/94	2.9%	2.8%
11/04/94	2.5%	3.1%
11/04/94	2.1%	1.7%
12/04/94	1.3%	1.5%
12/04/94	2.4%	2.5%
12/04/94	1.1%	0.9%
08/05/94	2.0%	1.8%
08/05/94	2.3%	2.2%
08/05/94	0.6%	0.4%
10/05/94	2.1%	5.5%
10/05/94	2.7%	2.4%
m_v	15.28	14.18
Fiber ID	36	62

Notes: All calculations were done at 5500Å.

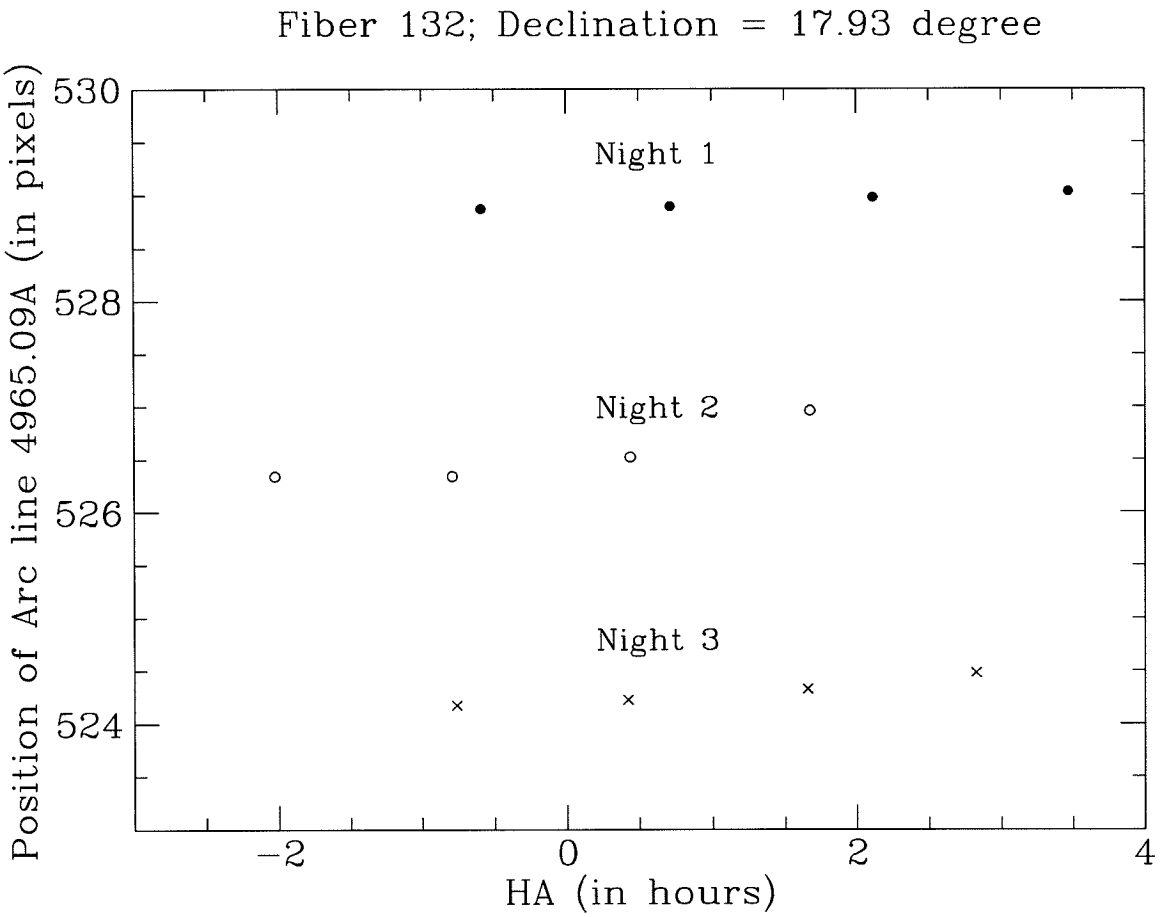

Figure 1 The Spectrograph Flexure

Figure 1 shows that the pixel position of 4965.09Å on the CCD along the dispersion direction varies as the telescope moves from the hour angle -2 to $+3$ hours at the declination 17.9 degree. The solid dots in the plot are for night 1 data, open circles, night 2, and crosses, night 3.